

Yury V. Kissin

# Polyethylene

End-Use Properties and their  
Physical Meaning

**HANSER**

Hanser Publishers, Munich

Hanser Publications, Cincinnati

*The Author:*

Yury V. Kissin,  
Rutgers, The State University of New Jersey, Department of Chemistry and Chemical Biology,  
Piscataway, New Jersey 08854-8087, USA

Distributed in North and South America by:

Hanser Publications  
6915 Valley Avenue, Cincinnati, Ohio 45244-3029, USA  
Fax: (513) 527-8801  
Phone: (513) 527-8977  
www.hanserpublications.com

Distributed in all other countries by

Carl Hanser Verlag  
Postfach 86 04 20, 81631 München, Germany  
Fax: +49 (89) 98 48 09  
www.hanser.de

The use of general descriptive names, trademarks, etc., in this publication, even if the former are not especially identified, is not to be taken as a sign that such names, as understood by the Trade Marks and Merchandise Marks Act, may accordingly be used freely by anyone.

While the advice and information in this book are believed to be true and accurate at the date of going to press, neither the authors nor the editors nor the publisher can accept any legal responsibility for any errors or omissions that may be made. The publisher makes no warranty, express or implied, with respect to the material contained herein.

Library of Congress Cataloging-in-Publication Data

Kissin, Y. V.

Polyethylene : end-use properties and their physical meaning / Yury V.

Kissin.

pages cm

ISBN 978-1-56990-520-3 (hardcover) -- ISBN 978-1-56990-521-0 (e-book) 1.

Polyethylene--Mechanical properties. 2. Molecular weights. 3. Gums and resins, Synthetic. I. Title.

TP1180.P65K47 2012

668.4'234--dc23

2012030832

Bibliografische Information Der Deutschen Bibliothek

Die Deutsche Bibliothek verzeichnet diese Publikation in der Deutschen Nationalbibliografie; detaillierte bibliografische Daten sind im Internet über <<http://dnb.d-nb.de>> abrufbar.

ISBN 978-1-56990-520-3

E-Book-ISBN 978-1-56990-521-0

All rights reserved. No part of this book may be reproduced or transmitted in any form or by any means, electronic or mechanical, including photocopying or by any information storage and retrieval system, without permission in writing from the publisher.

© Carl Hanser Verlag, Munich 2013

Production Management: Steffen Jörg

Coverconcept: Marc Müller-Bremer, [www.rebranding.de](http://www.rebranding.de), München

Coverdesign: Stephan Rönigk

Typesetted by Kösel, Krugzell

Printed and bound by CPI buch bücher.de gmbh

Printed in Germany

# Introduction

Every commercial information sheet describing a polyethylene resin, every professional discussion of the application range for a resin, every issue of the resin pricing—they all involve the same short list of resins' end-use properties. Although the items in the list may vary depending on application, they are universally understood throughout the “insider’s” word without any need for an explanation. For commercial film-grade LLDPE resins these parameters usually include the melt index, the melt flow ratio, the melting point, the dart impact strength, and the tear strength in two directions of the film. For blow-molding HDPE resins the usual parameters are the high-load melt index, environmental stress cracking resistance, the top-load strength, and so on. Tables I.1 and I.2 show two representative examples of these parameters taken from commercial product data-sheets.

**Table I.1** ExxonMobil LLDPE resin, LL 1001 Series

	SI units	English units
Density	0.918 g/cm <sup>3</sup>	0.0332 lb./in <sup>3</sup>
Melt index (190 °C, 2.16 kg)	1.0 g/10 min	1.0 g/10 min
Peak melting temperature	121 °C	250 °F
Tensile strength at yield, MD	9.4 MPa	1,400 psi
Tensile strength at yield, TD	9.5 MPa	1,400 psi
Tensile strength at break, MD	50 MPa	7,700 psi
Tensile strength at break, TD	35 MPa	5,100 psi
Elongation at break, MD	580 %	580 %
Elongation at break, TD	850 %	850 %
Secant modulus, MD, at 1 %	190 MPa	28,000 psi
Secant modulus, TD, at 1 %	220 MPa	32,000 psi
Dart drop impact strength	100 g	100 g
Elmendorf tear strength, MD	80 g	80 g
Elmendorf tear strength, TD	400 g	400 g

**Table I.2** Braskem GM7746C Blow Molding HDPE Resin

	SI units	English units
Density	0.944 g/cm <sup>3</sup>	0.0341 lb./in <sup>3</sup>
Melt index (190 °C, 21.6 kg)	4.5 g/10 min	4.5 g/10 min
Vicat softening point	126 °C	259 °F
Tensile strength at yield	23 MPa	3,340 psi
Tensile strength at break	42 MPa	6,090 psi
Elongation at yield	13%	13%
Elongation at break	880%	880%
Flexural (secant) modulus at 1%	890 MPa	129,000 psi
Secant modulus, TD, at 1%	220 MPa	32,000 psi
Environmental stress-cracking resistance (100% Igepal)	≥ 1,000 h	≥ 1,000 h

These terms and these values have become “the lingua franca” of all product engineers, plant operators, and catalyst chemists throughout the world involved in the production and testing of polyethylene resins. However, the exact physical meaning of the end-use properties and the correlations between their values and the basic “scientific” properties of polymers, such as the average molecular weight, the molecular weight distribution, the content of  $\alpha$ -olefin in an LLDPE resin or a VLDPE plastomer, are not clearly defined.

This book provides a necessary bridge between the values of engineering end-use parameters of polyethylene resins and their scientific molecular and structural characteristics. The main goal is to translate such common parameters as the melt index of a resin or the dart impact strength of a film sample into the universal language of the polymer science. After this translation is completed, many facets of the resin properties became transparent and easily explainable. For example:

- What happens with the melt flow ratio of a resin after the catalyst used to produce it is modified to increase its sensitivity to an  $\alpha$ -olefin?
- What happens with the dart impact strength or the tear strength of LLDPE film when butene is replaced with hexene or octene in an ethylene/ $\alpha$ -olefin copolymerization reaction employing the same catalyst and why does it happen?
- Why are the melting points of metallocene LLDPE resins so much lower compared to the melting points of LLDPE resins of the same density and molecular weight prepared with supported Ziegler-Natta catalysts?

These are the types of questions this book provides answers to. Detailed analysis of many such links between the end-use engineering properties of a resin and molecular characteristics of the polymer turn out to be quite complex. For this reason, a description of each such linkage is accompanied by numerous examples of practical significance and by explicit data for common commodity polyethylene resins.

This book is written with three audiences in mind. The first, the most populous, includes product engineers, the specialists who evaluate properties of resins and judge their usefulness (as well as pricing) for a particular application. These specialists are very adept at measuring and evaluation of end-use engineering properties of the resins they are working with. However, they are usually less surefooted when asked which of the molecular characteristics of the polymers they think should be changed, and in what direction, to improve a particular end-use property.

The members of the second audience are plant and pilot plant operators in the polyethylene industry. These individuals deal with large-scale, steady production processes and need to know which of the process variables they control are crucial for maintaining or achieving the desired end-use parameters of the resins.

The members of the third audience are catalyst chemists, specialists in designing new polymerization catalysts and modifying the existing ones. These professionals often judge success or a failure of the catalyst they develop based on properties of a small amount of polymer prepared in the laboratory, from ~ 10 to ~ 200 g. Their principal interest is to know which of the small-volume, bench-type tests of the polymers has the highest predictive power and how to translate the changes they make in the catalyst recipe into the changes in the end-use properties of the resins manufactured on the commercial scale. One has to take into account that the measurement of some end-use properties requires large quantities of resins far exceeding what can be prepared in the laboratory.

This book is intended to improve communication bridges between these three groups of specialists and to aid them in understanding each other better and faster.

*Yuri V. Kissin*

# Table of Content

<b>Introduction</b> .....	IX
<b>1 Educational Minimum: Manufacture, Structure, and Mechanical Properties of Polyethylene Resins</b> .....	1
1.1 Classification and Applications of Polyethylene Resins .....	1
1.2 Catalysts for Synthesis of Polyethylene Resins .....	4
1.3 Industrial Processes for the Manufacture of Polyethylene Resins .....	6
1.4 Chemistry of Ethylene Polymerization Reactions .....	8
1.5 Molecular Weight Distribution of Polymers and Methods of its Analysis .....	11
1.6 Examples of Molecular Weight Distribution of Polyethylene Resins .....	14
1.7 Copolymer Statistics and its Application to Description of LLDPE and VLDPE Resins .....	20
1.8 Compositional Uniformity of Commercial Polyethylene Resins .....	22
1.9 Morphology of Polyethylene Resins .....	26
1.10 Mechanical Deformation of Polyethylene Resins .....	29
References .....	31
<b>2 Melt Index and Melt Flow Ratio of Polyethylene Resin</b> .....	35
2.1 Introduction .....	35
2.2 Basics of Polymer Rheology; Melt Flow Through a Capillary .....	37
2.2.1 Flow of Polymer Melt Through a Cylindrical Capillary .....	39
2.2.2 Melt Index of Newtonian Liquid .....	40
2.3 Melt Flow of Monodisperse Polyethylene Resins .....	41
2.4 Additivity Rules for Viscosity; Calculation of Melt Indexes and Melt Flow Ratios from Molecular Weight Distribution Data .....	43
2.4.1 Additivity Rules for Zero-Shear Viscosity $\eta_0$ .....	43
2.4.2 Additivity Rules for Effective Viscosity and General Expressions for Flow of Non-Newtonian Multi-Component Melt .....	44

2.5	Examples of Melt Flow Rates and Melt Flow Ratios for Polyethylene Resins of Different Types	48
2.5.1	LLDPE Resins Produced with Supported Ziegler-Natta Catalysts	48
2.5.2	HDPE Resins with Broad Molecular Weight Distributions	51
2.5.3	Effect of Long-Chain Branching	53
	References	54
<b>3</b>	<b>Melting Point of Polyethylene Resin</b>	<b>57</b>
3.1	Introduction	57
3.2	Melting Point of HDPE Resin	58
3.3	DSC Melting Curves and Melting Points of LLDPE and VLDPE Resins Produced with Single-Site Catalysts	61
3.3.1	Crystallization Process of Compositionally Uniform Ethylene/ $\alpha$ -Olefin Copolymers	64
3.3.2	Model for Secondary Crystallization	65
3.3.3	Combined DSC Model for LLDPE and VLDPE Resins	66
3.4	DSC Melting Curves and Melting Points of LLDPE Resins Produced with Multi-Site Ziegler-Natta Catalysts	68
	References	71
<b>4</b>	<b>Crystallinity Degree and Density of Polyethylene Resins</b>	<b>73</b>
4.1	Crystallinity Degree	73
4.1.1	Measurement Methods	73
4.1.2	Definition of Crystallinity Degree of LLDPE and VLDPE Resins Based on Copolymer Statistics	75
4.2	Density	76
4.2.1	Measurement Methods	77
4.2.2	Physical Meaning of Polyethylene Density	77
	References	80
<b>5</b>	<b>End-Use Mechanical Properties of Polyethylene Film</b>	<b>83</b>
5.1	Mechanical Properties of Polyethylene Resins	83
5.1.1	Effect of Testing Speed on Mechanical Properties	84
5.1.2	Orientation in Polyethylene Film	85
5.2	Dart Impact Strength of LLDPE Film	87
5.2.1	Description of Dart Impact Test	87
5.2.2	Model of Dart Impact Test	89
5.2.2.1	Effects of Mechanical Properties of Resins	92

5.2.2.2	Comparison of Film Made from Ethylene/Butene and Ethylene/Hexene Copolymers . . . . .	93
5.2.2.3	Effect of Copolymer Composition . . . . .	94
5.2.2.4	Compositionally Uniform and Compositionally Nonuniform Resins . . . . .	95
5.3	Tear Strength of LLDPE and LDPE Film . . . . .	97
5.3.1	Description of Tear Test . . . . .	97
5.3.2	Physical Details of Tear Test . . . . .	97
5.3.3	Model of Tear Test . . . . .	102
5.3.3.1	Effect of Pendulum Speed . . . . .	107
5.3.3.2	Effects of Mechanical Properties of Resins . . . . .	107
5.3.3.3	Effect of Film Orientation . . . . .	108
5.3.3.4	Comparison of Tear Strength of Ethylene/Butene and Ethylene/Hexene Copolymers . . . . .	110
5.3.3.5	Low Density Polyethylene . . . . .	110
5.4	Comparison of Factors Determining Results of Tear Test and Dart Impact Test of LLDPE Film . . . . .	111
References	. . . . .	112
<b>6</b>	<b>End-Use Testing of High Molecular Weight HDPE and MDPE Resins . . . . .</b>	<b>115</b>
6.1	Top Load Test of HDPE Containers . . . . .	115
6.1.1	Mechanics of Top Load Test . . . . .	116
6.2	Dynamic Burst Test of HDPE Tubing and Pipes . . . . .	118
6.3	Static Burst Test and Long-Term Fatigue in Polyethylene . . . . .	119
6.3.1	Principal Equation for Low-Stress Failure . . . . .	120
6.3.2	Physical Mechanism of Polymer Failure under Low Stress . . . . .	122
6.4	Environmental Stress-Cracking Resistance . . . . .	125
6.4.1	Description of ESCR Test . . . . .	125
6.4.2	Physics of Environmental Stress Cracking . . . . .	126
6.4.3	Structural Parameters of HDPE Resins Affecting ESCR . . . . .	127
6.4.4	Relationship between ESCR and Long-Term Fatigue in Polyethylene . . . . .	130
6.4.5	Mechanism of Environmental Stress Cracking . . . . .	132
References	. . . . .	135
<b>Index</b>	. . . . .	<b>139</b>

## 1

# Educational Minimum: Manufacture, Structure, and Mechanical Properties of Polyethylene Resins

## ■ 1.1 Classification and Applications of Polyethylene Resins

The term “polyethylene resins” describes catalytically produced semicrystalline homopolymers and copolymers derived mostly from ethylene and used as commodity plastics, as well as ethylene polymers produced in radical polymerization reactions under high pressure. Some polyethylene resins contain strictly linear polymer chains, their chemical formula is  $-(\text{CH}_2-\text{CH}_2)_n-$ , where  $n$  is usually a very large number, from  $\sim 1,000$  to  $\sim 10,000$ . Other polyethylene resins contain branches in their chains. Most such resins are produced in ethylene/ $\alpha$ -olefin copolymerization reactions. The molecular structure of these resins can be represented by the formula



where the  $-\text{CH}_2\text{CH}_2-$  units come from ethylene and the  $-\text{CH}_2\text{CH}(\text{Branch})-$  units come from the  $\alpha$ -olefin molecule. The  $x$ ,  $y$ , and  $z$  values can vary from very small (4 to 5), to a very large number. All the branches in catalytically produced polyethylene resins are the same; they are alkyl substituents in the  $\alpha$ -olefin molecules: the ethyl group if the  $\alpha$ -olefin is butene, the butyl group if the  $\alpha$ -olefin is hexene, the hexyl group if the  $\alpha$ -olefin is octene, the isobutyl group if the  $\alpha$ -olefin is methylpentene. When ethylene is polymerized at a high pressure via the radical mechanism, branches of many different types are formed spontaneously due to peculiarities of the radical reactions. These branches are linear or branched alkyl groups. Their lengths vary widely within each polymer molecule. Two types of such branches are distinguished, the short-chain branches, from the methyl to the isooctyl group, and the long-chain branches, up to several thousand carbon atoms long.

In polymer science, the amount of  $\alpha$ -olefin in a copolymer is represented as the molar content of the  $\alpha$ -olefin,  $C_M^{\text{copol}}$ , mol %. In industry, the amount of  $\alpha$ -olefin in polyethylene resins is often represented by the value called *the branching degree*. It is defined as the number of branches per 1,000 carbon atoms, Branch/1,000C. Because all such branches usually end with the methyl group, the branching degree is often represented by the symbol  $\text{CH}_3/1,000\text{C}$ . The ratio between  $C_M^{\text{copol}}$  and the branching degree is given by

$$\text{CH}_3/1,000\text{C} = C_M^{\text{copol}} / (0.2 + 0.001 \cdot k \cdot C_M^{\text{copol}}) \quad (1.1)$$

where  $k$  is equal to 2 for ethylene/butene copolymers, 4 for ethylene/hexene copolymers, and 6 for ethylene/octene copolymers.

Classification of polyethylene resins has developed historically, in parallel with the discovery of new catalysts for ethylene polymerization and new polymerization processes. The classification is based on two parameters that could be easily measured in the 1950s in a commercial environment with a minimum of instrumentation: the rheological parameter called the *melt index*, which reflects the average molecular weight of the resin, and the *resin density* (the function of its crystallinity degree). The physical meaning of these two seemingly simple parameters is in reality quite complex. They are described in Chapters 2 and 4, respectively.

According to the American Society of Testing and Materials (ASTM D1248-05 and ASTM-D3350), all polyethylene materials are divided into various classifications. These classifications specify resins with uniform sets of properties. Density determines the type of the resin and the melt index determines its category. The commonly used commercial classification is given in Table 1.1.

**Table 1.1** Commercial Classification of Polyethylene Resins

		$\alpha$ -Olefin content, mol %	Crystallinity degree, %	Density, g/cm <sup>3</sup>
Resins of high density	HDPE	0 to <0.5	65 to 60	0.960 to 0.941
Resins of ultrahigh molecular weight	UHMW HDPE			0.935 to 0.930
Resins of medium density	MDPE	1 to 2	55 to 45	0.940 to 0.926
Resins of low density	LLDPE	2.5 to 3.5	45 to 30	0.925 to 0.915
Resins of very low density	VLDPPE	>4	<25	<0.915
Low density polyethylene, produced in high-pressure processes	LDPE	0	45 to 55	0.910 to 0.940

HDPE resins with nominal density of 0.941 to 0.959 g/cm<sup>3</sup> belong to Type III and those with nominal density higher than 0.960 belong to Type IV. Although they formally belong to Type II resins, some high molecular weight resins with density

lower than  $0.941 \text{ g/cm}^3$  and the resins with an ultrahigh molecular weight with density of  $\sim 0.930 \text{ g/cm}^3$  are also represented as HDPE resins because of their low branching degree.

The content of an  $\alpha$ -olefin in commercially manufactured ethylene/ $\alpha$ -olefin copolymers varies in a wide range, from  $<0.5$  up to 20 mol %. These copolymers, depending on the content of  $\alpha$ -olefin, are called *medium density polyethylene resins* (MDPE), *linear low density polyethylene resins* (LLDPE), or *very low density polyethylene resins* (VLDPE). The group of the VLDPE resins is further divided into two subgroups, polyethylene *plastomers* with the crystallinity degree of 10 to 20% and densities from  $0.915$  to  $0.900 \text{ g/cm}^3$  and completely amorphous ethylene *elastomers* with densities as low as  $0.86 \text{ g/cm}^3$ . By definition, all these resins contain only short-chain branches derived from the  $\alpha$ -olefins. However, polymerization reactions utilizing some metallocene catalysts and chromium oxide catalysts can also introduce long-chain branches in the polyethylene chains (Section 1.4).

Some metallocene catalysts can also copolymerize ethylene with cycloolefins, such as cyclopentene, cyclooctene, or norbornene. In this case, the branches in polyethylene chains are either small cycles containing from 5 to 10 carbon atoms, or two fused cycles. These materials form an additional resin type called *cycloolefin copolymers* (COC).

The five categories of polyethylene resins are specified according to their melt index measured according to ASTM D1238-10:

Category	1	2	3	4	5
Melt index, g/10 min	>25	10 to 25	1 to 10	0.4 to 1.0	below 0.4

Other characteristics of polyethylene resins, predominantly color, are specified by class. The three classes of polyethylene resins are designated as A, B, and C. The classes indicate color, amounts, and types of antioxidants, and other additives. Class A refers to naturally colored polyethylene resins, Class B includes white and black-colored resins, and Class C covers weather-resistant black resins containing more than 2% carbon black.

The classification of polyethylene resins in its present form affords a basic distinction between different resin types. However, the classification is often poorly suited to delineate fine differences between structures and properties of various resins that play an important role in the modern sophisticated resin market. After all, the market grades different resins mostly according to their end-use properties rather than by their general classification.

Taken together, polyethylene resins account for the largest fraction of the worldwide plastic production. The volume of HDPE resins manufactured in 2010 was close to  $40 \cdot 10^6$  metric tons and that of LLDPE  $27 \cdot 10^6$  metric tons. Applications of

polyethylene resins vary greatly by the grade. The applications of the two most important grades are:

HDPE resins	Blow molding (containers and bottles)	~ 31 %
	Film (biaxially oriented)	~ 28 %
	Injection molding	~ 22 %
	Other applications	~ 19 %
LLDPE resins	Film (blown and cast)	~ 80 %
	Injection molding	~ 7 %
	Wire and cable coating/insulation	~ 4 %
	Other applications	~ 9 %

## ■ 1.2 Catalysts for Synthesis of Polyethylene Resins

Commercial synthesis of most polyethylene resins is carried out with transition metal catalysts of different types [1–3]. Several groups of such catalysts are especially important.

*Supported titanium-based Ziegler-Natta catalysts* All these catalysts consist of two components. The first component called the *catalyst*, is a solid powder that contains a derivative of titanium. The second component is the *cocatalyst*. The cocatalyst is an organoaluminum compound, usually triethylaluminum. A variety of techniques were developed for supporting titanium compounds, mostly titanium tetrachloride, on such supports as silica and microcrystalline magnesium dichloride [1, 3]. Ziegler-Natta catalysts are used to synthesize several grades of HDPE and LLDPE resins. In industry, polyethylene resins are produced with these catalysts at temperatures between 80 and 95 °C and at ethylene partial pressures of 0.7 to 1.5 MPa (100 to 200 psi). All these resins intrinsically have a very high molecular weight (see Section 1.4) and in order to decrease it, ethylene polymerization reactions with Ziegler-Natta catalysts are nearly always carried out in the presence of hydrogen, which serves as a chain-length control agent. In addition to polyethylene resins, Ziegler-Natta catalysts are also used for the commercial production of other important polyolefins including isotactic polypropylene, polybutene, and polymethylpentene, as well as synthetic rubbers based on polybutadiene and polyisoprene.

Several types of titanium-based Ziegler-Natta catalysts are used for the manufacture of special grades of polyethylene called *bimodal polyethylene resins* (see Section 1.6). These resins are ~ 1 : 1 mixtures of two finely intermixed fractions, one

with a very high molecular weight and another with a very low molecular weight. The mixtures are produced in two reactors connected in a series. The fraction with a very low molecular weight (~ 10,000 to 20,000), is produced first in the presence of a large amount of hydrogen, and then the second component with a very high molecular weight (~ 400,000 to 600,000) is produced with a very low amount of hydrogen. The telltale signature of these polymers is their molecular weight distribution curves which consist of two clearly identifiable broad components (Section 1.6). The main requirements for the catalysts employed in these polymerization reactions are very high activity and an easy control of molecular weight.

A special type of titanium-based catalysts is widely used in industry in solution polymerization processes for the synthesis of ethylene/octene copolymers. These polymerization reactions are performed in heavy hydrocarbons (mixtures of C<sub>8</sub> to C<sub>10</sub> alkanes) at high temperatures of 130 to 200 °C, and at a reactor pressure of 3.5 to 20 MPa (500 to 3,000 psi). Catalysts of very high activity are used in these processes. The catalysts are formed directly in the reactor by combining an organomagnesium compound, such as dibutyl magnesium, with a source of chlorine atoms, such as butyl chloride, to produce a support of finely dispersed magnesium dichloride. The active ingredient in these catalysts is usually also titanium tetrachloride.

*Chromium oxide catalysts (Phillips catalysts)* Chromium oxide catalysts are used for the synthesis of HDPE resins of various grades, particularly for the manufacture of HDPE resins with linear chains and a broad molecular weight distribution. Similar catalysts are also used for the synthesis of ethylene/ $\alpha$ -olefin copolymers. Such resins are usually designated as *low density linear polyethylene* (LDLPE) resins to distinguish them from common LLDPE resins. All chromium oxide catalysts are supported on inert porous substrates, usually on silica.

*Organochromium catalysts* Several commercially important catalysts for the synthesis of injection molding-grade HDPE resins utilize organochromium compounds, such as bis(triphenylsilyl)chromate or bis(cyclopentadienyl)chromium. All these compounds are silica-supported.

*Metallocene catalysts (Kaminsky catalysts)* Metallocene catalysts are mostly used for the synthesis of HDPE and LLDPE resins of high compositional uniformity and a narrow molecular weight distribution. These catalysts are employed either in a soluble form or supported on inert carriers. The catalysts contain two components. The first component is a metallocene complex of zirconium or titanium. The second component, called a *cocatalyst*, is either a special organoaluminum compound, methylalumoxane (usually abbreviated as MAO), or a fluoroboronaromatic compound. Metallocene catalysts are also used to produce crystalline syndiotactic polypropylene and polystyrene, ethylene/propylene elastomers, and engineering ethylene/cycloolefin plastics.

*Bimetallic catalysts* Several HDPE applications require resins with an especially broad, preferably bimodal molecular weight distribution. Such materials cannot be produced simply by physical mixing of pellets of two HDPE resins with vastly different molecular weights. Instead, these resins are either obtained using Ziegler-Natta catalysts in special technological processes employing two or several polymerization reactors in a series or in a single reactor using bimetallic catalysts. The idea behind such catalysts is to combine within each catalyst particle two active ingredients that operate under identical conditions but which produce polymers with vastly different molecular weights.

## ■ 1.3 Industrial Processes for the Manufacture of Polyethylene Resins

Four technological processes are used to manufacture polyethylene resins in catalytic and radical reactions.

*Polymerization in slurry* Polymerization processes in hydrocarbon slurry, usually in light hydrocarbons such as isobutane, hexane, or heptane, were historically the first commercial ethylene polymerization processes. These processes using chromium oxide and Ziegler-Natta catalysts still enjoy high popularity due to their versatility and convenience of operation [2, 4]. The slurry technology accounts for the manufacture of nearly 60% of all polyethylene resins. The slurry reactions afford the production of the full range of polyethylene resins, from low molecular weight waxes to resins with a very high molecular weight. These processes are also used to produce resins of ultrahigh molecular weight.

Several types of slurry processes are used in industry [5, 6]:

1. Loop reactors with a low-boiling diluent circulating at a high speed through a long circular pipe,
2. Continuous stirred-tank reactors with a high-boiling diluents, and
3. “Liquid pool” processes in which the polymerization reaction takes place in a light diluent such as propane or isobutane.

All of these reactors usually operate at 80 to 90 °C and a total pressure of 1 to 3 MPa (150 to 300 psi). The residence time of catalyst particles in the reactors varies from 2 to 3 h.

*Polymerization in the gas phase* Many polymerization catalysts, including both Ziegler-Natta catalysts, chromium oxide catalysts, and supported metallocene catalysts, were adopted for use in the gas phase [2, 7–13]. Gas-phase processes account for over 20% of the world polyethylene capacity. These processes are very eco-

nomical due to the absence of the solvent recovery stage. They are flexible and can accommodate a large variety of supported catalysts capable of polymerization at a relatively low pressure.

A typical gas-phase reactor is a tall cylindrical tower with a diameter that ranges from 3 to 6 m (10 to 20 ft) and a height-to-diameter ratio of ~6 to 7. The tower is half-filled with a bed of polymer particles. The particles are agitated either by employing the fluidized-bed technique (blowing a stream of ethylene through numerous openings in the reactor's bottom) or with a mechanical stirrer. A fresh catalyst in the form of small spherical particles is continuously added to the polymer bed, and polymer particles are continuously removed from the reactor. During their stay in the reactor (the average residence time is usually 1 to 4 h), the catalyst particles circulate through the polymer bed and gradually increase in size as the polymerization reaction proceeds, but they retain their spherical shape. The fluidized-bed reactors exhibit high versatility with respect to the type of polymerization catalyst they can accommodate.

Several modifications of the gas-phase reactor technology have been developed. In one modification, two gas-phase fluidized bed reactors are connected together. The connection allows the manufacture of bimodal polyethylene resins with a very broad molecular weight distribution [14, 15]. Another reactor scheme uses a combination of two different reactor types: a small slurry loop pre-reactor followed by one or two gas-phase fluidized-bed reactors that accommodate a Ziegler-Natta catalyst [16, 17].

*Polymerization in solution* Two solution polymerization technologies are practiced. Processes of the first type employ heavy solvents, while processes of the second type use molten polyethylene itself as the polymerization medium [6, 18, 19].

Many hydrocarbons dissolve polyethylene at 120 to 150 °C. Because the viscosity of the polyethylene solution rapidly increases with molecular weight, solution polymerization processes are employed primarily for the production of low molecular weight resins. A variety of Ziegler-Natta and metallocene catalysts survive high temperatures for short periods of time and can be used in the solution processes [2]. Reactions in solution are carried out at 150 to 200 °C at a total pressure of ~5 to 10 MPa (720 to 1,500 psi); they are very fast with residence times usually from 5 to 15 minutes. If a heavy solvent is used, these processes require the removal of the solvent from the polymer as the last step.

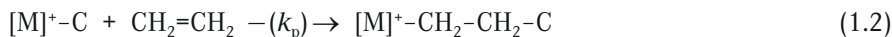
*Radical polymerization reactions* LDPE resins are produced in radical polymerization reactions at a very high pressure. These reactions are carried out either in long tubular reactors with diameters of 2.5 to 6.5 cm (1 to 2.5 in) and the lengths from 500 to 1,000 m (~6,500 to 13,000 ft) or in stirred autoclaves with a volume of ~0.5 m<sup>3</sup>. In both cases, the reactor pressure is very high, from 120 to 300 MPa (18,000 to 45,000 psi), and the temperature ranges from 130 to 350 °C, depending on the resin grade. Under these conditions, ethylene is kept in a supercritical state

and it readily dissolves polyethylene. These polymerization reactions are initiated with oxygen or with organic peroxides. The reactions are very fast; the typical residence time varies from 2 to 10 minutes, which allows the production of up to 20 ton/h of polyethylene in a single reactor.

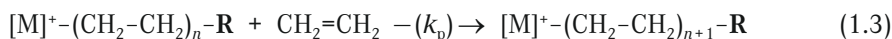
## ■ 1.4 Chemistry of Ethylene Polymerization Reactions

Polymerization reactions of ethylene and copolymerization reactions of ethylene and  $\alpha$ -olefins with all classes of catalysts discussed in Section 1.2 are catalytic in the same sense as other catalytic reactions: a single active center produces many polymer molecules, one after another, over a period of time dictated by the technology, from several minutes in high-temperature solution processes to several hours in gas-phase and slurry processes. The real chemical structure of the active centers is firmly established only for metallocene catalysts. A metallocene complex  $Cp_2ZrCl_2$  (here the  $Cp$  symbol stands for any ligand with the cyclopentadienyl group) reacts with a cocatalyst, MAO, or with trimethylaluminum present in MAO, and is converted to an active center, a metallocenium cation  $Cp_2Zr^+-CH_3$ . The negatively charged counter-ion is positioned within the MAO molecule. The structure of active centers in other polymerization catalysts is not known definitely yet but it is generally assumed that they all contain the  $[M]^+-C$  bond. Here  $M$  is a Ti or a Cr atom and the brackets  $[ ]$  signify that other atoms attached to the  $M$  atom, as well as the nature of the negatively charged counter-ion, are not yet definitely known.

The principal chemical step in any catalytic polymerization reaction of ethylene is the insertion of the double bond of an ethylene molecule into this  $[M]^+-C$  bond:

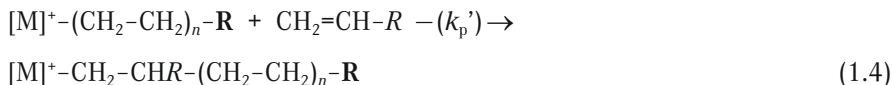


In polymer chemistry, this reaction is called the *chain growth* (or *chain propagation*) reaction. Reaction 1.2 is very fast; thousands of these reactions occur over a period of a few seconds. This repeated insertion reaction constitutes the process of the growth of a single polymer chain. Each such step can be written in a general form as an increase of the polymer chain length while the chain remains attached to the transition metal atom:

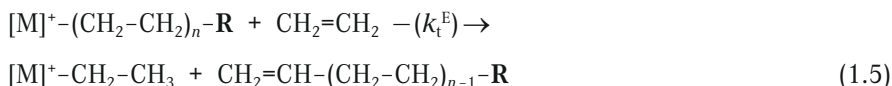


where  $R$  is the starting end-group of a polymer chain, for example, the  $CH_3$  group in the metallocene catalyst.

When an  $\alpha$ -olefin  $CH_2 = CH-R$  is present in the reactor, another chain growth reaction can take place:



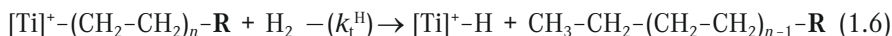
Reactions 1.3 and 1.4 are the principal steps in the formation of ethylene/ $\alpha$ -olefin copolymers. Ethylene is the monomer of the highest reactivity in catalytic polymerization reactions and Reaction 1.4 always proceeds at a lower rate than Reaction 1.3. Very infrequently, an ethylene molecule reacts with the growing polymer chain in a different manner than in Reaction 1.3:



Reaction 1.5 is called the *chain transfer reaction to a monomer* (ethylene in this case). The reaction results in the disengagement of the polymer chain from the active center. Such separated chains are called dead polymer chains to distinguish them from growing polymer chains. The new active center  $[M]^+\text{-CH}_2\text{-CH}_3$  still has the  $[M]^+\text{-C}$  bond and retains the ability to insert ethylene molecules in Reaction 1.2 and grow a new polymer chain.

Reaction 1.5 is the principal chain transfer reaction in ethylene polymerization reactions with chromium oxide and metallocene catalysts. The frequency of Reaction 1.5 strongly depends on temperature: the higher the temperature, the more frequent the reaction is and, as a result, the lower is the polymerization number  $n$  in the dead polymer molecule  $\text{CH}_2=\text{CH-(CH}_2\text{-CH}_2)_{n-1}\text{-R}$ .

When titanium-based Ziegler-Natta catalysts are used for ethylene polymerization, Reaction 1.5 occurs very rarely and the dead polymer chains contain, on average, a very large number of ethylene units; the  $n$  value can range from ten to fifty thousand. Polymers with such a high molecular weight are difficult to process; they have found a commercial use only as components of bimodal resins (Sections 1.6 and 2.5.2). As mentioned in Section 1.2, a special chemical agent, hydrogen, is nearly always added to the ethylene polymerization reactions with Ziegler-Natta catalysts. It hydrogenates the  $[\text{Ti}]^+\text{-C}$  bond in the growing polymer chain:



Reaction 1.6 is called the *chain transfer reaction to hydrogen*. The center with the  $[\text{Ti}]^+\text{-H}$  bond remains active and can also insert the double bond of an ethylene molecule, similarly to Reaction 1.2. Reaction 1.6 proceeds with a much higher rate than Reaction 1.5, and the molecular weight of ethylene polymers produced with Ziegler-Natta catalysts in the presence of hydrogen is always significantly lower.

Commercial ethylene polymerization reactions are always carried out at a constant ethylene partial pressure  $P_E$  and, therefore, at a constant ethylene concentration  $C_E$ . The polymerization rate, the rate of ethylene consumption in Reaction 1.3, is expressed as

$$R_{\text{pol}} = k_p \cdot C^* \cdot C_E \quad (1.7)$$

Here  $C^*$  is the concentration of the active centers  $[M]^+ - C$  in the catalyst. The experimental evaluation of the  $C^*$  value is very difficult [3]; therefore, the product of two values in Eq. 1.7,  $k_p$  and  $C^*$ , which is called the *effective rate constant*  $k_{\text{eff}}$ , is often used as a combined parameter to characterize the catalyst activity. Some polymerization catalysts are stable; their  $C^*$  and  $k_{\text{eff}}$  values do not change over the reaction time. However, the majority of the catalysts are unstable; their  $C^*$  value initially increases rapidly for several minutes and then gradually decreases.

The average molecular weight of a polyethylene chain formed in Reactions 1.3, 1.5, and 1.6 is equal to the ratio between the probability (or the reaction rate) of the chain growth reaction (Reaction 1.3) and the combined probability of two chain transfer reactions, Reactions 1.5 and 1.6:

$$\begin{aligned} MW_{\text{av}} \approx 28 \cdot k_p \cdot C^* \cdot C_E / (k_t^E \cdot C^* \cdot C_E + k_t^H \cdot C^* \cdot C_H) = \\ 28 \cdot k_p \cdot C_E / (k_t^E \cdot C_E + k_t^H \cdot C_H) \end{aligned} \quad (1.8)$$

Here  $C_H$  is the hydrogen concentration;  $k_p$ ,  $k_t^E$ , and  $k_t^H$  are the rate constants of Reactions 1.3, 1.5, and 1.6, respectively; 28 is the molecular weight of an ethylene molecule.

When chromium oxide catalysts or metallocene catalysts are employed, hydrogen is usually not added; thus  $C_H = 0$  and  $MW_{\text{av}} \approx 28 \cdot k_p / k_t^E$ , which means that the average molecular weight of the produced polyethylene does not depend on the ethylene concentration in the reactor. On the other hand, most ethylene polymerization reactions with Ziegler-Natta catalysts are carried out at a significant hydrogen pressure when  $k_t^E \cdot C_E$  is much lower than  $k_t^H \cdot C_H$ . Consequently,  $MW_{\text{av}} \approx 28(k_p/k_t^H)(C_E/C_H)$ ; that is, the average molecular weight of polyethylene resins produced in these reactions depends on the ratio between concentrations of ethylene and hydrogen.

One more chemical reaction is essential for understanding the rheological and mechanical properties of some polyethylene resins. The dead polymer chain formed in Reaction 1.5,  $\text{CH}_2=\text{CH}-(\text{CH}_2-\text{CH}_2)_{n-1}-\mathbf{R}$ , has the same vinyl double bond  $\text{CH}_2=\text{CH}-$  as any  $\alpha$ -olefin molecule  $\text{CH}_2=\text{CH}-\mathbf{R}$  employed in ethylene/ $\alpha$ -olefin copolymerization reactions (synthesis of LLDPE resins). The difference between these two  $\alpha$ -olefin molecules is merely the size of the alkyl group  $R$  attached to the vinyl bond. This alkyl group is small in  $\alpha$ -olefin molecules used in the copolymerization reactions but it can be very large in dead polymer molecules. It has been proven experimentally that when ethylene polymerization reactions are catalyzed by some metallocene or chromium oxide catalysts, such dead polymer molecules containing vinyl double bonds indeed participate in copolymerization reactions with ethylene, in Reaction 1.4 [20–22]. These dead polymer molecules produce long side-groups (long-chain branches) in polyethylene molecules. Although the

long-chain branches are always present in a very low concentration, they greatly affect the rheology of the polymer melt (Section 2.5.3).

## ■ 1.5 Molecular Weight Distribution of Polymers and Methods of its Analysis

A typical active center  $[M]^+-C$  in a polymerization catalyst has the life-span from several minutes (if the polymerization reactions are carried out at a very high temperature) to several hours. During this period, every center produces several thousand polymer molecules. The formation of a single macromolecule containing from two to ten thousand monomer units typically takes from several seconds to a minute.

The length of time each macromolecule grows before disengaging from the active center in Reactions 1.5 or 1.6 is determined by pure statistics; the majority of the dead macromolecules are quite short, but others are very long. The simplest case of the molecular weight distribution describes relative fractions of macromolecules of different length, that is, macromolecules containing different number of ethylene units,  $n$ . It is usually referred to as the Flory-Schulz distribution function [3, 2–26]. This function applies to polymerization processes in which all active centers have the same properties and the same reactivity, when the probability of chain separation from an active center does not depend on the length of the chain,  $n$ , and when the concentrations of all ingredients in the polymerization reaction remain constant during a given polymerization reaction. The last condition is typical for commercial polymerization processes which are usually continuous and when all the concentrations of all the reactants are kept constant and are closely monitored.

The theory of the molecular weight distribution states that if a polymerization reaction produces macromolecules of a high molecular weight, the distribution function of polymer chains,  $F_{\text{number}}(n)$ , is given by the following equation [3, 23–26]:

$$F_{\text{number}}(n) = \mathbf{n}_{\text{av}}^{-1} \cdot \text{Exp}(-n/\mathbf{n}_{\text{av}}) \quad (1.9)$$

Here  $F_{\text{number}}(n)$  is the fraction of polymer chains containing  $n$  monomer units and  $\mathbf{n}_{\text{av}}$  is the average polymerization degree of the produced mixture of polymer chains. In the case of polyethylene resins, a polymer chain containing  $n$  monomer units has the molecular weight  $MW$  of  $28 \cdot n$ , and the number-average molecular weight of the polymer described by the Flory-Schulz equation is  $M_n = 28 \cdot \mathbf{n}_{\text{av}}$ . The Flory-Schulz distribution signifies that a given polymerization reaction is characterized by a single  $\mathbf{n}_{\text{av}}$  value and that the  $\mathbf{n}_{\text{av}}$  value is constant in the course of a given polymerization reaction.

The  $F_{\text{number}}(n)$  function clearly states that the shorter a given polymer chain (the lower the  $n$  value) the higher is the fraction of such chains in the polymer mixture. However, as far as the polymer properties are concerned, the amount that matters is not the fraction of given polymer chains but the relative *weight fraction* of the polymer in these chains. The weight distribution function,  $F_{\text{weight}}(n)$ , represents the normalized weight fraction of polymer chains consisting of  $n$  monomer units:

$$F_{\text{weight}}(n) = n \cdot F_{\text{number}}(n) / \int [n \cdot F_{\text{number}}(n)] \cdot dn = (n/n_{\text{av}}^2) \cdot \text{Exp}(-n/n_{\text{av}}) \quad (1.10)$$

The weight-average polymerization degree  $n_{\text{weight}}$  of such a polymer is equal to  $2 \cdot n_{\text{av}}$ ; the weight-average molecular weight is  $M_w = 56 \cdot n_{\text{av}}$ ; and the width of the molecular weight distribution, which is defined as the  $M_w/M_n = n_{\text{weight}}/n_{\text{av}}$  ratio, is equal to 2.

Figure 1.1 shows an example of the shape of these two functions,  $F_{\text{number}}(n)$  and  $F_{\text{weight}}(n)$ , for a polymer with  $n_{\text{av}} = 1,000$ . The  $F_{\text{number}}(n)$  is an exponentially decreasing function whereas the  $F_{\text{weight}}(n)$  function has a maximum at  $n = n_{\text{av}}$ .

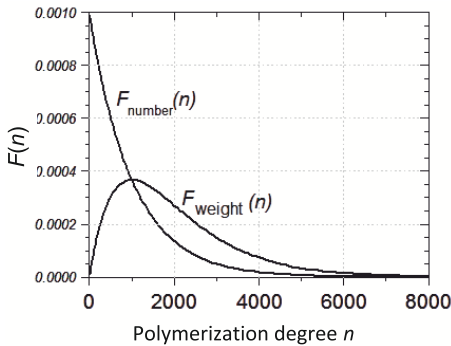


**Figure 1.1** Functions  $F_{\text{number}}(n)$  and  $F_{\text{weight}}(n)$  for polymer with  $n_{\text{av}} = 1,000$

At the present time, gel permeation chromatographic (GPC) method is the universal technique for the measurement of average molecular weights and the molecular weight distribution of polyethylene resins. Another name of this technique is size-exclusion chromatography or SEC [3, 27]. Several instruments for this analysis are commercially produced. To carry out the GPC analysis, a dilute solution of the resin in a good solvent (usually ortho-dichlorobenzene or 1,2,4-trichlorobenzene) passes at a high temperature (110 to 120 °C) through a set of columns filled with a cross-linked polystyrene gel. Due to differences in the diffusion rates of polymer molecules of different sizes through layers of the swelled gel, the average residence time of a particular polymer molecule in the columns is in a reciprocal dependence to its molecular weight: the longest molecules leave the columns rapidly whereas shorter molecules meander through the gel for a significant period of time. The concentration of polymer molecules exiting the last column in a GPC instrument is measured with a highly sensitive detector.

*Flory distribution function in GPC coordinates* A typical GPC curve of a polyethylene resin produced with a single-site metallocene catalyst is shown in Fig. 1.2. The abscissa of this curve is the logarithm of the molecular weight or, in the case of polyethylene resins,  $\log(28 \cdot n)$ .

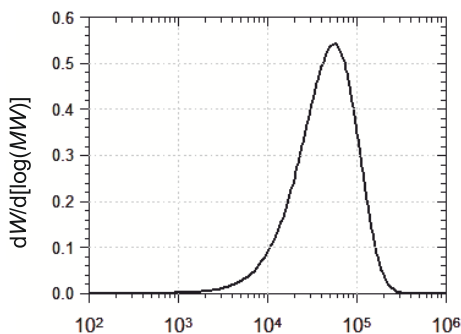


**Figure 1.2** GPC curve of polyethylene resin produced with single-site catalyst

The curve has a relatively sharp maximum and is noticeably asymmetrical. In order to determine the shape of the GPC curve of a polymer with the molecular weight distribution that is theoretically described by Eq. 1.10, one has to take into account a peculiar nature of GPC analysis: a nearly perfect linear correlation exists between the time a given polymer molecule spends in a GPC column and the logarithm of its polymerization degree  $n$ . Employing this relationship, the expression for the Flory weight distribution function,  $F_{\text{weight}}(n)$  from Eq. 1.10, is transformed in the GPC coordinates [3, 28, 29] to

$$\mathbf{n}_{\text{av}}^{-2} \cdot \text{Exp}\{2 \cdot \ln(10) \cdot \log(n) - \mathbf{n}_{\text{av}}^{-1} \cdot \text{Exp}[\ln(10) \cdot \log(n)]\}$$

as a function of  $\log(n)$ ;  $[\ln(10) \approx 2.3]$  (1.11)

Equation 1.11 represents the same weight distribution function as the  $F_{\text{weight}}(n)$  function in Eq. 1.10 and in Fig. 1.1 but with a different abscissa,  $\log(28 \cdot n)$  instead of  $n$ . Figure 1.2 shows the theoretical GPC curve of a Flory-distributed polymer with  $M_w = 56,000$ , which is the polymer with the same distribution as that shown in Fig. 1.1. The calculated plot is also an asymmetric curve with a sharp maximum. Equation 1.11, as well as the  $F_{\text{weight}}(n)$  function in Eq. 1.10, contains only one variable, the number-average polymerization degree  $\mathbf{n}_{\text{av}}$ , and it does not have any adjustable parameters for the width of the GPC peak. The maximum of the Flory function in the GPC coordinates (Eq. 1.11) is positioned at  $\log(n)_{\text{max}} = \log(2 \cdot \mathbf{n}_{\text{av}})$ , that is, at  $n_{\text{max}} = n_{\text{weight}} = 2 \cdot \mathbf{n}_{\text{av}}$  (or at  $MW^{\text{max}} = M_w$ ).

Equation 1.11 can be readily applied to describe the molecular weight distribution of a variety of resins produced in catalytic polymerization reactions under stationary conditions. Several examples in the next section demonstrate that all GPC curves of polyethylene resins, however broad and complex, can be represented in a

satisfactory manner as combinations of several Flory curves in the GPC coordinates, each described by Eq. 1.11.

The overwhelming majority of polyethylene resins are polymer mixtures containing several (j) Flory components with various number-average molecular weights  $M_{n,j}$  and respective average polymerization degrees  $n_j$ . The amount of each component in the mixture is given by its fraction  $FR_j$ . Many examples of such mixtures are described in the next section. The combined distribution function of the mixture of polymer molecules with respect to their polymerization number  $n$  is (similarly to Eq. 1.9) is

$$F_{\text{number}}(n)^{\text{total}} = FR_j \cdot \mathbf{n}_{\text{av},j}^{-1} \cdot \text{Exp}(-n/\mathbf{n}_{\text{av},j}) \quad (1.12)$$

and the combined distribution function of the weight of polymer molecules with respect to their polymerization number  $n$  is (similarly to Eq. 1.10) is

$$F_{\text{weight}}(n)^{\text{total}} = n \cdot \sum FR_j \cdot \mathbf{n}_{\text{av},j}^{-2} \cdot \text{Exp}(-n/\mathbf{n}_{\text{av},j}) \quad (1.13)$$

The number-average molecular weight of such a multi-component mixture,  $M_n^{\text{av}}$ , is

$$M_n^{\text{av}} = [\sum FR_j / M_{n,j}]^{-1} \quad (1.14)$$

The weight-average molecular weight of such a mixture,  $M_w^{\text{av}}$ , is

$$M_w^{\text{av}} = [\sum FR_j \cdot 2 \cdot M_{n,j}]^{-1} \quad (1.15)$$

The width of the molecular weight distribution of the mixture,  $(M_w/M_n)^{\text{av}}$ , is

$$(M_w/M_n)^{\text{av}} = M_w^{\text{av}}/M_n^{\text{av}} \quad (1.16)$$

The most advanced variants of GPC instruments currently on the market employ two detectors and carry out a second analysis of the polymer solution leaving the GPC columns, in addition to measuring the polymer content in the solution. The first technique was developed for the analysis of ethylene/ $\alpha$ -olefin copolymers [30–32]. It measures the composition of eluted copolymer molecules. Another double-detector method is used to analyze the molecular weight distribution of resins containing long-chain branches in LDPE and in some metallocene resins [33]. In this case, the second detector is an online viscometer.

## ■ 1.6 Examples of Molecular Weight Distribution of Polyethylene Resins

Polyethylene resins with the narrowest molecular weight distribution,  $M_w/M_n \sim 2.0$ , can be produced only with soluble, single-site metallocene catalysts and only at a high [MAO]:[metallocene] ratio. One such example is given in Fig. 1.3. It shows

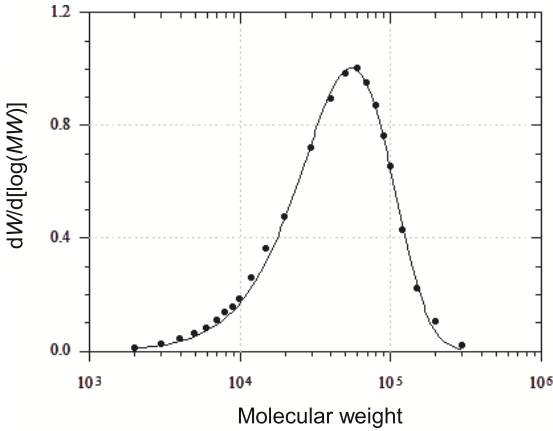


**Figure 1.3** GPC curve of polyethylene resin produced with metallocene catalyst. The line is a single Flory component curve calculated with Eq. 1.11. The data points are for an ethylene/hexene copolymer with  $C_M^{\text{copol}} = 2.0$  mol %

the GPC curve of an LLDPE resin produced with a soluble metallocene catalyst at an [MAO]:[metallocene] ratio of  $\sim 10,000$  (dots) [28]. The solid line represents the GPC curve of a single Flory component calculated with Eq. 1.11.

Resins with such a narrow molecular weight distribution represent a rare exception. Even the resins prepared with soluble metallocene catalysts at low [MAO]:[metallocene] ratios, and all the resins prepared with supported metallocene catalysts always have a noticeably broader molecular weight distribution. As an example, Fig. 1.4 shows the GPC curve of a VLDPE resin (ethylene/hexene copolymer with  $C_M^{\text{copol}} = \sim 17$  mol %) produced with a soluble metallocene catalyst at an [MAO]:[metallocene] ratio of  $\sim 1,000$ . This material consists of two Flory components with molecular weights  $M_w$  of 1,700 and 4,100, respectively, in a  $\sim 0.7:1$  weight ratio [28].

Figure 1.5 shows the GPC curve of an HDPE resin produced with a supported Ziegler-Natta catalyst at  $80^\circ\text{C}$  and its resolution into Flory components. The average molecular weight  $M_w^{\text{av}}$  of the resin calculated with Eq. 1.15 is 133,000 and the width of the molecular weight distribution  $(M_w/M_n)^{\text{av}}$  calculated with Eq. 1.16 is 6.0.

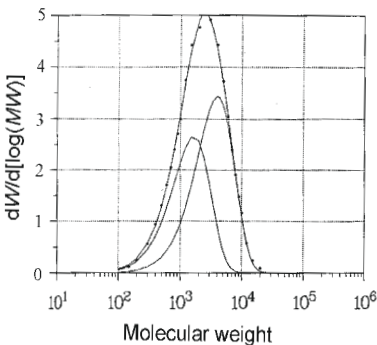


**Figure 1.4** GPC curve of VLDPE resin produced with metallocene catalyst. The lines are individual Flory components. The data points are for an ethylene/hexene copolymer with  $C_M^{\text{copol}} \sim 17$  mol %

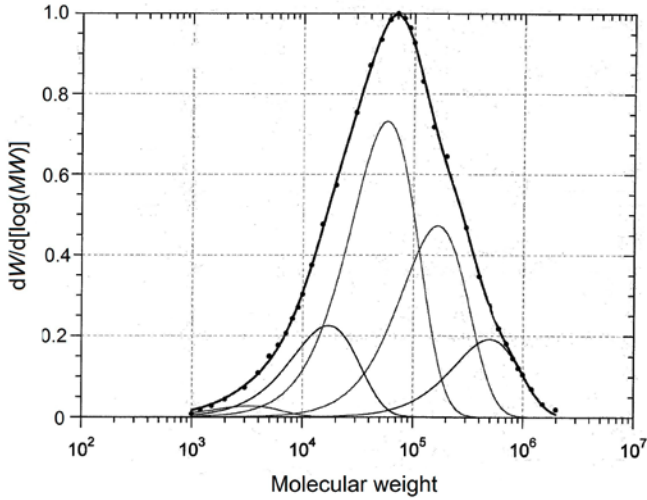


**Figure 1.5** GPC curve of HDPE resin produced with supported Ziegler-Natta catalyst at 80 °C and its resolution into Flory components

Table 1.2 gives parameters of each Flory component in this polymer mixture. The distribution of macromolecules with respect to their molecular weight is quite broad: the highest and the lowest molecular weights of the Flory components differ by a factor of ~100.

**Table 1.2** Flory Components in HDPE Resin Produced with Supported Ziegler-Natta Catalyst

Flory component	$M_w$	Content, %
I	~3,300	~1.5
II	15,700	13.7
III	47,900	44.4
IV	124,400	28.6
V	342,900	11.6

Figure 1.6 shows the GPC curve of an LLDPE resin (ethylene/hexene copolymer with  $C_M^{\text{copol}} = 3.5$  mol %) produced with a supported Ziegler-Natta catalyst at 85 °C and its resolution into Flory components [34]. The average molecular weight  $M_w^{\text{av}}$  of the resin is ~109,000 and the width of the molecular weight distribution ( $M_w/M_n^{\text{av}}$ ) is 4.0.

Table 1.3 gives parameters of each Flory component in the polymer mixture. The distribution of copolymer molecules with respect to their molecular weight is also quite broad, similar to the results for the HDPE resin produced with a similar catalyst.

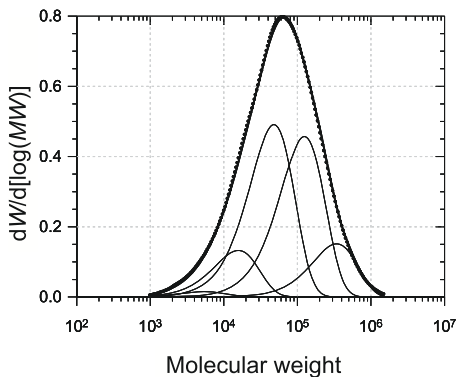


**Figure 1.6** GPC curve of LLDPE resin (ethylene/hexene copolymer with  $C_M^{\text{copol}} = 3.5$  mol %) produced with supported Ziegler-Natta catalyst and its resolution into Flory components

**Table 1.3** Flory Components in LLDPE Resin Produced with Supported Ziegler-Natta Catalyst

Flory component	$M_w$	Content, %	$C_M^{\text{copol}}$ , mol %
I	~5,600	~1	15 to 18
II	15,700	10.6	8 to 10
III	47,900	39.4	~4
IV	124,400	36.6	0.6 to 0.8
V	342,900	12.2	0.3 to 0.4

Figure 1.7 shows the GPC curve of a typical HDPE resin prepared with a chromium oxide catalyst. The molecular weight distribution of such resins is always very broad. Table 1.4 lists molecular weights of all components in an HDPE resin produced at 90 °C.

The range of molecular weights of the components in the mixture is very large, from 2,000 to nearly two million. As a result, the width of the molecular weight distribution, the  $(M_w/M_n)^{\text{av}}$  ratio, is also high, ~12. Obviously, the *average* molecular weight of such a resin,  $M_w^{\text{av}} \sim 227,000$ , is a poor predictor of its physical and mechanical properties.

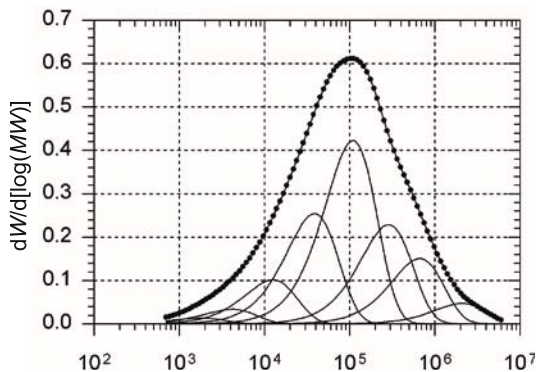


**Figure 1.7** GPC curve of HDPE resin produced with chromium oxide catalyst and its resolution into Flory components

**Table 1.4** Flory Components in HDPE Resin Produced with Chromium Oxide Catalyst

Flory component	$M_w$	Content, %
I	3,200	2.6
II	12,100	9.9
III	38,500	23.5
IV	96,700	25.2
V	228,000	21.2
VI	598,900	14.5
VII	1,848,000	3.1

Figure 1.8 shows the GPC curve of an HDPE resin prepared with a bicomponent metallocene/Ziegler-Natta catalyst and the GPC curves of all the polymer components. The two components with the lowest molecular weights are produced by the metallocene catalyst, which together account for ~40% of the total resin. All the other components are produced by the titanium catalyst.

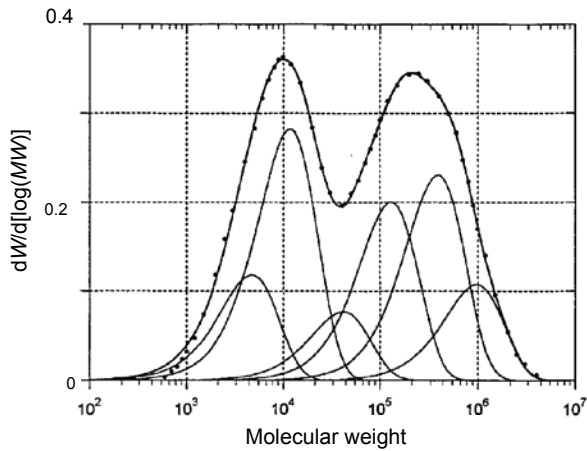
**Figure 1.8** GPC curve of HDPE resin produced with a bicomponent metallocene/Ziegler-Natta catalyst and its resolution into Flory components

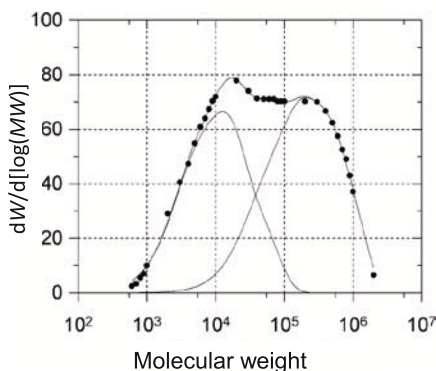
Table 1.5 gives one example of the molecular weight characteristics of both fractions in a pipe-grade HDPE resin prepared with such a bicomponent catalyst. The resin fraction produced with the metallocene catalyst has a very low molecular weight, ~10,000 and mechanical properties that are very poor. The principal function of this fraction in the polymer mixture is to serve as a low-viscosity diluent for the high molecular weight material produced by the Ziegler-Natta catalyst. The latter fraction, if produced separately, forms a very viscous melt but provides the necessary strength for articles manufactured from the bicomponent resins (Chapter 6). As with the example of the HDPE resin produced with a chromium oxide

**Table 1.5** Components of Film-Grade HDPE Resin Produced with Bicomponent Ziegler-Natta/Metallocene Catalyst

Resin	$M_w^{av}$	$(M_w/M_n)^{av}$	Content, %
Total polymer	187,000	20.0	100
Fraction produced with Ziegler-Natta catalyst	275,800	4.7	67.0
Fraction produced with metallocene catalyst	10,200	3.0	33.0

catalyst (Fig. 1.7), the value of the average molecular weight in such complex mixtures does not reflect any end-use properties of the resins.

Finally, Fig. 1.9 shows the GPC curve of another type of a bimodal HDPE resin. This resin was prepared with the use of a single Ziegler-Natta catalyst in two slurry reactors connected in a series. The concentration of the chain transfer agent, hydrogen, was very different in the two reactors, and as a result, the final resin is the mixture of two materials; one with a very high molecular weight and another with a very low molecular weight.

**Figure 1.9** GPC curve of bimodal HDPE resin produced with supported Ziegler-Natta catalyst in two slurry reactors connected in series

Parameters of the total resin and its two components are listed in Table 1.6. The GPC curve of this resin can be viewed as an overlap of two nearly identical combinations of four Flory components shifted by a factor of  $\sim 19$  in terms of their average molecular weights.

**Table 1.6** Components of Film-Grade HDPE Resin Produced with Ziegler-Natta Catalyst in Two-Reactor Process

Resin	$M_w^{av}$	$(M_w/M_n)^{av}$	Content, %
Total polymer	248,400	26.4	100
Low-MW fraction	17,800	3.9	55.0
High-MW fraction	343,500	3.9	45.0

## ■ 1.7 Copolymer Statistics and its Application to Description of LLDPE and VLDPE Resins

All commercially produced LLDPE and VLDPE resins are copolymers of ethylene with  $\alpha$ -olefins, butene, hexene, octene, or methylpentene. They differ by the amount of the  $\alpha$ -olefin (Table 1.1), but this amount is always relatively low. For example, all LLDPE resins, whatever their manufacturer, the catalyst employed or the reactor process involved, contain between 2.5 and 3.5 mol % of  $\alpha$ -olefin.

Any copolymer macromolecule containing ethylene monomer units,  $-\text{CH}_2-\text{CH}_2-$ , and the monomer units of an  $\alpha$ -olefin,  $-\text{CH}_2-\text{CHR}-$ , can be viewed as consisting of sets of monomer blocks (monomer sequences):

Blocks of  $n$  ethylene units,  $-\text{CH}_2-\text{CHR}-(\text{CH}_2-\text{CH}_2)_n-\text{CH}_2-\text{CHR}-$  or  $\text{M}-(\text{E})_n-\text{M}$ ,

Blocks of  $m$   $\alpha$ -olefin units,  $-\text{CH}_2-\text{CH}_2-(\text{CH}_2-\text{CHR})_m-\text{CH}_2-\text{CH}_2-$  or  $\text{E}-(\text{M})_m-\text{E}$ .

By definition, each block is flanked by two monomer units of the opposite kind: the ethylene blocks are  $\text{M}-(\text{E})_n-\text{M}$  and the  $\alpha$ -olefin blocks are  $\text{E}-(\text{M})_m-\text{E}$ . The number of monomer units in the blocks,  $n$  or  $m$ , can vary starting from one (isolated monomer units, sequences  $\text{M}-\text{E}-\text{M}$  or  $\text{E}-\text{M}-\text{E}$ ) to any large number.

Because the content of  $\alpha$ -olefin in LLDPE resins is low, the blocks of  $\alpha$ -olefin units are all short; most  $m$  values are either 1 or, rarely, 2 or 3. The crystallinity level of all these materials and the value of their melting point are entirely determined by the presence of relatively long ethylene sequences. The ethylene/ $\alpha$ -olefin copolymers are random, that is, the ethylene and the  $\alpha$ -olefin units are positioned along the copolymer chain in a strictly statistical manner. Statistical expressions for calculating the contents of ethylene units in blocks  $\text{M}-(\text{E})_n-\text{M}$  with different  $n$  values are well known [2, 3]. The principal parameter is the molar percent of  $\alpha$ -olefin in the copolymer  $C_{\text{M}}^{\text{copol}}$ . The higher the  $C_{\text{M}}^{\text{copol}}$  value the shorter (on average) are the ethylene blocks and the lower is the fraction of ethylene units in the long blocks.

Two statistical functions are usually used to describe ethylene blocks in random copolymers [2, 3, 35]:

- I) The fraction of ethylene units in blocks containing  $n$  units [blocks  $\text{M}-(\text{E})_n-\text{M}$ ] normalized to the total molar content of ethylene in the copolymer  $(1 - C_{\text{M}}^{\text{copol}}/100)$ :

$$\delta(\text{E})_n = n \cdot (C_{\text{M}}^{\text{copol}}/100)^2 \cdot [1 - (C_{\text{M}}^{\text{copol}}/100)]^{n-1} \quad (1.17)$$

- II) The fraction of ethylene units in the sum of all long ethylene blocks starting with the block containing  $n$  units; that is, the fraction of ethylene units in the sum of blocks  $M-(E)_n-M$ ,  $M-(E)_{n+1}-M$ ,  $M-(E)_{n+2}-M$ , and so on, also normalized to the total molar content of ethylene in the copolymer. This is expressed as

$$\Sigma(E)_n = [(C_M^{\text{copol}}/100) \cdot (n - 1) + 1] \cdot \{[1 - (C_M^{\text{copol}}/100)]\}^{n-1} \quad (1.18)$$

Two examples of the  $\delta(E)_n$  function are shown in Fig. 1.10. One example is for the copolymer with  $C_M^{\text{copol}} = 3$  mol %, which is a typical composition of an LLDPE resin. Another example is for a copolymer with  $C_M^{\text{copol}} = 8$  mol %, a typical composition of an ethylene plastomer. It is obvious that most ethylene units in both resins are positioned in long sequences, a fact that accounts for their polyethylene-type crystallinity. The distribution of ethylene units strongly depends on the copolymer composition: the lower the  $C_M^{\text{copol}}$  value, the higher is the fraction of ethylene units in long (crystallizable) blocks. In the case of the copolymer with  $C_M^{\text{copol}} = 3$  mol %, the largest fraction of ethylene units is in blocks ranging from  $M-(E)_{30}-M$  to  $M-(E)_{35}-M$ , whereas in the case of the copolymer with  $C_M^{\text{copol}} = 8$  mol % the most abundant blocks are shorter, from  $M-(E)_{12}-M$  to  $M-(E)_{14}-M$ .

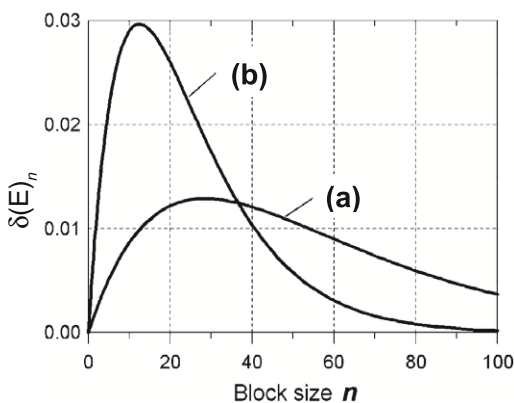


**Figure 1.10** Distribution of ethylene units in blocks of different size in ethylene/ $\alpha$ -olefin copolymers. (a) LLDPE resin with  $C_M^{\text{copol}} = 3$  mol %, (b) VLDPE resin with  $C_M^{\text{copol}} = 8$  mol %

The degree of crystallinity of ethylene/ $\alpha$ -olefin copolymers is usually measured by the X-ray method or by the differential scanning calorimetry method. The degree of crystallinity can be approximately estimated by assuming that crystallinity is a function of the fraction of ethylene units in the sum of sufficiently long ethylene blocks, Eq. 1.18; see Section 4.1 in Chapter 4.

## ■ 1.8 Compositional Uniformity of Commercial Polyethylene Resins

The term *compositional uniformity* is used here to describe differences in the composition of different copolymer molecules in polyethylene resins of LLDPE and VLDPE grades. Some polyethylene resins are compositionally uniform. Any copolymer molecule in such resins, taken at random, contains about the same fraction of  $\alpha$ -olefin units,  $C_M^{\text{copol}}$  (the same amount of branches), as any other copolymer molecule. The majority of LLDPE and VLDPE resins produced with metallocene catalysts belong to this category. In contrast, all LLDPE and VLDPE resins produced with supported Ziegler-Natta catalysts and with chromium oxide catalysts are mixtures of copolymer molecules with very different contents of  $\alpha$ -olefins. Some macromolecules in these mixtures contain a very small fraction of  $\alpha$ -olefin units, while other copolymer molecules contain a relatively large number of the units.

At the present time, two complimentary automated fractionation techniques exist: analytical temperature-rising elution fractionation (TREF) [36–41] and crystallization fractionation (CRYSTAF) [42–48]. Both techniques provide the basis of most detailed investigations of composition uniformity in LLDPE and VLDPE resins that are produced with multi-site Ziegler-Natta and chromium oxide catalysts. Both techniques exploit the same principle that copolymer molecules of a different composition crystallize from solution at different temperatures. The first step in both methods is dissolution of a small resin sample in a suitable solvent at a high temperature. The two most often used solvents are ortho-dichlorobenzene and 1,2,4-trichlorobenzene. The dissolution temperature is 130 to 140 °C. The hot, well-mixed solution is slowly cooled, at a rate of several degrees/h, resulting in slow crystallization of the polymer. In the CRYSTAF method, the concentration of the polymer remaining in solution is monitored with an infrared detector as a function of temperature. In the TREF method, the polymer is completely crystallized on some inert inorganic carrier, then slowly redissolved in a fresh solvent at a gradually increasing temperature. The concentration of the dissolved polymer is monitored as a function of temperature. Fully automated TREF and CRYSTAF instruments are commercially available that afford a very thorough resolution of copolymer mixtures into compositionally uniform fractions [42, 43]. Special curve-resolution techniques have been developed to identify individual compositionally uniform components in complex TREF and CRYSTAF curves [39, 48].

Figure 1.11 gives one example of the resolving ability of these techniques and the results of the computer simulation of complex multi-peak curves. The figure shows the CRYSTAF curve of a 1 : 1 mixture of two compositionally uniform LLDPE resins (ethylene/butene copolymers) with different comonomer contents (6 and 17 mol %) and its computer resolution into two individual components [48].

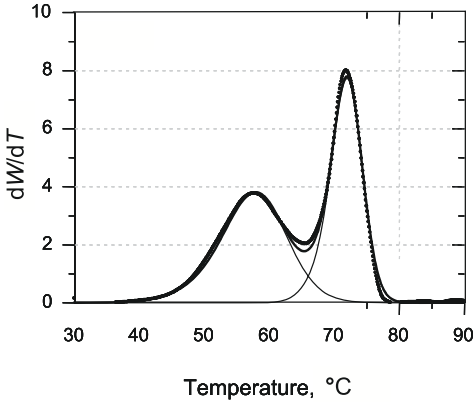


**Figure 1.11** CRYSTAF curve of a mixture of two compositionally uniform LLDPE resins with different comonomer contents and its computer resolution into components

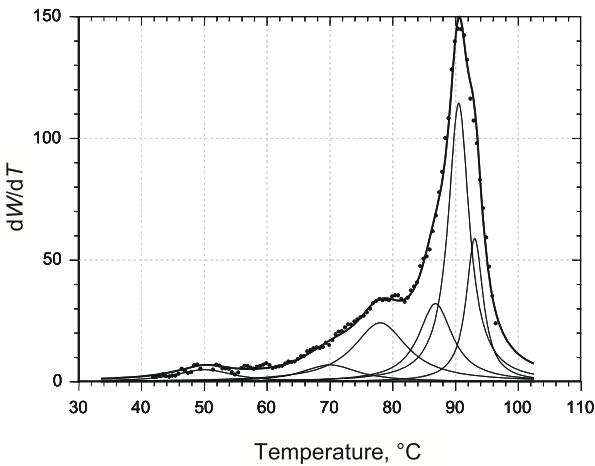


**Figure 1.12** TREF curve of LLDPE resin (ethylene/butene copolymer with  $C_{M}^{\text{copol}} = 2.8$  mol %) produced with supported Ziegler-Natta catalyst and its resolution into compositionally uniform components

Other examples of curve-resolution methods are shown in Figs. 1.12 and 1.13, Figure 1.12 shows the TREF curve of an LLDPE resin, which is an ethylene/butene copolymer with  $C_{M}^{\text{copol}} = 2.8$  mol %, produced with a supported Ziegler-Natta catalyst at 80 °C, and the curve's resolution into compositionally uniform fractions [39]. Parameters of these fractions are given in Table 1.7.

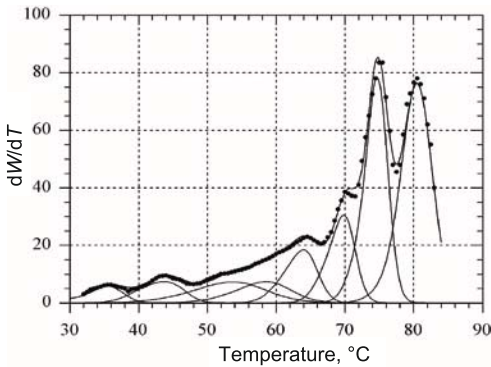
**Table 1.7** Compositionally Uniform Components in LLDPE Resin (Ethylene/Butene Copolymer with  $C_{M}^{\text{copol}} = 2.8$  mol %) Produced with Supported Ziegler-Natta Catalyst; TREF analysis

Fraction:	A	B	C	D	E	F
$T_{\text{cryst}}$ , °C:	93.1	90.5	86.8	78.0	70.0	50.0
$C_{M}^{\text{copol}}$ , mol %:	~0.3	0.8	1.5	3.1	4.6	8.6
Content, %:	15.5	37.0	16.9	20.3	6.0	4.4

The data in the table show that this resin is a mixture of macromolecules with a different butene content ranging from components with very low  $C_M^{\text{copol}}$  (Fractions A and B) to components with very high  $C_M^{\text{copol}}$  (Fraction F). The latter material has a very low crystallinity degree; it is easily dissolved in such solvents as hexane or heptane. Some manufacturers measure the amount of this component by extracting it with a light solvent (usually hexane) and report it as *soluble material* or *extractable material*.

Chromium oxide catalysts are widely used for the synthesis of HDPE resins. They are also suitable for the manufacture of ethylene/ $\alpha$ -olefin copolymers (LDLPE resins). Table 1.4 shows that these catalysts contain many different types of active centers and produce polymer mixtures with a broad molecular weight distribution. When these catalysts are employed for the synthesis of LDLPE resins, different centers produce copolymer fractions of different composition.

For example, an HDPE resin (ethylene homopolymer) produced with a chromium oxide catalyst contains only linear polymer chains, it melts in a narrow temperature range, 134.3 to 135 °C, and it has a crystallinity degree of ~70%. The CRYSTAF curve of such a resin contains a single narrow crystallization peak with the maximum at ~84 °C. Figure 1.13 shows the CRYSTAF curve of a VLDLPE resin, an ethylene/hexene copolymer with  $C_M^{\text{copol}} = 4.7$  mol %, produced with the same chromium oxide catalyst at 90 °C and its resolution into compositionally uniform components [49]. This resin has a quite broad compositional distribution. It contains several crystallization peaks at temperatures ranging from 80.6 to 36 °C.



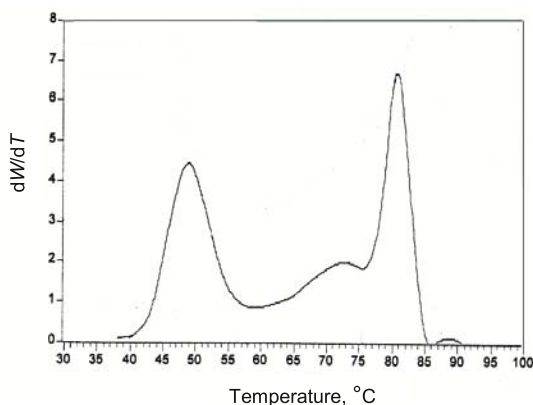
**Figure 1.13** CRYSTAF curve of LLDPE resin (ethylene/hexene copolymer with  $C_M^{\text{copol}} = 4.7$  mol %) produced with chromium oxide catalyst at 90 °C and its resolution into compositionally uniform components.

Table 1.8 lists the compositions and the contents of eight individual fractions in this resin. Their  $C_M^{\text{copol}}$  values vary from ~0.7 mol % for the fraction crystallizing at the highest temperature (Component A) to > 6 mol % for the fraction crystallizing at the lowest temperature. In addition, the resin contains 12.5% of a completely amorphous material with an even higher  $C_M^{\text{copol}}$  value.

**Table 1.8** Components of VLDPE Resin (Ethylene/Hexene Copolymer with  $C_M^{\text{copol}} = 4.7$  mol %) Produced with Chromium Oxide Catalyst; CRYSTAF analysis

Component:	A	B	C	D	E	F	G	H
$T_{\text{cryst}}$ , °C:	80.6	74.9	70.2	64.6	59.4	54.7	~45	~36
$C_M^{\text{copol}}$ , mol %:	~0.7	1.3	1.8	2.5	3.1	3.6	~5	~6.5
Content, %:	29.7	22.7	10.0	7.4	4.9	6.5	~4	~2.5

Figures 1.12 and 1.13 give examples of compositional nonuniformity in LLDPE resins that develops naturally as a result of the presence of several types of active centers with different copolymerization ability in the same catalyst. LLDPE resins with strongly expressed compositional nonuniformity can also be produced artificially by blending different LLDPE resins. From the resin-processing viewpoint, such blending is very difficult to achieve if one attempts to physically mix comparable amounts of two LLDPE resins with different properties. However, the mixing is significantly simplified if both resins are manufactured as solutions in a heavy hydrocarbon solvent (see Section 1.3).



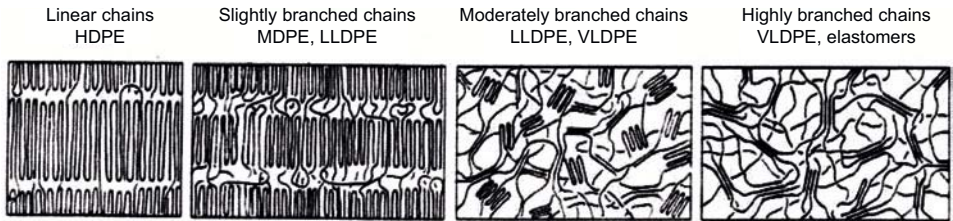
**Figure 1.14** CRYSTAF curve of blend of two LLDPE resins (ethylene/octene copolymers). One resin produced with Ziegler-Natta catalyst and another with metallocene catalyst

Figure 1.14 shows the CRYSTAF curve of a commercially manufactured blend of two ethylene/octene LLDPE resins. The first resin is produced with a Ziegler-Natta catalyst designed for the use in such solution processes (Section 1.2). As with all the other LLDPE resins produced with catalysts of this type, this resin is, by itself, compositionally nonuniform. It contains a copolymer component with a low octene content of ~0.5 mol % (its crystallization peak is at 81°C), two components with higher octene contents of ~1.5 and 2.5 mol % (the broad crystallization area between 75 and 60°C), and an amorphous component with a high  $C_M^{\text{copol}}$  value, which does not crystallize. Overall, this material is similar in terms of its composition distribution to the ethylene/butene copolymer produced with another Ziegler-

Natta catalyst, which has a CRYSTAF curve shown in Fig. 1.12. The second resin in the LLDPE blend in Fig. 1.14 is produced with a modified single-site metallocene catalyst. It is compositionally uniform and its crystallization temperature is 49.1 °C. The two resins have similar average molecular weights; they are blended in a 1.5:1 ratio. These blends exhibit superior mechanical properties and a very good sealing performance in packaging applications.

## ■ 1.9 Morphology of Polyethylene Resins

All polyethylene resins, with the exception of some VLDPE resins with very high  $\alpha$ -olefin content, are semicrystalline plastics. The structure of crystalline regions in the resins depends on the level of branching in polyethylene macromolecules. Figure 1.15 shows four principal smallest morphological features in polyethylene resins of different types. A clear separation of these structural elements is possible only in the case of compositionally uniform LLDPE resins in which all the macromolecules have the same composition.



**Figure 1.15** Morphological features in polyethylene resins of different types

The length of a typical HDPE molecule with the molecular weight of 200,000 is about 1,800 nm. When such polymer molecules crystallize, they fold on themselves several times and form the structural element called a *lamella*. The folds form amorphous regions in HDPE resins. Each lamella has a sandwich structure consisting of the crystalline core of folded chains and two amorphous regions adjacent to the core. X-ray, infrared, and wide-angle neutron scattering analyses show that the nature of the folds depends on crystallization conditions. When an HDPE resin is slowly crystallized from solution, the folding is tight and the chains fold in such a manner that it allows for an adjacent re-entry of the chain into the same lamella. When the same HDPE resin rapidly crystallizes from the melt (which is the typical crystallization condition in industry), the chain folding is much looser and resembles the old-fashioned telephone switchboard, as shown in Fig. 1.16 [50, 51]. In the majority of cases, a macromolecule, after forming a loose fold, still

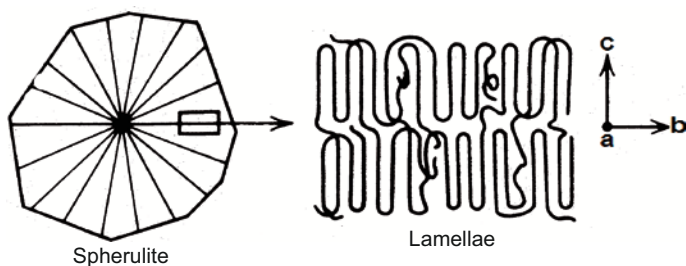


**Figure 1.16** Structure of HDPE spherulite

enters the same lamella. However, some chains (called *tie macromolecules*) after folding may enter neighboring lamellae.

If polyethylene macromolecules are slightly branched (for example, MDPE resins containing from 0.5 to ~1.5 mol % of  $\alpha$ -olefin) and the fraction of long ethylene segments  $-M-E_n-M-$  (it as given by Eq. 1.18) is high, these segments form lamellae of the same type as in HDPE resins. However, the folds are even less tight, the amorphous regions are significantly thicker, and the number of the tie macromolecules is higher. A further increase in the level of branching leads to a continuing decrease in the fraction of long ethylene sequences capable of crystallization, resulting in a large decrease of the lamella thickness (see Chapter 3) and an increase of the volume of the amorphous phase. Finally, VLDPE resins with the  $\alpha$ -olefin content approaching 8 to 10 mol % contain only relatively short ethylene sequences and cannot form lamellae anymore.

It should be taken into account that LLDPE resins produced with Ziegler-Natta catalysts contain copolymer chains with very different contents of  $\alpha$ -olefins, including both the macromolecules with low  $C_M^{\text{copol}}$  values, below 0.5 to 1.0 mol %, and the macromolecules with high  $C_M^{\text{copol}}$  values of above 10% (Section 1.8, Tables 1.7 and 1.8). These macromolecules crystallize separately at different temperatures and form lamellae of different types (see Chapter 3).

The largest morphological unit of all HDPE and MDPE resins crystallized from the melt under typical conditions is a spherulite, a small anisotropic spherical object with a diameter ranging from 1 to 5  $\mu\text{m}$ . The spherulites can be clearly seen in polyethylene film under medium magnification with an optical microscope equipped with a polarizer. Figure 1.17 shows a typical microphotograph of spherulites in film made from an HDPE resin. The spherulites are formed as a result of a complex crystallization process of polyethylene macromolecules. The main structural subunits in the spherulites are thin rod-like fibrils (rays) radiating in all directions from the center to the periphery of the spherulite. The fibrils consist of stacked lamellae; they frequently branch and fill the whole volume of the spherulite, as shown in Fig. 1.17.



**Figure 1.17** Spherulites in HDPE film [52]

The principal crystalline form of polyethylene is orthorhombic [52], the same as in linear paraffins. Parameters of its cell are:  $a = 0.740$  nm,  $b = 0.493$  nm, and  $c$  (the direction of polymer chains) = 0.253 nm. This  $c$  value corresponds to the length of one ethylene unit in the polyethylene chain,  $-\text{CH}_2-\text{CH}_2-$ . The  $c$  axis and the  $a$  axis of the crystals are perpendicular to the fibril axis, and the  $b$  axis, the direction of chain crystallization, is parallel to the fibril direction. The theoretical density of this crystalline form is  $1.0$  g/cm<sup>3</sup>. The presence of short-chain branches leads to a small expansion of the orthorhombic cell; the  $a$  length increases to  $\sim 0.77$  nm and  $b$  to  $\sim 0.5$  nm. This expansion leads to a decrease in crystal density.

The second important crystalline form of polyethylene is pseudomonoclinic [52]. This crystalline modification is always formed when polyethylene is crystallized rapidly and in polyethylene articles subjected to low-temperature working, such as stretching of film. The cell parameters of the pseudomonoclinic form are:  $a = 0.405$  nm,  $b = 0.485$  nm,  $c = 0.254$  nm (the same as in the orthorhombic cell), and angles  $\alpha = \beta = 90^\circ$ ,  $\gamma = 105^\circ$ . The theoretical density is  $0.965$  g/cm<sup>3</sup>. The pseudomonoclinic modification is stable only at temperatures below  $50^\circ\text{C}$  and converts to the orthorhombic modification at higher temperatures.

## ■ 1.10 Mechanical Deformation of Polyethylene Resins

All grades of polyethylene resins, when used above their brittle point (typically, from  $-70$  to  $-80$  °C), are materials with strongly expressed ductile properties and a low fracture toughness. Any forced stretching of a polyethylene sample, film, or rod, is accompanied by a series of structural transformations and mechanical changes. These mechanical changes are traditionally represented by a stress/strain curve.

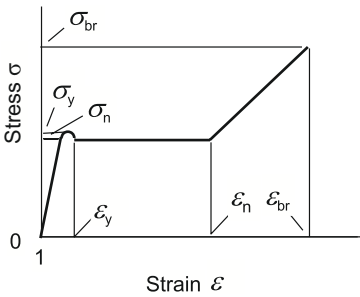


**Figure 1.18** Idealized stress/strain curve of ductile polymer

Figure 1.18 shows the stress/strain curve of a typical semicrystalline polyethylene resin, such as HDPE or LLDPE, and gives definitions of characteristic stresses  $\sigma$  and strains  $\varepsilon$ . The  $\varepsilon$  values in the figure are the ratios of the lengths of the strained and the original sample:  $\varepsilon = \text{elongation} + 1$ ; the minimum  $\varepsilon$  value is 1. The stress/strain curve in Fig. 1.18 is defined by six parameters:

The *yield stress*,  $\sigma_y$ , and the *yield strain*,  $\varepsilon_y$ ,

The *necking stress*,  $\sigma_n$ , and the *end-of-necking strain*,  $\varepsilon_n$ ,

The *breaking (tensile) stress*,  $\sigma_{br}$  and the *breaking strain*,  $\varepsilon_{br}$ .

All the stresses are calculated with respect to the cross section of the original sample. Typical stress values for HDPE resins are  $\sigma_y \approx 2.9$  to  $3.3$  kg/mm<sup>2</sup> (29 to 33 MPa),  $\sigma_y/\sigma_n \approx 1.05$  to 1.1, and  $\sigma_{br} \approx 3$  to  $4$  kg/mm<sup>2</sup> (30 to 40 MPa). The same parameters for LLDPE resins are:  $\sigma_y \approx \sigma_n \approx 0.9$  to  $1.5$  kg/mm<sup>2</sup> (9 to 15 MPa) depending on the resin type,  $\sigma_y/\sigma_n \approx 1.05$  to 1.1, and  $\sigma_{br} \approx$  from 2.0 to 3.0 kg/mm<sup>2</sup> (20 to 30 MPa).

Mechanical changes shown in Fig. 1.18 are accompanied by cardinal and irreversible structural changes in the polymer sample. At deformations below  $\sim 0.5\%$ , spherulites deform elastically. Stiffness of the sample at this stage is characterized by its elastic (Young) modulus  $M_Y \approx \sigma_y/(\varepsilon_y - 1)$ . This parameter is traditionally measured as a tangent to the stress/strain curve at a 1% elongation point (at  $\varepsilon_y - 1 = 0.01$ ) or at a 2% elongation point [ASTM method D5323-92 (2011)] and is

called the *secant modulus*. The stress/strain curve at low elongations is practically a straight line (Fig. 1.18) and the secant modulus (1%) is close to  $M_Y$ .

Further straining of the polymer sample leads to a gradual breaking of bridges between the lamellae, slipping of the lamellae in the fibrils, splitting of the fibrils, and to other structural changes. These processes can be viewed as a succession of partial “melting” of the initial morphological features of the resins, spherulites and fibrils. At the yield point, a neck develops in the sample. The neck is an area consisting of highly oriented bundles of macromolecules. As the stretching proceeds, two of the initial morphological features, the spherulites and fibrils in them, are completely disassembled as the length of the neck increases. As a result, the resin sample continues to elongate at a nearly constant stress  $\sigma_n$  until all the material becomes highly oriented, as shown in Fig. 1.18.

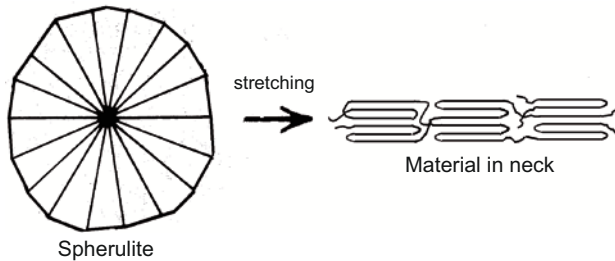


**Figure 1.19** Structural changes in drawn polyethylene resin

After the neck region has extended to the whole length of the stretched sample, the third stage of straining begins, which is called the *strain-hardening* stage. This is the elastic stretching of the completely oriented material, culminating in its breaking at an arbitrary point along the stretched range of the sample. The length of this elastic deformation zone depends on the grade of the resin. HDPE resins break soon after the beginning of the strain-hardening stage and their  $\sigma_y$  and  $\sigma_{br}$  values are relatively close. In contrast, LLDPE resins have a relatively long strain-hardening stage (Fig. 1.18) and their  $\sigma_{br}$  value is always much higher than the  $\sigma_y$  value. These differences are attributed to the mechanism of strain-hardening. Strain-hardening is essentially the straining process of the segments of tie macromolecules holding together highly oriented crystalline lamellae (Fig. 1.18). The number of these tie segments is significantly lower than the total number of polymer segments in the amorphous regions of stretched samples. In essence, the behavior of the tie molecules under strain is described by mechanical features of amorphous elastic polymers [53].

It should be kept in mind that all the  $\sigma$  values in Fig. 1.18 are given with respect to the original cross section of the sample. The real cross section is dramatically reduced at the beginning of the necking stage (by a factor of  $\sim \epsilon_{br}^2$ ) and at the break-

ing point (by a factor of  $\sim \varepsilon_{br}^2$ ); consequently, the real  $\sigma_n$  and  $\sigma_{br}$  values are, respectively, much higher.

Parameters of the stress/strain curve strongly depend on the molecular weight of polyethylene resins. Low molecular weight HDPE resins are brittle and break at a strain of  $<10\%$  without the neck development. HDPE resins with a molecular weight in the range of 80,000 to  $\sim 1,000,000$  always develop the neck. Increasing the molecular weight of such resins is accompanied by a decrease of the  $\varepsilon_{br}$  value from  $\sim 15$  to  $\sim 3$  and by a significant increase of the  $\sigma_{br}$  value from  $\sim 3$  to  $\sim 6$  kg/mm<sup>2</sup> ( $\sim 30$  to 60 MPa). Finally, HDPE resins of ultrahigh molecular weight, over  $1.5$  to  $2 \cdot 10^6$ , do not develop the neck at all and uniformly elongate by 200 to 400%. Such resins can be processed at pressures of 2,000 to 3,000 atm and temperature below 100 °C into film that is very strongly stretched and nearly perfectly oriented, both in the crystalline and in the amorphous phase. This film contains a large fraction of tie macromolecules [54, 55]; it has a very high tensile strength ( $\sigma_{br} = 50$  to 60 kg/mm<sup>2</sup> or 500 to 600 MPa) and a very high modulus, up to  $\sim 1 \cdot 10^4$  kg/mm<sup>2</sup> ( $\sim 1 \cdot 10^5$  MPa).

## ■ References

1. Nowlin, T.E., Mink, R.I., Kissin, Y.V., In *Transition Metal Polymerization Catalysts*. Hohh, R., Mathers, R.T. (Eds.) (2009) John Wiley & Sons, Hoboken, p. 131
2. Krentsel, B.A., Kissin, Y.V., Kleiner, V.I., Stotskaya, S.S., *Polymers and Copolymers of Higher  $\alpha$ -Olefins* (1997) Hanser, Munich, Chapter 8
3. Kissin, Y.V., *Alkene Polymerization Reactions with Transition Metal Catalysts* (2008) Elsevier, Amsterdam, Chapter 4
4. *Metallocene Technology in Commercial Applications*. Benedikt, G.M. (Ed.) (1999) Plastics Design Library, Norwich
5. *Polyolefins Through the 80s – A Time of Change* (1983) SRI International, Menlo Park, CA
6. Choi, K.-Y., Ray, W.H., *J. Macromol. Sci.-Rev. Macromol. Chem., Phys.* (1985) C25, p. 57
7. *Advances in Polyolefins*. Cheng, T.C., Seymour R.B. (Eds.) (1989) Plenum, New York
8. Karol, F.J., Jacobson, F.I., In *Catalytic Polymerization of Olefins*. Keii T., Soga K. (Eds.) (1986) Elsevier, Amsterdam, p. 323
9. Hsieh, J.T.T., Simonsen, J.C., *U.S. Patent* 5 096 868 (1992)
10. Lo, F.Y., Nowlin, T.E., Shirodkar, P.P., *U.S. Patent* 5 032 562 (1991)
11. Miller, A.R., *U.S. Patent* 4 003 712 (1977)
12. Goeke, G.L., Wagner, B.E., Karol, F.J., *U.S. Patent* 4 302 565 (1981)

13. Furtek, A.B., Proceedings from *MetCon'93*, Houston, TX, (1993) p. 125
14. Ali, A.H., Hagerty, R.O., Ong, S.C., *Canadian Patent* 2 078 655 (1993)
15. Yi, K.C.H., Maraschin, N.J., In *Maack'90 International Business Conference*, (1990) Zurich
16. Miller, B., *Plastic World* (1992) p. 46
17. Knuutila, H., Lehtinen, A., Nummila-Pakarinen, A., *Adv. Polym. Sci.* (2004) 169, p. 13
18. Short, J.N., In *Transition Metal Catalyzed Polymerizations: Alkenes and Dienes*. Quirk, R.P. (Ed.) (1983) Harwood Academic Publishers, New York, p. 651
19. Hamilton, M.A., Zboril, V.G., U.S. Patent 4 547 473 (1985)
20. Lai, S.Y., Wilson, J.R., Knight, G.W., Stevens, J.C., Chum, P.S., *U.S. Patents* 5 272 236 (1993) and 5 278 272 (1994)
21. McKnight, A.L., Waymouth, R.M., *Macromolecules* (1999) 32, p. 2816
22. Shapiro, P.J., Bunel, E.E., Schaefer, W.P., Bercaw, J.E., *Organometallics* (1990) 9, p. 867
23. Flory, P.J., *Principles of Polymer Chemistry* (1953) Cornell University Press, Ithaca
24. Schulz, G.V., *Z. Phys. Chem., B* (1939) 43, p. 25
25. Bamford, C.H., In *Encyclopedia of Polymer Science and Engineering*. Mark, H.F., Bikales, N.M., Overberger, C.G., Manges, G. (Eds.) (1986) John Wiley & Sons, New York, Vol. 13, p. 845
26. Peebles, L.H., *Molecular Weight Distributions in Polymers* (1971) Wiley-Interscience, New York
27. You, W., Kirkland, J., Bly, D., *Modern Size-Exclusion Liquid Chromatography* (1979) John Wiley & Sons, New York, Chapter 3
28. Kissin, Y.V., *J. Polym. Sci., Part A: Polym. Chem.* (1995) 33, p. 227
29. Soares, J.B.P., Hamielec, A.E., *Polymer* (1995) 36, p. 2257
30. Faldi, A., Soares, J.B.P., *Polymer* (2001) 42, p. 3057
31. Ver Strate, G., Cozewith, C., West, R.K., Davis, W.M., Capone, G.A., *Macromolecules* (1999) 32, p. 3837
32. Luruli, N., Grumel, V., Brüll, R., Du Toit, A., Pasch, H., Van Reenen, A.J., Raubenheimer, H.G., *J. Polym. Sci., Part A: Polym. Chem.* (2004) 42, p. 5121
33. Thorshaug, K., Mendici, R., Boggioni, L., Tritto, I., Trinkle, S., Friedrich, C., Mülhaupt, R., *Macromolecules* (2002) 35, p. 2903
34. Kissin, Y.V., Mink, R.I., *J. Polym. Sci., Part A: Polym. Chem.* (2010) 48, p. 4219
35. Kissin, Y.V., *Adv. Polym. Sci.* (1974) 15, p. 91
36. Soares, J.B.P., Hamielec, A.E., *Polymer* (1995) 36, p. 1639
37. Mingozzi, I., Cecchin, G., Morini, G., *Int. J. Polym. Anal. & Charact.* (1997) 3, p. 293
38. Mirabella, F.M., *J. Polym. Sci. Part B: Polym. Phys.* (2001) 39, pp. 2800, 2819
39. Kissin, Y.V., Mirabella, F.M., Meverden, C.C., *J. Polym. Sci., Part A: Polym. Chem.* (2005) 43, p. 4351
40. Wild, L., *Adv. Polym. Sci.* (1991) 98, p. 1

41. Kakugo, M., Miyatake, T., Naito, Y., Mizunuma, K., In *Transition Metal Catalyzed Polymerizations. Ziegler-Natta and Metathesis Polymerization*. Quirk, R.P. (Ed.) (1989) Cambridge University Press, New York, p. 624
42. Monrabal, B., *J. Appl. Polym. Sci.* (1994) 52, p. 491
43. Soares, J.B.P., Monrabal, B., *Macromol. Chem. Phys.* (1998) p. 1917
44. Soares, J.B.P., Hamiliec, A.E., *Macromol. Theory Simul.* (1995) 4, p. 305
45. Monrabal, B., *Makromol. Chem., Macromol. Symp.* (1996) 110, p. 81
46. Britto, L.J.D., Soares, J.B.P., Penlidis, A., *J. Polym. Sci. Part B: Polym. Phys.* (1999) 37, p. 539
47. Chu, K.J., Soares, J.B.P., Penlidis, A., *Macromol. Chem. Phys.* (2000) 201, p. 340
48. Kissin, Y.V., Fruitwala, H.A., *J. Appl. Polym. Sci.* (2007) 106, p. 3872
49. Kissin, Y.V., Brandolini, A.J., Garlick, J.L., *J. Polym. Sci., Part A: Polym. Chem.* (2008) 46, p. 5315
50. Stamm, M., *J. Polym. Sci., Part B: Polym. Phys.* (1982) 20, p. 235
51. Wignall, G.D., Mandelkern, L., Edwards, C., Glotin, M., *J. Polym. Sci., Part B: Polym. Phys.* (1982) 20, p. 245
52. Miller, R.L., In *Crystalline Olefin Polymers, Part 1*. Ruff, R.A.V., Doak, K.W. (Eds.) (1965) Interscience, New York, p. 577
53. Ward, I.M., *Mechanical Properties of Solid Polymers*, 2<sup>nd</sup> edition (1983) John Wiley & Sons, New York, Chapter 3
54. Ward, I.M., *Polym. Eng. Sci.* (1984) 24, p. 724
55. Zachariades, A.E., Porter, R.S., *J. Macromol. Sci., Part B: Phys.* (1981) 19, p. 377

## 2

# Melt Index and Melt Flow Ratio of Polyethylene Resin

## 2.1 Introduction

The melt index of a polyethylene resin is universally accepted in industry as the indicator of its weight-average molecular weight. Melt indexes are measured using an instrument called an *extrusion plastometer*. The measurement procedures are specified in the American Society for Testing and Materials (ASTM) method D1238-10, Conditions E and F, and in the International Organization for Standardization (ISO) 1133. Figure 2.1(a) shows the schematics of the melt flow measurement. A small amount of resin ( $\sim 6$  g) is placed in a heated cylindrical barrel with a round capillary opening at its bottom, 2.095 mm in diameter and 8 mm in length. The resin is kept at  $190^\circ\text{C}$  for 6 minutes to achieve its complete melting. After that, the melt is pressurized by loading a metal weight on the stem at the top of the plunger inserted into the barrel. The pressure of the plunger forces the melt through the capillary opening. By definition, the melt index is the weight of poly-

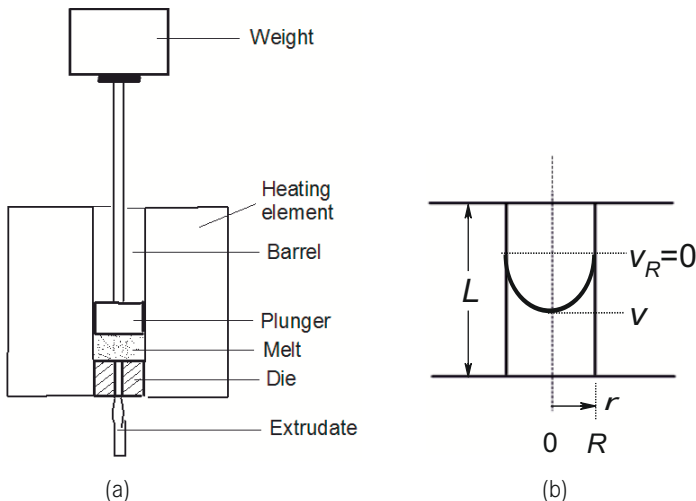


**Figure 2.1** (a) Schematics of melt flow measurement; (b) Flow of viscous liquid through capillary

mer melt discharged through the capillary opening over a period of 10 minutes. The amount of the extruded melt is determined by weighing or, when modern extrusion plastometers are used, by measuring the speed of the plunger movement. Depending on the type of resin, four different standard weights can be used to measure melt indexes, 2.16, 5.16, 10.16, and 21.6 kg. The melt indexes are respectively designated as  $I_2$ ,  $I_5$ ,  $I_{10}$ , and  $I_{21}$ . If no indication of the weight is given, the  $I_2$  value is traditionally reported.

The melt index of a polyethylene resin is a *very precise relative measure* of its weight-average molecular weight. Modern equipment can measure melt indexes with a precision of  $\pm 2$  to 3%. It is instructive to examine an empirical correlation between the molecular weight and the melt index  $I_2$  of polyethylene resins with a narrow molecular weight distribution ( $M_w/M_n \sim 2$ ) produced with soluble metallocene catalysts. One such correlation is shown in Fig. 2.2.

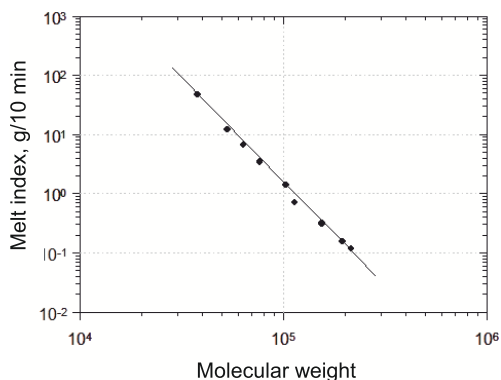


**Figure 2.2** Dependence between the melt index  $I_2$  and the average molecular weight for polyethylene resins with narrow molecular weight distribution

It is represented by an empirical expression:

$$\log(I_2) = 17.45 - 3.451 \cdot \log(M_w) \quad (2.1)$$

Another empirical correlation for the same type of material is:

$$I_2 = 6.16 \cdot 10^{17} \cdot M_w^{-3.5} \quad (2.2)$$

Several examples of the latter dependence are:

$M_w$ :	90,000	92,500	95,000	97,500	100,000	150,000
$I_2$ , g/10 min:	2.24	2.04	1.85	1.69	1.55	0.37

These data show that a 2.5% difference between  $M_w$  values of two resins (a difference which would require the use of very precise and expensive GPC equipment and would take several hours to measure) can be easily noticed when the resins'  $I_2$  values are compared. In this example, the  $I_2$  values differ by 8.3%. This difference can easily be established in routine measurements over a period of  $\sim 15$  minutes.

Similarly, a 50% difference in the molecular weight leads to a fourfold change in the  $I_2$  value.

The principal uncertainty in using dependencies like those in Eqs. 2.1 and 2.2 is that all the numerical parameters in such equations depend on the molecular weight distribution of the resins. For example, a similar correlation for resins with a broader molecular weight distribution, such as HDPE resins produced with supported Ziegler-Natta catalysts is:

$$I_2 = 9.52 \cdot 10^{18} \cdot M_w^{-3.79} \quad (2.3)$$

The molecular weight distribution of a polyethylene resin is characterized in industry by a ratio of two melt indexes measured with different loads. The commonly used ratios are  $I_{21}/I_2$  (often called the *melt flow ratio*, or *MFR*) and  $I_{10}/I_2$ . Both of these ratios approximately correlate with the  $M_w/M_n$  ratio of the resin. For example, an empirical correlation between the  $M_w/M_n$  ratio and the  $I_{21}/I_2$  ratio for LLDPE resins with a medium-broad molecular weight distribution produced with supported Ziegler-Natta catalysts is [1, 2]:

$$M_w/M_n \approx 0.238 \cdot (I_{21}/I_2) - 2.4 \quad (2.4)$$

Melt index ratios are quite sensitive to the presence of long-chain branching in polyethylene resins. As an example, if a compositionally uniform ethylene/ $\alpha$ -olefin copolymer produced with a metallocene catalyst has a small amount of long-chain branches, its  $I_{10}/I_2$  ratio increases from  $\sim 5$  to a range of 8 to 12 [3–6].

## ■ 2.2 Basics of Polymer Rheology; Melt Flow Through a Capillary

All polyethylene resins in the molten state are viscous non-Newtonian liquids. This statement requires a definition of what a Newtonian and a non-Newtonian liquids are. In very simple terms, a Newtonian liquid is a liquid in which viscosity does not depend on the shear applied to it. Because any shear would force the liquid to flow, a Newtonian liquid can be defined as a liquid in which the viscosity does not depend on the speed at which it flows. The melt of a polyethylene resin never exhibits such a behavior; in contrast, the faster it flows the less viscous it becomes. This phenomenon becomes immediately obvious when melt indexes of the resins are measured under different loads. If a polyethylene resin were a Newtonian liquid, its  $I_{21}/I_2$  value would always be  $\sim 10$ , whatever the molecular weight of the resin is (Section 2.2.1). In reality, the  $I_{21}/I_2$  ratio of any polyethylene melt is always higher than 10 because when the weight is increased from 2.16 to 21.6 kg, the melt start flowing faster, its viscosity decreases, and the amount of the melt discharged

through the capillary increases disproportionately. The lowest experimentally determined  $I_{21}/I_2$  ratio, 15 to 16, was measured for resins with a narrow molecular weight distribution prepared with soluble single-site metallocene catalysts, whereas the resins with a broad bimodal molecular weight distribution (see Figs. 1.8 and 1.9) can have the  $I_{21}/I_2$  ratio in excess of 150.

This deviation from the Newtonian flow behavior has a simple explanation. Every macromolecule with a molecular weight  $MW$ , whether it is in solution or in the melt, acquires the form of a sphere (a coil) with the radius (radius of gyration)  $R_g$ :

$$R_g = k_g \cdot (0.5/6^{0.5}) \cdot MW^{0.5} \quad (2.5)$$

where  $k_g$  is a parameter characterizing the “quality” of the surrounding medium. The better the solvent quality (such solvents are called “good”), the higher is the  $k_g$  value and the bigger is the radius of the coil. If external stress is applied to the coil, its shape changes from spherical to ellipsoidal. As Fig. 2.3 shows, the higher the stress, the more elongated the ellipsoid becomes. Because the resistance of a polymer coil to movement in the flow is proportional to its cross section in the direction of the flow (to the square of its effective radius shown in Fig. 2.3), any decrease of the effective radius reduces its resistance to flow and, therefore, increases the overall speed of the flowing melt.

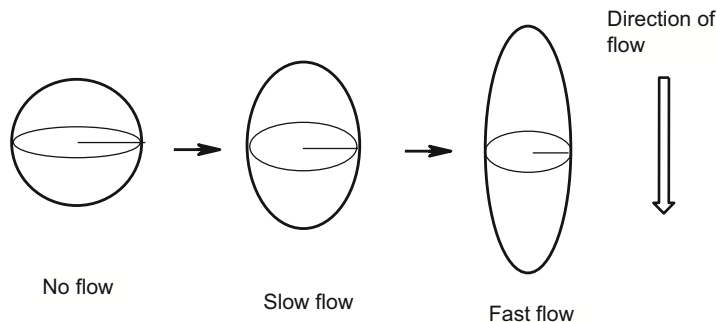


**Figure 2.3** Distortion of macromolecule coil under stress

When the shear (the speed of the melt flow) is very small, viscous properties of the melt are quite similar to those of a Newtonian liquid. The melt viscosity measured at a very low shear is called the zero-shear viscosity  $\eta_0$ . This value is closely related to the molecular weight of the resin. If all macromolecules in a given polymer sample have exactly the same length (a situation which never exists in commercial polyethylene resins), the correlation between the zero-shear viscosity  $\eta_0$  and the polymerization degree  $n$  is described by a firmly established theoretical expression, which has been confirmed in numerous experimental measurements for polyethylene fractions with a narrow molecular weight distribution [6–8]:

$$\eta_{0,n} = k \cdot n^\gamma \quad (2.6)$$

where the  $\gamma$  parameter is equal to 3.5. The  $k$  parameter in Eq. 2.6 is not known in advance; it should be estimated from experimental data, as described below.

The issue of interpreting the physical meaning of the melt index can be separated into three subjects:

1. What is the melt index of a viscous Newtonian liquid?
2. What is the melt index of an ideal non-Newtonian liquid, such as a polymer with all macromolecules of the same length?
3. What is the melt index of a real polymer containing macromolecules of different lengths?

### 2.2.1 Flow of Polymer Melt Through a Cylindrical Capillary

Figure 2.1(b) shows the diagram of a liquid flow through a cylindrical capillary with the radius  $R$  and the length  $L$  under the pressure  $P$ . In the case of extrusion plastometers used for the melt index measurement,  $P$  is calculated as

$$P(\text{MPa}) = 9.81 \cdot \text{Weight (kg)} / [\pi (D_{\text{bar}} \cdot 10^{-3}/2)^2] \cdot 10^{-6} \quad (2.7)$$

where  $D_{\text{bar}}$  is the diameter of the barrel in the plastometer, 9.55 mm (Fig. 2.1(a)).

When an incompressible viscous liquid flows through a capillary, the flow velocity  $v_r$  at a distance  $r$  from the cylinder axis varies from  $v_R = 0$  at  $r = R$  (the flow velocity at the capillary wall is zero), to a certain maximum velocity along the central axis of the capillary, at  $r = 0$ . The following definitions and derivation steps are commonly used [3, 20], assuming that the flow remains laminar in the total range of the flow speeds:

The definition of the shear rate  $D_r$  at a radius  $r$ :

$$D_r = -dv_r/dr \quad (2.8)$$

The definition of the shear strain  $\tau_r$  in the melt (the Stokes equation):

$$\tau_r = (P/2L) \cdot r \quad (2.9)$$

The definition of viscosity  $\eta$ :

$$\eta = \tau_r/D_r \quad (2.10)$$

A combination of Eqs. 2.9 and 2.10 gives the principal expression for the viscous flow through a capillary. This expression represents the starting point of all calculations of a non-Newtonian flow:

$$(P/2L) \cdot r (= \tau_r) = \eta \cdot D_r \quad (2.11)$$

The elementary flow volume  $dV_r$  at a radius  $r$  is:

$$dV_r = 2\pi \cdot r \cdot dr \cdot v_r \quad (2.12)$$

where  $dr$  is the thickness of the elementary layer and  $2\pi r \cdot dr$  is its cross-section. Boundary conditions at the wall of the capillary (at  $r = R$ ) are:  $\tau_R = (P/2L) \cdot R$  and  $\eta_R = \tau_R/D_r$ . Hence,  $D_r = \tau_R/\eta_R = (P/2L) \cdot R/\eta_R$ , which signifies that the shear rate in the elementary layer at the wall,  $D_r$ , is the highest.

The total flow volume  $V$  through the capillary is the integral of  $dV_r$  over  $r$ :

$$V = \int_0^R 2\pi \cdot r \cdot v_r \cdot dr \quad (2.13)$$

The easiest way to perform integration in Eq. 2.13 is to change its variable from  $r$  to  $\tau_r$ . The following replacements are traditionally made:  $dr = (P/2L)^{-1} \cdot d\tau_r$  and  $dv_r = -(\tau_r/\eta_r) \cdot dr = (P/2L)^{-1} \cdot \eta_r^{-1} \cdot \tau_r \cdot d\tau$  (from Eqs. 2.8 and 2.10). The final expression for the flow rate  $v_r$  at a distance  $r$  from the center of the capillary is produced after the replacement and integration in Eq. 2.13, 0 to a given  $\tau_r$ :

$$v_r = \int_{v_{r=0}}^{v_r} dv_r = v_{r=0} - (P/2L)^{-1} \cdot \int_0^{(P/2L) \cdot r} \eta_r^{-1} \cdot \tau_r \cdot d\tau \quad (2.14)$$

where the lower limit in the first integral,  $v_r = 0$ , is the maximum melt velocity in the center of the capillary.

## 2.2.2 Melt Index of Newtonian Liquid

The solution of Eq. 2.14 is well known for a Newtonian liquid when  $\eta_r$  is always equal to  $\eta_0$  [6]. In this case, the integration of Eq. 2.14 gives:

$$v_r = v_{r=0} - 0.5(P/2L)^{-1} \cdot \eta_0^{-1} \cdot \tau_r^2 = v_{r=0} - 0.5(P/2L) \cdot \eta_0^{-1} \cdot r^2 \quad (2.15)$$

The  $v_{r=0}$  value is determined from the boundary condition:  $v_r = 0$  at  $r = R$ ; therefore,  $v_{r=0} = 0.5 \cdot (P/2L) \cdot \eta_0^{-1} \cdot R^2$ . The final expression for the velocity  $v_r$  as a function of the radius  $r$  is a parabolic function:

$$v_r = 0.5(P/2L) \cdot \eta_0^{-1} \cdot (R^2 - r^2) \quad (2.16)$$

Introduction of Eq. 2.16 into Eq. 2.14 and integration from  $r = 0$  to  $R$  gives the melt flow volume of a Newtonian liquid (the Hagen-Poiseuille equation):

$$V^{\text{Newton}} = \pi \cdot P \cdot R^4 / (8 \cdot L \cdot \eta_0) \quad (2.17)$$

Equation 2.17 states that when a Newtonian liquid with viscosity  $\eta_0$  flows through a capillary, the volume of the flow (the melt index) is proportional to the pressure  $P$  in the capillary; that is, it is proportional to the weight of the load placed on the stem of the plunger. The equation also shows that the volume of the Newtonian melt is proportional to the square of the capillary cross section ( $S_{\text{cap}} = \pi \cdot R^2$ ) and that it is in a reciprocal dependence on the capillary length  $L$ .

## 2.3 Melt Flow of Monodisperse Polyethylene Resins

All polyethylene resins are non-Newtonian liquids, and Eq. 2.17 does not describe their flow through a capillary because the viscosity of all these resins is not constant but varies depending on the speed of the flow,  $v_r$ . The simplest example of such a deviation can be observed when one measures the melt flow of model polymers that have all their macromolecules the same length (the same  $n$  value). Such polymers are called monodisperse polymers. Polyethylene resins of this type cannot be produced with any polymerization catalyst. However, they have been prepared artificially in a series of chemical reactions that include anionic polymerization of butadiene with a butyl lithium initiator followed by hydrogenation of the produced polybutadiene [19]. The final products of these two reactions are very similar to ethylene/butene MDPE resins in terms of their molecular structure but they have a very narrow molecular weight distribution:  $M_w/M_n \sim 1.04$  to  $1.06$ . Figure 2.4 shows the dependence between the melt index and the weight of the load for one such polymer with  $MW$  of 146,000 and the melt index  $I_2$  of 0.48. When the loads are small, up to 5 kg, the relationship between the melt index and the load is linear; that is, it agrees with Eq. 2.17, which signifies that the polymer melt behaves as a Newtonian liquid. This flow range provides the basis for the measurement of the zero-shear viscosity  $\eta_0$  using Eq. 2.17. When the load increases above 5 kg, an upward deviation from the linear dependence becomes obvious, demonstrating the non-Newtonian nature of the melt at a high strain. However, the deviation from the Newtonian behavior in Fig. 2.4 is not large; the  $I_{21}/I_2$  ratio for this melt is merely 12.8, just slightly higher than that for a Newtonian melt in which the  $I_{21}/I_2$  ratio is expected to be 10.

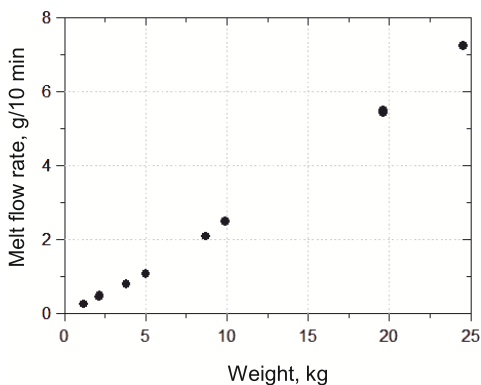


**Figure 2.4** Melt flow of monodisperse polymer with  $MW = 146,000$  showing the dependence between melt index and load weight

This deviation from Newtonian flow behavior has no universally accepted theoretical interpretation and is usually expressed by *empirical* functions, such as [6, 12, 21, 22]:

$$\eta/\eta_0 = [1 + k_\eta \cdot (D \cdot \eta_0)^\beta]^{-1} \quad (2.18)$$

where  $D$  is the shear rate (see Eq. 2.8) and  $k_\eta$  and  $\beta$  are two empirical parameters that are estimated from experimental data. Equation 2.18 signifies that as the shear rate increases, the intrinsic viscosity  $\eta$  decreases in comparison with  $\eta_0$ ; the existence of such a decrease constitutes the definition of non-Newtonian flow. In everyday practice of melt index measurements, this phenomenon is usually called *shear thinning* of a polymer melt. The deviation from the Newtonian flow behavior for the melt in Fig. 2.4 is too small to determine the  $k_\eta$  and  $\beta$  values with sufficient precision. More dependable estimations have been carried out for complex polymer mixtures, as described below; they give  $k_\eta \approx 1 \cdot 10^{-5}$  and  $\beta \approx 0.81$ .

The introduction of Eq. 2.18 into Eq. 2.11 and the use of Eq. 2.8 produce the expression for the elementary flow volume  $dV_r$  at a radius  $r$  (compare to Eq. 2.12). In principle, continuing this derivation in a manner similar to that used for the derivation of Eqs. 2.13 to 2.17 would provide the expression for the flow volume (melt index) of a non-Newtonian melt consisting of macromolecules of the same length. However, such straightforward analytical derivations are not possible anymore because the viscosity  $\eta$ , by itself, is a complex function of the shear rate  $D$ , which is empirically described by Eq. 2.18. Instead, a numerical solution of the problem can be carried out. The calculations require knowledge of the polyethylene melt density at 190 °C, which is 0.764 g/cm<sup>3</sup>. Some representative results are given in Table 2.1. The results are clear: monodisperse polymers, even when they have a quite high molecular weight, behave very similarly to Newtonian liquids. Their  $I_{21}/I_2$  ratios are not significantly higher than 10, and their melt indexes  $I_2$  are close to the melt indexes for Newtonian melts,  $I_2^{\text{Newton}}$ .

**Table 2.1** Calculated Melt Indexes of Monodisperse Polyethylene Resins

<i>MW</i> :	25,000	50,000	75,000	100,000	200,000
$\eta_0$ , kPa/s:	0.54	5.29	21.9	59.9	665
$I_2^{\text{Newton}}$ , g/10 min:	15.0	1.52	0.37	0.13	0.01
$I_2$ , g/10 min:	15.3	1.56	0.38	0.14	0.012
$I_{21}/I_2$ :	11.5	11.5	11.5	11.5	11.5

## ■ 2.4 Additivity Rules for Viscosity; Calculation of Melt Indexes and Melt Flow Ratios from Molecular Weight Distribution Data

### 2.4.1 Additivity Rules for Zero-Shear Viscosity $\eta_0$

Before the relationships between molecular weights and the widths of the molecular weight distribution of polyethylene resins and their melt indexes and melt flow ratios are examined, one principal issue should be addressed: what is the zero-shear viscosity of a mixture of macromolecules with different molecular weights? For example, consider the simplest case in which melts of two monodisperse polymers, one with  $MW_1$  and  $\eta_{0,1}$  and another with  $MW_2$  and  $\eta_{0,2}$ , are mixed in a given weight proportion, *fraction* and  $1 - \textit{fraction}$ . What would the  $\eta_{0,\text{mix}}$  value of such a mixture be? There is no good theoretical answer to this question, but several empirical rules have been proposed in the literature. The first one is the log-additive rule of mixing [12, 22, 23]:

$$\log(\eta_{0,\text{mix}}) = \textit{fraction} \cdot \log(\eta_{0,1}) + (1 - \textit{fraction}) \cdot \log(\eta_{0,2}) \quad (2.19)$$

The second mixing rule makes use of Eq. 2.6. The underlying assumption is that the  $\eta_{0,\text{mix}}$  value can be estimated from Eq. 2.6 for the weight-average molecular weight of the binary mixture,  $M_w = \textit{fraction} \cdot MW_1 + (1 - \textit{fraction}) \cdot MW_2$  [2, 24]. According to Eq. 2.6, the polymerization degree of a monodisperse polymer is related to its zero-shear viscosity as  $n = MW/28 = (\eta_{0,n}/k)^{-\gamma}$  where  $\gamma = 3.5$ . Therefore,

$$\eta_{0,\text{mix}} = [\textit{fraction} \cdot (\eta_{0,1})^{-\gamma} + (1 - \textit{fraction}) \cdot (\eta_{0,2})^{-\gamma}]^{\gamma} \quad (2.20)$$

The applicability of Eq. 2.20 for the description of average melt indexes of binary mixtures is demonstrated in Fig. 2.5. It shows the experimentally determined dependence of the melt flow rate for an equal by-weight mixture (*fraction* = 0.5)

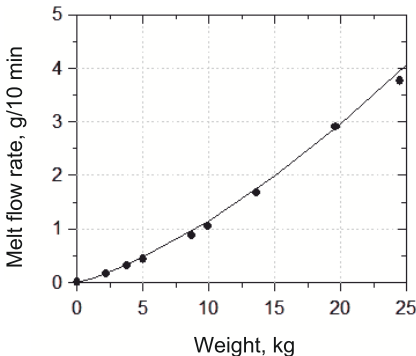


**Figure 2.5** Melt flow of 1:1 mixture of two monodisperse polymers with  $MW = 146,000$  and  $51,000$ ; dependence between melt index and load

of two monodisperse polymers with molecular weights of 146,000 and 51,000, respectively. The  $\eta_{0,\text{mix}}$  value for the mixture was calculated with Eq. 2.20 for  $k = 2.0 \cdot 10^{-9}$ , and then the dependence between the flow rate and the weight of the load was numerically calculated for this  $\eta_{0,\text{mix}}$  value in the same manner as done for a single monodisperse polymer described above.

Of course, any real polyethylene resin contains not two but a very large number of macromolecules with different polymerization degrees  $n$  (different molecular weights  $MW_n \approx 28 \cdot n$ ). The weight-average molecular weight for such mixtures is  $M_w = \Sigma(\text{fraction}_n \cdot MW_n)$ . Calculations of  $\eta_{0,\text{mix}}$  values for such mixtures is based on the general form of Eq. 2.20:

$$\eta_{0,\text{mix}} = \Sigma[\text{fraction}_n \cdot (\eta_{0,n})^{-\gamma}]^{\gamma} \quad (2.21)$$

with  $\gamma = 3.5$ . The values of  $\text{fraction}_n$  are determined from gel permeation chromatographic (GPC) analysis of resins, as described in Sections 1.4 and 1.5 of Chapter 1 and in Sections 2.4.2 and 2.5 below.

### 2.4.2 Additivity Rules for Effective Viscosity and General Expressions for Flow of Non-Newtonian Multi-Component Melt

All commercially produced polyethylene resins are complex mixtures of macromolecules, and their melts exhibit pronounced non-Newtonian behavior [14–18, 25–27]. These melts can be viewed as assemblies of closely packed macromolecular coils of different radii. The situation is even more complicated because the coils interpenetrate each other, and each given coil is to some degree entangled with its neighbors. The theoretical treatment of such mixtures of non-Newtonian liquids is a very challenging subject [25–27]. The analysis of the melt behavior presented below is based on a simplified version of this model where the entanglement of neighboring molecular coils is not taken into account. This simplified theory cannot be expected to provide exact values of melt flow rates for a given resin. Instead, the simple model provides a semiquantitative description of the melt behavior, which helps in the interpretation of such basic (and easily experimentally determined) values as  $I_2$  or  $I_{21}/I_2$ .

When a viscous liquid flows through a capillary, it is subjected to shear strain  $\tau_r$ , which is calculated with the Stokes equation, Eq. 2.9. The shear strain is equal to zero in the center of the capillary and reaches a maximum at the capillary wall. The simple analysis of the rheology of multicomponent blends presented below is based on three conjectures:

1. In a given elemental volume of a flowing melt positioned at a distance  $r$  from the capillary axis (Fig. 2.1(b)), all of its components (all macromolecular coils in the mixture) are subjected to the same shear stress  $D_r$ .

2. The effective viscosity of the multicomponent melt in this elemental volume is governed by the same blending rule for the components of the mixture as the blending rule for the zero-shear viscosity  $\eta_0$  (Eq. 2.20 or Eq. 2.21). This conjecture is represented by a general equation similar to Eq. 2.21:

$$\eta_{\text{mix},D} = \Sigma [\text{fraction}_n \cdot (\eta_{n,D})^{-\gamma}]^{\gamma} \quad (2.22)$$

where  $\text{fraction}_n$  is the fraction of polymer molecules with the polymerization degree  $n$  and  $\eta_{n,D}$  is its real viscosity at a shear rate  $D$ .

3. As the shear stress increases, the viscosity of each component in the blend is reduced according to Eq. 2.18 (the shear thinning effect). In other words, the viscosity term  $\eta_{n,D}$  in Eq. 2.22 depends on a given shear rate  $D_r$ : the higher the  $D_r$  value, the lower is the viscosity of macromolecules with the polymerization degree  $n$ ,  $\eta_{n,D}$ , with respect to the zero-shear viscosity of the same macromolecules,  $\eta_{0,n}$ .

Equation 2.18 states that the degree of deviation from Newtonian behavior (the degree of shear thinning) depends on the molecular weight (that is, on the zero-shear viscosity) of the polymer component: the higher the  $n$  value (and the higher  $\eta_{0,n}$ ), the larger is the deviation. This circumstance accounts for a significant difference in the behavior of the melts of monodisperse polymers (Table 2.1) and the melts of commercial polyethylene resins. When the melt of a monodisperse polymer flows through a capillary, all of its macromolecules change their shape from spherical to ellipsoidal (Fig. 2.3) to the same degree; they are more elongated near the capillary wall but retain the spherical shape in the center of the capillary. In contrast, when the melt of a real polyethylene resin produced in a catalytic polymerization reaction flows through the capillary, the macromolecules with a higher molecular weight form more elongated ellipsoids whereas the surrounding shorter macromolecules mostly retain their spherical shape.

As an example of the steps required for the calculation of the melt flow rate of a real polyethylene resin, we examine the simplest case: a polymer produced with a soluble single-site metallocene catalyst. In this case, the expression for  $\text{fraction}_n$  in Eq. 2.22 is straightforward; this is the weight content of macromolecules containing  $n$  monomer units for a single-Flory polymer (the same as in Eq. 1.10)

$$\text{fraction}_n = \delta(E)_n = (n/\mathbf{n}_{\text{av}})^2 \cdot \text{Exp}(-n/\mathbf{n}_{\text{av}}) \quad (2.23)$$

where  $\mathbf{n}_{\text{av}}$  is the number-average polymerization degree of the resin. The zero-shear viscosity of such a polymer mixture is (using Eqs. 2.21 and 2.6):

$$\eta_{0,\text{mix}} = \int [(n/\mathbf{n}_{\text{av}})^2 \cdot \text{Exp}(-n/\mathbf{n}_{\text{av}}) \cdot k^{-\gamma}]^{\gamma} \quad (2.24)$$

with  $\gamma = 3.5$ .

A combination of three equations, the additivity rule for viscosities of polymer components in Eq. 2.6, Eq. 2.18, and Eq. 2.22, gives the final expression for the effective viscosity of a single-Flory polymer mixture subject to shear at a rate  $D_r$ :

$$\eta_{\text{mix},D}^{\text{Flory}} = \int [(n/\mathbf{n}_{\text{av}})^2 \cdot \text{Exp}(-n/\mathbf{n}_{\text{av}}) \cdot (\eta_{n,D})^{-\gamma}]^{\gamma} = \int [(n/\mathbf{n}_{\text{av}})^2 \cdot \text{Exp}(-n/\mathbf{n}_{\text{av}}) \cdot \{k \cdot n^{\gamma} \cdot [1 + k_{\eta} \cdot (D_r \cdot k \cdot n^{\gamma})^{\beta}]^{-1}\}^{-\gamma}]^{\gamma} \quad (2.25)$$

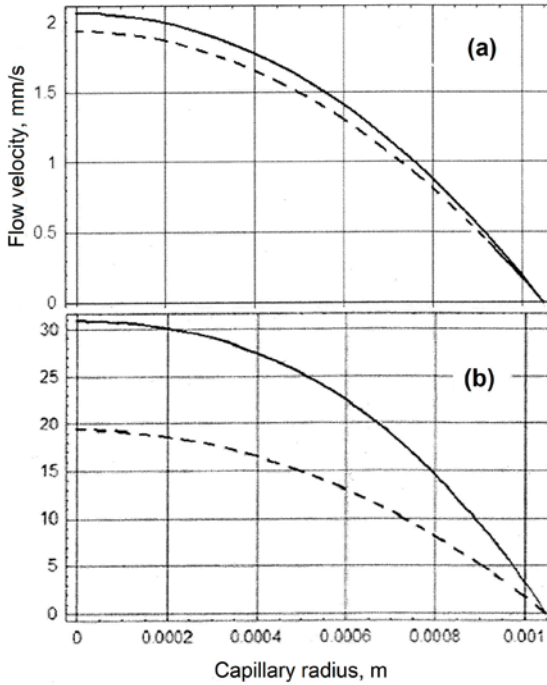
with the integration range from 0 to  $\infty$ . In principle, the expression for  $\eta_{\text{mix},D}^{\text{Flory}}$  can be combined with Eq. 2.13 to calculate the elementary flow rate  $v_r$ , at a distance  $r$  from the capillary axis, and the result of this integration can be introduced for integration into Eq. 2.14 to calculate the total volume of the melt flowing from the capillary; that is, to calculate the melt index. However, the expression in Eq. 2.25 is too cumbersome to integrate analytically. The alternative option is to resort to numerical integration. These calculations were carried out with the Mathematica program.

Table 2.2 gives the results of such calculations for a series of single-Flory resins in a broad range of average molecular weights. The results are very informative. When the weight of the load is small, 2.16 kg, the  $I_2$  values of these non-Newtonian melts are only slightly higher than the  $I_2^{\text{Newton}}$  values calculated under the assumption that the melts exhibit Newtonian behavior; the differences do not exceed 7 to 8%. However, the calculated  $I_{21}$  values are significantly higher than the  $I_{21}^{\text{Newton}}$  values. (Recall that  $I_{21}^{\text{Newton}} = 10 \cdot I_2^{\text{Newton}}$ .) The differences between  $I_{21}$  and  $I_{21}^{\text{Newton}}$  are of the order of 40%. The calculated  $I_{21}/I_2$  ratios, 15.9, match the range of experimentally determined  $I_{21}/I_2$  values for polyethylene resins produced with single-site catalysts, 15 to 16. Figure 2.6 compares flow rates of a single-Flory melt with  $M_w = 100,000$  as a function of the radius in the capillary. Two flow rates, one for the Newtonian melt and another for the non-Newtonian melt, are very close at the low weight, 2.16 kg, but differ significantly at the high weight, 21.6 kg.

**Table 2.2** Calculated Melt Indexes of Single-Flory Polyethylene Resins Produced with Single-Site Metallocene Catalysts

$M_w$ :	50,000	75,000	100,000	125,000	150,000
$\eta_0$ , kPa/s:	0.46	1.92	5.25	11.5	21.7
$I_2^{\text{Newton}}$ , g/10 min:	17.3	4.18	1.53	0.70	0.37
$I_2$ , g/10 min:	18.7	4.51	1.65	0.76	0.40
$I_{21}$ , g/10 min:	298	71.9	26.3	12.1	6.4
$I_{21}/I_2$ :	15.9	15.9	15.9	15.9	15.9

As described in Chapter 1 (Section 1.5), commercial single-Flory polyethylene resins are quite rare. The overwhelming majority of polyethylene resins are polymer mixtures containing several ( $j$ ) Flory components with various number-average molecular weights  $M_{n,j}$  and respective average polymerization degrees  $\mathbf{n}_{\text{av},j}$ . The  $j$  number usually varies from 4 to 8 depending on polymerization catalyst. Many examples of relative contents of different Flory components,  $Fr_j$ , and their  $M_{n,j}$  values in such multi-Flory resins are given in Tables 1.2 to 1.5. The weight fraction of



**Figure 2.6** Melt flow of single-Flory polymer with  $M_w = 100,000$  at two different loads, 2.16 kg (a) and 21.6 kg (b) in coordinates “flow velocity, mm/s as a function of radius, m”; solid lines are for a non-Newtonian melt and dashed lines are for a Newtonian melt

macromolecules containing  $n$  ethylene units for a multi-Flory polymer (the same as in Eq. 1.13) is  $n \cdot \sum FR_j \cdot \mathbf{n}_{av,j}^{-2} \cdot \text{Exp}(-n/\mathbf{n}_{av,j})$  (compare to Eq. 2.23).

By following the same reasoning that is used for the derivation of Eqs. 2.24 and 2.25, the final expression for the effective viscosity of a multi-Flory polymer subject to shear at a shear rate  $D_r$  is:

$$\eta_{\text{mix},D}^{\text{multi-Flory}} = \sum_i FR_j \cdot \int [(n/\mathbf{n}_{av,j})^2 \cdot \text{Exp}(-n/\mathbf{n}_{av,j}) \cdot \{k \cdot n^\nu \cdot [1 + k_\eta \cdot (D_r \cdot k \cdot n^\nu)]^\beta\}^{-1}]^{-\nu} \quad (2.26)$$

with the integration range from 0 to  $\infty$ . The equation in Eq. 2.26 can be only integrated numerically. Equation 2.26 was combined with Eq. 2.13 to calculate the elementary flow rate  $v_r$  at a distance  $r$  from the capillary axis, and the results of this integration were introduced into Eq. 2.14 to calculate melt flow rates of multi-Flory resins.

## ■ 2.5 Examples of Melt Flow Rates and Melt Flow Ratios for Polyethylene Resins of Different Types

The principal difficulty in using the simple theory of the melt flow outlined above is that several of its parameters,  $k$  and  $\gamma$  in Eq. 2.6 and  $k_n$  and  $\beta$  in Eq. 2.18, are empirical and must be determined from experiment. The simple theory does not take into account entanglement of polymer coils in the melt. The degree of entanglement is different depending on the radii of the coils and the differences between these radii. The coils are the same in size in the melt of a monodisperse polymer but differ greatly in radius in melts of all commercial resins. As a result, parameters in Eqs. 2.6 and 2.18 may differ depending on the makeup of a resin and the ratio of long, medium-length, and short macromolecules in the mixture. When a new type of a resin is produced, it is always much more reliable and much faster to measure  $I_2$  and  $I_{21}$  values experimentally, rather than analyze the molecular weight distribution of the resin by GPC and calculate the  $I_2$  and  $I_{21}$  values. The principal application of the simple melt flow theory is the interpretation of the experimentally measured rheological characteristics and the prediction of possible changes in the melt flow. These changes can be caused by procedures such as co-blending small amounts of extraneous polymers to the resins or by modification of catalyst recipes that may produce small changes in the molecular weight distribution of the resins.

### 2.5.1 LLDPE Resins Produced with Supported Ziegler-Natta Catalysts

Figure 2.7 show the dependence of the melt flow rate as a function of the weight of the load for a typical ethylene/hexene LLDPE resin prepared with a supported Ziegler-Natta catalyst.

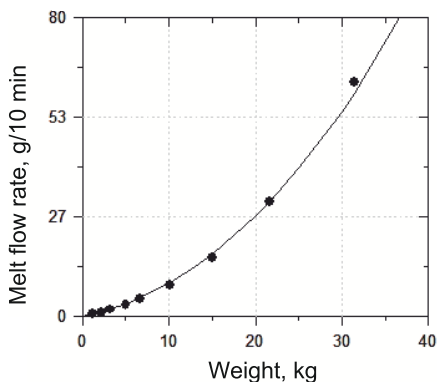


**Figure 2.7** Melt flow of a multi-Flory LLDPE resin prepared with Ziegler-Natta catalyst as a function of load weight (●) and its theoretical simulation

Technological parameters of this resin are: density = 0.917 g/cm<sup>3</sup>,  $C_M^{\text{copol}} = 3.3$  mol %,  $M_w \sim 102,000$ ,  $M_w/M_n = 4.9$ ,  $I_2 = 1.08$ , and  $I_{21}/I_2 = 28.5$ . The GPC curve of the resin contains five Flory components; their parameters are listed in Table 2.3. Calculations with Eq. 2.26 provided the means for the determination of the parameters in the rheological model:  $k = 4.5 \cdot 10^{-9}$  and  $\gamma = 3.5$  in Eq. 2.6;  $k_\eta = 1.05 \cdot 10^{-5}$ , and  $\beta = 0.81$  in Eq. 2.18.

**Table 2.3** Molecular Weight Distribution of LLDPE Resin Produced with Ziegler-Natta Catalyst

Flory component:	I	II	III	IV	V
$M_w$ :	4,000	14,300	43,400	110,700	303,400
Fraction, wt %:	1.5	11.5	36.8	35.2	14.9

As Fig. 2.7 shows, these parameters provide an adequate description of the melt flow for such LLDPE resins. The calculations produce the following results. The zero-shear viscosity of this resin is 12.9 kPa/s and the melt index  $I_2$  for the Newtonian melt with this  $\eta_0$  value would be 0.62, which is  $\sim 40\%$  lower compared to the real (and the calculated)  $I_2$  value of 1.08. This means that the melt of the polymer flows faster than the melt of a Newtonian liquid with the same zero-shear viscosity would. The difference becomes even more pronounced when  $I_{21}$  values are compared: the calculated  $I_{21}$  value and the  $I_{21}^{\text{Newton}}$  value are 30.9 and 6.22 g/10 min, respectively. Still another measure of shear thinning of this melt comes from the comparison of maximum velocities of the melt in the center of the capillary. The ten-fold increase in the weight of the load produces a nearly 27-fold increase of the maximum velocity, from 1.3 to  $\sim 34.5$  mm/s.

The simple rheological model also provides an analysis of the changes one can expect when the molecular weight of each Flory component in the resin is slightly changed (by changing the partial pressure of hydrogen in a polymerization reactor) or when the relative contents of the Flory components are changed, a task achieved by catalyst modification. Several examples of these changes are given in Table 2.4.

The first two changes (columns 2 and 3) describe the effect of a proportional change in the molecular weight of each Flory component as a result of a change in the concentration of hydrogen in a polymerization reactor by  $\pm 10\%$ . Such changes do not affect the width of the molecular weight distribution of the resin (the  $M_w/M_n$  ratio) or the melt flow ratio of the resin. However, these changes greatly affect both the  $I_2$  and the  $I_{21}$  value. These data emphasize importance of a precise control of reaction parameters in commercial processes: a 5 to 7% drift in some parameters could easily lead to the production of an off-spec material.

Commercial manufacturers of polyethylene resins often attempt to modify Ziegler-Natta catalysts with the goal of producing resins of better quality and a higher

**Table 2.4** Calculated Melt Indexes of and Melt Flow Ratios of Several LLDPE Resins Produced with Ziegler-Natta Catalyst

Resin:	Original resin	Molecular weight increased	Molecular weight decreased	Flory components I & II decreased	Flory component V decreased
$M_w$ :	102,000	113,000	92,700	109,000	85,800
$M_w/M_n$ :		4.9	4.9	4.9	3.8
$\eta_{0r}$ , kPa/s:	12.9	296	9.2	16.4	7.1
$I_2^{\text{Newton}}$ , g/10 min:	0.62	0.43	0.87	0.49	1.14
$I_2$ , g/10 min:	1.08	0.75	1.51	0.81	1.9
$I_{21}$ , g/10 min:	30.9	21.3	43.3	21.3	49.2
$I_{21}/I_2$ :	28.6	28.6	28.6	26.4	26.2

commercial value. Two hypothetical results of such modification are shown in the last two columns of Table 2.4. Table 1.3 lists the parameters of Flory components in a LLDPE resin produced with a supported Ziegler-Natta catalyst. The Flory components in the resins have different compositions. Component I has very high hexene content. This is a completely amorphous sticky material of little commercial value. If the polymerization reactions are carried out in a hydrocarbon solvent, this material dissolves in the solvent under polymerization conditions (temperatures between 70 and 85 °C) and the subsequent blending of the separated components is difficult. Some types of chemical modification allow a nearly complete elimination of the active centers in the catalysts which produce this amorphous material. Unfortunately, this modification is usually accompanied by significant reduction in the yield of Flory component II as well. The example in the fifth column of Table 2.4 describes the rheological consequences of such a modification when the whole component I and one-half of component II are absent from the resin. As expected, this mixture has a narrower molecular weight distribution (the  $M_w/M_n$  ratio is reduced from 4.9 to 3.8) and has a significantly lower melt flow ratio, 26.4 instead of 28.6.

The example in the last column of Table 2.4 shows the outcome of another attempt at catalyst modification. Flory component V has very low hexene content, below 0.4 mol %. This is a highly crystalline material with a very high molecular weight (Table 1.3). If the fraction of this component in the mixture is reduced by one-half, the remaining material has higher average hexene content, a lower average molecular weight, and its melt index nearly doubles. As Table 2.4 shows, this material also has a significantly narrower molecular weight distribution and a lower  $I_{21}/I_2$  value. Although both types of catalyst modification produce LLDPE resins with lower  $I_{21}/I_2$  ratios, two different corrective measures should be carried out in the respective polymerization processes. If the centers I and II are poisoned, the copo-

lymerization reaction should be carried out at a higher  $\alpha$ -olefin concentration to compensate for the loss of these Flory components and to bring the average hexene content to the original level,  $\sim 3$  mol %. If the amount of component V is reduced, the concentration of  $\alpha$ -olefin in the reactor should be decreased to decrease the average hexene content in the resin and to avoid the formation of excessive amounts of components I and II.

## 2.5.2 HDPE Resins with Broad Molecular Weight Distributions

Figure 1.8 shows a typical GPC curve of a pipe-grade polyethylene resin produced with a bicomponent Ziegler-Natta/metalocene catalyst. The titanium-based Ziegler-Natta component in the catalyst produces the high molecular weight fraction in this mixture and the metalocene catalyst component produces the low molecular weight fraction. Table 2.5 lists the data on the molecular weight distribution of both fractions. Each fraction by itself has a relatively narrow molecular weight distribution; the respective  $M_w/M_n$  ratios are 2.9 and 6.0. However, molecular weights of these two fractions differ greatly: the  $M_w$  value for the low molecular weight material is  $\sim 10,000$  and that for the high molecular weight material is  $\sim 640,000$ . As a result, the  $M_w/M_n$  ratio for the total resin is very high,  $\sim 50$ .

**Table 2.5** Flory Components in Pipe-Grade HDPE Resin Produced with Bicomponent Ziegler-Natta/Metalocene Catalyst

	Flory component	$M_w$	$M_w/M_n$	Content, %
Total polymer:		352,200	50.0	100
Low-MW fraction:		9,800	2.9	46.0
	I	3,430		9.1
	II	6,170		18.4
	III	16,570		18.5
High-MW fraction:		644,400	6.0	54.0
	I	76,360		13.0
	II	230,500		15.3
	III	588,600		12.4
	IV	1,729,500		13.3

Table 2.6 gives the calculated rheological results. They were determined using the same parameters as those given above for the resins produced with Ziegler-Natta catalysts. In rheological terms, the two resin fractions are very different. Their zero-shear viscosities differ by a factor of  $3.4 \cdot 10^6$  and their high-load melt indexes  $I_{21}$  by a factor of  $4.7 \cdot 10^7$ . The high molecular weight component is very viscous; if

produced separately, its  $I_{21}$  value of 0.077 would be barely measurable. Such resins cannot be processed with modern extruders. On the other hand, the low molecular weight fraction is practically a wax; its viscosity, if measured at 190 °C, would not differ significantly from the viscosity of water. This resin fraction does not contribute anything to the mechanical properties of the total resin; its only purpose is to serve as a diluent for the high molecular weight fraction during those several minutes when the resin melt is processed.

**Table 2.6** Rheological Parameters of Pipe-Grade HDPE Resin Produced with Bicomponent Ziegler-Natta/Metallocene Catalyst

	$\eta_0$ , kPa/s	$I_{21}^{\text{Newton}}$ , g/10 min	$I_2$ , g/10 min	$I_{21}$ , g/10 min	$I_{21}/I_2$
Total polymer, experimental values			0.045	6.2	139
Total polymer, calculated values	995	$8.1 \cdot 10^{-3}$	0.052	7.2	140
Low-MW fraction (33%), calculated values	$2.4 \cdot 10^{-3}$	$3.27 \cdot 10^4$	$4.94 \cdot 10^3$	$1.49 \cdot 10^5$	$\sim 30$
High-MW fraction (67%), calculated values	$8.26 \cdot 10^3$	$\sim 1 \cdot 10^{-3}$	$1.9 \cdot 10^{-3}$	0.077	$\sim 40$

Figure 2.8 compares the melt flow of this bicomponent resin at a 2.16 kg load in the coordinates “flow velocity, mm/s, as a function of radius, m” with the melt flow of the Newtonian melt with the same zero-shear viscosity. This plot clearly demonstrates that the rheological behavior of resins with a broad molecular weight distribution differs very strongly from the melt behavior of resins with Newtonian rheological properties, even under relatively small loads.

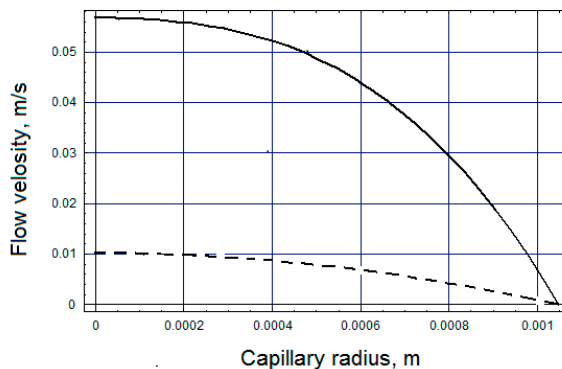


**Figure 2.8** Melt flow of bicomponent resin (parameters in Table 2.6) at 2.16 kg load in coordinates “flow velocity, mm/s as a function of radius, m”; the solid line is for a non-Newtonian melt and the dashed line is for a Newtonian melt

Figures 2.8 and 2.6 (b) show another characteristic feature of the flow of melts with a strongly expressed non-Newtonian behavior: a large velocity gradient near the wall of the capillary at  $r \approx 1$  mm. All rheological theories of viscous fluids, both Newtonian and non-Newtonian, assume that the flow velocity at the wall of the capillary is zero (Fig. 2.1(b), the low integration limit in Eq. 2.14). This assumption usually holds in a broad range of loads. However, when the loads are very high, this rule fails and the melt starts slipping along the capillary wall. The slipping usually proceeds in a stop-and-go manner, and as a result, the surface of the out-flowing melt, after it solidifies, acquires a specific rough appearance usually called “shark skin”. The appearance of the shark skin pattern on the surface of an extrudate makes all melt index measurements and all melt index calculations meaningless. When the melt starts slipping with respect to the capillary wall, the amount of the extrudate becomes dependent not only on the load but on the smoothness of the capillary surface as well; the smoother the surface, the higher is the load leading to the melt slipping and to the development of the shark skin effect.

Figure 1.9 gives another example of a bimodal HDPE resin, which was produced with the use of a single Ziegler-Natta catalyst in two slurry reactors connected in a series. In terms of the molecular weight distribution, this resin can be viewed as a combination of two sets of four Flory components shifted by a factor of  $\sim 20$  in their average molecular weight (Table 1.6). Table 2.7 gives calculated rheological parameters of this resin. Overall, the results of the rheological analysis for the two resins reported in Tables 2.6 and 2.7 are very similar. In the latter example (Table 2.7), zero-shear viscosity of the two resin fractions differs by a factor of  $3.8 \cdot 10^5$  and their high-load melt index  $I_{21}$  by a factor of  $2.4 \cdot 10^6$ . To take advantage of excellent mechanical properties of the high molecular weight polymer fraction in both mixtures, they must be diluted with a polymer material of a very low molecular weight to allow processing of the resin melts.

**Table 2.7** Rheological Parameters of Film-Grade HDPE Resin Produced with Single Ziegler-Natta Catalyst in Two-Reactor Process

	$\eta_{01}$ , kPa/s	$I_2^{\text{Newton}}$ , g/10 min	$I_{21}$ , g/10 min	$I_{211}$ , g/10 min	$I_{211}/I_2$
Total polymer	130	0.62	0.20	15.6	77.3
Low-MW fraction (45%)	0.024	$3.29 \cdot 10^3$	558	$1.79 \cdot 10^5$	$\sim 32$
High-MW fraction (55%)	911	$\sim 0.09$	0.014	0.405	$\sim 29$

### 2.5.3 Effect of Long-Chain Branching

Three types of polyethylene resins have long-chain branches in their macromolecules: LDPE resins produced via the radical mechanism in high-pressure polymeri-

zation reactors, some MDPE and HDPE resins prepared with special types of metallocene catalysts, and HDPE resins produced with chromium oxide catalysts. To be rheologically significant, such branches must be longer than the critical entanglement length, which is equal to  $\sim 140$  carbon atoms in the case of polyethylene [28, 29].

Effects of long-chain branching on the rheology of polyethylene resins have been studied both experimentally and theoretically [5, 18, 26] but still remain a very complex subject. The single empirical rule for the description of such an effect is: the higher the content of long branches in the macromolecules, the larger is their deviation from standard rheological models. In particular, the higher the content of long branches, the higher are the melt flow ratios of such resins compared to the melt flow ratios of resins of the same molecular weight but lacking long-chain branches.

Calculations of the  $I_{21}/I_2$  ratios for a typical HDPE resin prepared with a chromium oxide catalyst can serve as an example. All these resins have a broad molecular weight distribution with a characteristic triangular shape shown in Fig. 1.7. Parameters of the constituting Flory components in one such resin are listed in Table 1.4. The average molecular weight of these resins is usually 220,000 to 250,000 and the  $M_w/M_n$  ratios are in the 12 to 15 range (11.9 in this particular case). The calculated zero-shear viscosity of the resin is 213 kPa/s; a Newtonian melt with this  $\eta_0$  value would have the  $I_{21}$  value of  $\sim 0.38$  g/10 min. Of course, the resin has a broad molecular weight distribution and exhibits an expressed non-Newtonian behavior: the  $I_{21}$  value of the resin calculated with the simple model would be 5.65 g/10 min and the  $I_{21}/I_2$  value would be  $\sim 45$ . However, experimentally measured  $I_{21}/I_2$  values for HDPE resins produced with chromium oxide catalysts usually range between 120 and 150. These large differences between the experimental and the calculated  $I_{21}/I_2$  values are a clear manifestation of the long-chain branching effect on the rheological behavior of polyethylene resins.

## ■ References

1. Kissin, Y.V., Nowlin, T.E., Wagner, K.P., *J. Polym. Sci., Part A: Polym. Chem.* (1988) 26, p. 755
2. Kissin, Y.V., Brandolini, A.J., Mink, R.I., Nowlin, T.E., *J. Polym. Sci., Part A: Polym. Chem.* (2009) 47, p. 3271
3. Lai, S.Y., Wilson, J.R., Knight, G.W., Stevens, J.C., Chum, P.S., *U.S. Patent* 5 272 236 (1993)
4. Knight, G.W., Lai, S., *SPE Polyolefins VIII International Conference* (1993) Houston, TX, p. 226

5. Seung, J.P., Larson, R.G., *J. Rheol.* (2005) 49, p. 523
6. Carley, J.F., In *Rheology, Theory and Applications*, vol. 4. Eirich, F.R. (Ed.) (1967) Academic Press, New York, p. 425
7. Bird, R.B., Armstrong, R.C., Hassager, O., *Dynamics of Polymer Fluids*, vol. 1 (1987) John Wiley, New York, p. 105
8. Graessley, W.W., *Adv. Polym. Sci.* (1974) 16, p. 1
9. Larson, R.G., *The Structure and Rheology of Complex Fluids* (2001) Oxford University Press, New York
10. Dealy, J.M., Larson, R.G., *Structure and Rheology of Molten Polymers: From Structure to Flow Behavior* (2006) Hanser, Munich
11. Macosco, C.W., *Rheology: Principles, Measurements and Applications* (1994) Wiley-VCH, New York
12. Larson, R.G., Qiang, Z., Sachin, S., Seung, J.P., *AIChE J.* (2007) 53, p. 542
13. Berry, G.C., Fox, T.G., *J. Polym. Sci., Part A: Polym. Chem.* (1968) 5, p. 261
14. Tung, L.H., *J. Polym. Sci.* (1960) 46, p. 409
15. Williamson, G.R., Wright, B., Howard, R.N., *J. Appl. Chem.* (1964) 14, p. 131
16. Raju, V.R., Smith, G.G., Marin, G., Knox, J.R., Graessley, W.W., *J. Polym. Sci., Part B: Polym. Phys.* (1979) 17, p. 1183
17. Pearson, D.S., Ver Strate, G., von Meerwall, E., Schilling, F.C., *Macromolecules* (1987) 20, p. 1133
18. Mavridis, H., Shrorr, R., *J. Polym. Sci., Part A: Polym. Chem.* (1993) 49, p. 299
19. Coolbaugh, T.S., Loveless, F.C., Matthews, D.N., *U.S. Patent* 5 276 100 (1994)
20. Oka, S., In *Rheology, Theory and Applications*, vol. 3. Eirich, F.R. (Ed.) (1960) Academic Press, New York, p. 21
21. Vinogradov, G.V., Malkin, A.Y., *J. Polym. Sci., Part A-2* (1966) 4, p. 135
22. Bondi, A., In *Rheology, Theory and Applications*, vol. 4. Eirich, F.R. (Ed.) (1967) Academic Press, New York, p. 70
23. Utracki, L.A., *Polymer Alloys and Blends. Thermodynamics and Rheology* (1990) Hanser, Munich, Part 3.3.1
24. Muñoz-Escalona, A., Lafuente, P., Vega, J.F., Muñoz, M.E., Santamaria, A., *Polymer* (1997) 38, p. 589
25. Wasserman, S.H., Graessley, W.W., *J. Rheol.* (1992) 36, p. 543
26. Inkson, N.J., McLeish, T.C.B., Groves, D.J., Harlen, O.G., *J. Rheol.* (1999) 43, p. 873
27. Anderssen, R.S., Mead, D.W., *J. Non-Newton. Fluid Mech.* (1998) 76, p. 299
28. Janzen, J., Colby, R.H., *J. Molec. Struct.* (1999) 569, p. 485
29. Fetters, J., Lohse D.J., Colby, R.H., In *Physical Properties of Polymers Handbook*. Mark, J.E. (Ed.) (1996) AIP Press, New York, p. 335

# 3

## Melting Point of Polyethylene Resin

### ■ 3.1 Introduction

The melting point of a polyethylene resin is its essential technical characteristics. The melting points are measured using the method of differential scanning calorimetry (DSC). The position of the peak maximum on a DSC melting curve (the melting point) and the width of the melting transition, as well as the heat of fusion (see Chapter 4), provide important information about the molecular structure of the resin, its crystallinity degree, and its structural uniformity. The value of the melting point gives the first qualitative information about the nature of the resin and, to some degree, about mechanical properties that can be expected from the articles manufactured from the resin. This is particularly true for linear low density polyethylene (LLDPE) and very low density polyethylene (VLDPE) resins produced with single-site metallocene catalysts. All such resins are compositionally uniform ethylene/ $\alpha$ -olefin copolymers and they all have strongly depressed melting points compared to those of high density polyethylene (HDPE) resins [1–7]. On the other hand, melting points of compositionally nonuniform LLDPE resins produced with multi-site Ziegler-Natta catalysts and with chromium oxide catalysts are always relatively high (120 to 130 °C) and they only weakly depend on the average copolymer composition [7–15].

It is customary to measure the melting point and the heat of fusion of a polyethylene resin in a three-step procedure. First, a small sample of the resin (5 to 10 mg) is placed in a small aluminum pan and heated to 140 or 150 °C at a high heating rate, for example 10 °C/min. The melted sample is then cooled to ~30 °C at a slow rate, from 0.5 to 2 °C/min, to achieve its thorough annealing. Finally, the melting curve of the crystallized/annealed sample is recorded at different heating rates, from 2 to 10 °C/min [16].

## ■ 3.2 Melting Point of HDPE Resin

HDPE resins crystallize from a melt in a chain-folded lamellar morphology (see Section 1.9). A clear proof of the chain folding was originally discovered for individual linear paraffins starting from  $n\text{-C}_{150}\text{H}_{302}$ . A linear polymer segment of this size would correspond to an ethylene block  $\text{M}-(\text{E})_n\text{-M}$  containing  $\sim 75$  monomer units [17]. The type of folding in paraffin crystals is schematically shown in Fig. 3.1. In the case of individual paraffins, the length of the straight segment ( $l$ ) is an integer reciprocal to the full chain length of the paraffin. The methyl end-groups of the paraffins and the folds are excluded from the crystals; they are located at the surfaces of the lamellae (Fig. 3.1). The folds are tight, and the paraffin chains adjacently re-enter into the same crystal.

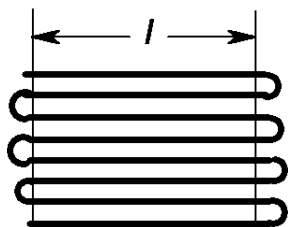


**Figure 3.1** Scheme of polyethylene lamellae

Polyethylene lamellae have a similar structure. They consist of tightly packed linear stretches of the same macromolecule or of several macromolecules [18–20]. The bent segments of the polymer chains between the neighboring linear stretches (the folds) are called loops (see Fig. 1.16). The loops are usually relatively short and consist of a few ethylene units. The average length of the straight segment of a polymer chain between two loops is called the average lamella thickness,  $l_{\text{av}}$ ; its size is usually given either as the physical length, in ångströms ( $\text{Å}$ ), or as the average number of ethylene units in the segment,  $n_l$ . The  $n_l$  number in a lamella with the thickness of  $l_{\text{av}}$   $\text{Å}$  is  $n_l = l_{\text{av}}/2.54$  where  $2.54 \text{ Å}$  is the length of one ethylene unit in a polyethylene chain. The thickness of the lamellae of linear polyethylene strongly depends on the crystallization conditions, especially on the crystallization temperature. For example, an HDPE resin, when crystallized at a constant temperature of  $120^\circ\text{C}$ , initially produces lamellae with  $l_{\text{av}} \sim 220 \text{ Å}$  ( $\sim 90$  ethylene units), but after the resin is kept for three hours at this temperature the lamellae thicken to  $\sim 330 \text{ Å}$  or  $\sim 130$  ethylene units. If the crystallization is carried out at  $128^\circ\text{C}$ , the respective numbers are  $260 \text{ Å}$  ( $\sim 100$  ethylene units) and  $480 \text{ Å}$  ( $\sim 190$  ethylene units) [18].

This variability of lamella thickness is the principal reason why the melting points of polyethylene resins are usually measured during the second melting step. The complex “melting  $\rightarrow$  cooling (crystallization/annealing)  $\rightarrow$  second melting” proce-

ture is used to erase the previous thermal history of the sample. The first rapid melting of the resin is preferably followed by a stage of slow cooling/crystallization and annealing of the lamellae, and the melting curve is recorded after the lamellae are formed under standardized conditions. It is obvious also that the DSC crystallization conditions (slow cooling) cannot result in the formation of lamellae with a strictly constant thickness. Rather, HDPE lamellae have a certain distribution with respect to thickness (see Eq. 3.2) and the  $l_{av}$  value represents their average thickness.

Our understanding of the melting behavior of polyethylene resins is based on detailed experimental data on the melting of crystalline paraffins. Paraffins with a carbon atom number lower than about  $n-C_{100}$  crystallize in the fully extended form. These crystals can be viewed as analogs of polyethylene lamellae (without the folds). The length of these crystals depends, of course, on the carbon atom number of the paraffin molecule. From the theoretical point of view, the dependence between the melting temperature ( $T_m$ ) of a paraffin crystal and its crystal thickness  $l$  (or between the melting temperature of a polyethylene lamella and its thickness,  $l_{av}$ ) is given by the Thompson-Gibbs equation [18, 21]:

$$T_m(K) = T_m^\circ(1 - \chi/l) \quad (3.1)$$

Here  $T_m^\circ$  is the equilibrium melting temperature of the infinitely thick polyethylene crystal and  $\chi$  is a constant related to the free energy of the fold surface,  $\sim 125$  erg/cm<sup>2</sup>, and to the bulk free energy of fusion,  $2.8 \cdot 10^9$  erg/cm<sup>3</sup> [18]. Various estimations give the  $T_m^\circ$  range from 419.2 K [18] to 414.6 K [21]. In the case of polyethylene crystals, the  $\chi$  value in Eq. 3.1 depends on the crystallization conditions, and various empirical expressions are usually used to describe dependencies between experimental  $T_m$  of polyethylene and  $l_{av}$ . Several such expressions are described in the literature [16, 18, 22]; all of them provide quite close results.

It should be noted that when a polyethylene resin of a very high molecular weight is crystallized from the melt at a very high pressure, the thickness of its lamellae greatly increases. At the limit, such chains can also crystallize in the fully extended form and produce very thick crystals with melting points in excess of 142 °C [23, 24], which are similar to the predictions for  $T_m^\circ$  shown above.

Modeling DSC curves of HDPE resins is based on two assumptions:

1. There exists an average thickness of the crystalline lamella,  $l_{av}$  (Å) that is determined by the thermodynamics of chain folding and crystallization kinetics. The  $l_{av}$  for a given sample of linear polyethylene with a particular thermal history cannot be estimated strictly from the theoretical viewpoint; it can only be evaluated from the  $T_m$  value using Eq. 3.1, provided that  $T_m$  is experimentally measured under isothermal conditions. The average number of ethylene units in such a lamella,  $n_{av}$ , is  $l_{av}/2.54$ .

2. The thickness of different polyethylene lamellae in a given resin is not strictly uniform. One can assume that it is distributed according to the Gauss law [16]:

$$Fr(l) = [\sigma \cdot \sqrt{2\pi}]^{-1} \cdot \text{Exp}[-(l_{\text{av}} - l)^2/2\sigma^2] \quad (3.2)$$

where  $Fr(l)$  is the fraction of lamellae with thickness  $l$  (Å) and  $\sigma$  is the width of the thickness distribution. This assumption is based on the fact that melting curves of linear polyethylene samples always have a significant width, from 6 to 8 °C, which is higher than the width of DSC melting curves of low molecular weight organic crystals.

Plotting Eq. 3.2 in the coordinates “ $Fr(l)$  as a function of  $l$ ” gives a symmetric Gauss curve with a half-width of  $\sigma$ . However, DSC melting curves are plotted in different coordinates: “heat flow  $\Delta H$  (W/g) or heat capacity (J/K mol) as a function of temperature.” This peculiarity of the DSC coordinates requires a transformation of the Gauss function: instead of the dependence “ $Fr(l)$  as a function of  $l$ ” in Eq. 3.2, a different dependence “ $\Delta H$  as a function of  $T_m$ ” should be used. This change of coordinates [16] gives the following expression for the shape of the melting curve of linear polyethylene in the DSC coordinates:

$$\begin{aligned} \Delta H = T_m^0 \cdot \chi \cdot (T_m^0 - T_m)^{-2} / (\sigma \cdot \sqrt{2\pi}) \cdot \\ \text{Exp}\{-(T_m^0 \cdot \chi)^2 / 2\sigma^2 \cdot (T_m^0 - T_m^{\text{av}})^{-1} - (T_m^0 - T_m)^{-1}\}^2 \} \\ \text{as a function of } T_m \text{ (K)} \end{aligned} \quad (3.3)$$

Figure 3.2 compares two melting curves of linear polyethylene. The curve in Fig. 3.2(a) is the experimental curve of an HDPE resin prepared with a single-

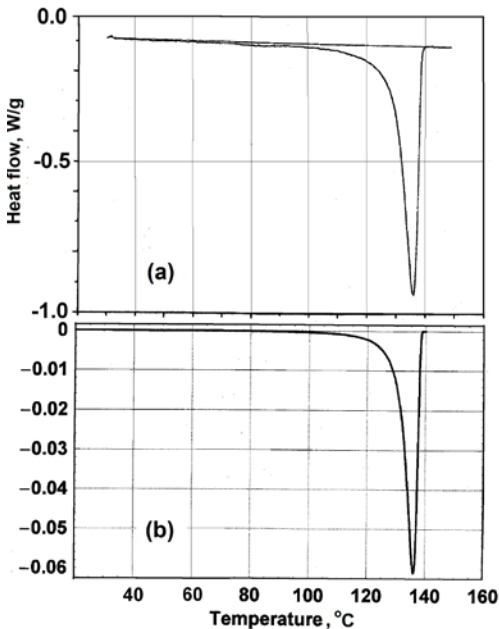


**Figure 3.2** Modeling the melting DSC curve of linear HDPE resin: (a) experimental DSC melting curve of linear polymer produced with single-site catalyst; (b) calculation with Eq. 3.3

site metallocene catalyst. The curve in Fig. 3.2(b) is calculated with Eq. 3.3 for  $T_m^{\text{av}} = 134.5^\circ\text{C}$ , using parameters of the Thompson-Gibbs equation from ref. [22]. The effective  $\sigma$  value in Eq. 3.3 is the sum of two numbers: the instrumental broadening (which is specific for a particular DSC instrument and for particular recording conditions) and the real  $\sigma$  value in Eq. 3.2 characterizing the distribution of lamella thickness. A comparison of the two curves in Fig. 3.2 shows that Eq. 3.3 provides an adequate model for the specific asymmetric shape of the melting curve of an HDPE resin.

Several features of DSC curves of HDPE resins require attention. Due to the nature of Eq. 3.3, plotting a Gauss function in the DSC coordinates results in a shift of the curve's maximum. The maximums of melting curves calculated with Eq. 3.3 are 1.0 to 1.5 °C higher than the  $T_m$  values used in the calculations. This peculiarity means that the real  $T_m^{\text{av}}$  values of HDPE resins, as well as those of medium density polyethylene (MDPE) resins with low  $\alpha$ -olefin content, are slightly lower than the temperatures at the maximums of their DSC curves.

The distortion of the Gauss function in the DSC coordinates described by Eq. 3.3 (see Fig. 3.2(b)) explains a noticeable difference in the shapes of the sides of DSC melting curves. The shape of such a curve at temperatures below the maximum is determined by the existence of lamellae that are thinner than the average lamella. On the other hand, the presence of thicker lamellae, with  $l > l_{\text{av}}$ , which melt at higher temperatures, is virtually unnoticed in the DSC coordinates. In the literature, the intercept of the tangent to the low-temperature side of the melting curve and its baseline is sometimes used as the position of the "melting point". This is the standard procedure when melting points of low molecular weight organic crystals or inorganic substances are measured. However, the existence of the distribution in the lamella thickness (Eq. 3.2) does not justify this practice in the case of polymers. The shape of the low-temperature side of the DSC melting curve of an HDPE resin is mostly determined by melting of thinner lamellae, and the positioning of the tangent to such curves is arbitrary.

### ■ 3.3 DSC Melting Curves and Melting Points of LLDPE and VLDPE Resins Produced with Single-Site Catalysts

Figure 3.3 shows melting points of a series of compositionally uniform ethylene/hexene copolymers produced with single-site metallocene catalysts. The copolymers contain from 0.5 to 3.5 mol % of hexene. Each melting temperature corresponds to the maximum at the melting curve. The melting point value decreases

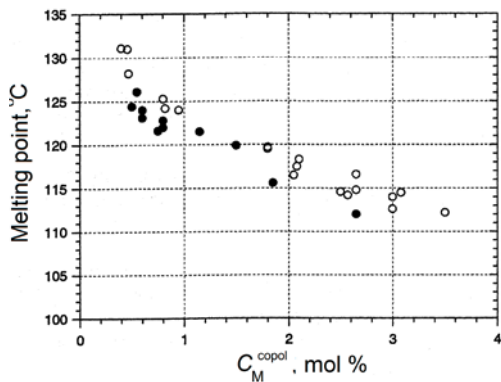


**Figure 3.3** Melting temperatures of ethylene/hexene copolymers produced with single-site catalyst; heating rates are 10 °C/min (●) and 2 °C/min (○)

sharply with an increase in the hexene content in the copolymers. The DSC model presented in this section provides an explanation for the steep dependence evident from Fig. 3.3.

Basic statistical expressions used for modeling the melting behavior of compositionally uniform ethylene/ $\alpha$ -olefin copolymers are presented in Section 1.7 of Chapter 1. For the goal of DSC modeling, a copolymer chain can be viewed as consisting of a set of monomer sequences: blocks of ethylene units,  $M-(E)_n-M$ , and blocks of  $\alpha$ -olefin units,  $E-(M)_m-E$ . All commercial LLDPE and VLDPE resins contain relatively small fractions of  $\alpha$ -olefins; their  $C_M^{\text{copolymer}}$  value varies from 2 to 10 mol % and most of their  $E-(M)_m-E$  blocks are very short, with  $m$  from 1 to 3. Crystallinity of all these materials, and therefore all their DSC features, are entirely determined by the presence of long ethylene blocks  $M-(E)_n-M$  in the copolymer chains.

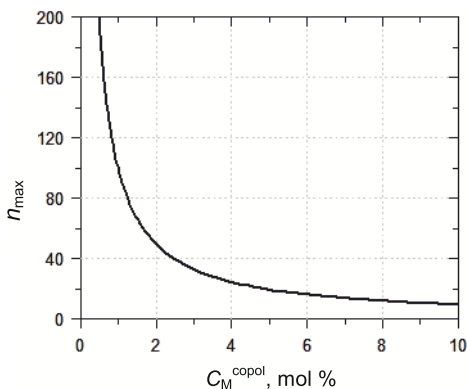
Section 1.7 gives two statistical functions that describe the distribution of ethylene units in blocks of different size. The first statistical function is  $\delta(E)_n$ , the fraction of ethylene units in blocks containing  $n$  monomer units,  $M-(E)_n-M$ , normalized to the total molar content of ethylene in the copolymer (Eq. 1.17), and the second function is  $\Sigma(E)_n$ , the fraction of ethylene units in the sum of all long ethylene blocks starting with a block containing  $n$  monomer units, that is, the fraction of ethylene units in the sum of blocks  $M-(E)_n-M$ ,  $M-(E)_{n+1}-M$ ,  $M-(E)_{n+2}-M$ , and so on (Eq. 1.18). Both these expressions contain a single variable, the molar percent of  $\alpha$ -olefin in the copolymer,  $C_M^{\text{copolymer}}$ . Two examples of the  $\delta(E)_n$  function represented by Eq. 1.17 are shown in Fig. 1.10: one for a copolymer with  $C_M^{\text{copolymer}} = 3$  mol %, which is a typical composition of an LLDPE resin, and another for a copolymer with  $C_M^{\text{copolymer}} = 8$  mol %, a typical composition of a VLDPE resin. A comparison of two curves in Fig. 1.10 demonstrates that the lower the  $\alpha$ -olefin content in a copolymer, the higher is the fraction of ethylene units in longer (crystallizable) blocks.

As Fig. 1.10 shows, every distribution of ethylene units in blocks  $M-(E)_n-M$  has a maximum which corresponds to the size of the most abundant ethylene sequence.

The position of this maximum is a function of the copolymer composition. The maximum of the  $\delta(E)_n$  function is positioned at  $d[\delta(E)_n]/dn = 0$ . Differentiation of Eq. 1.17 gives the position of the maximum:

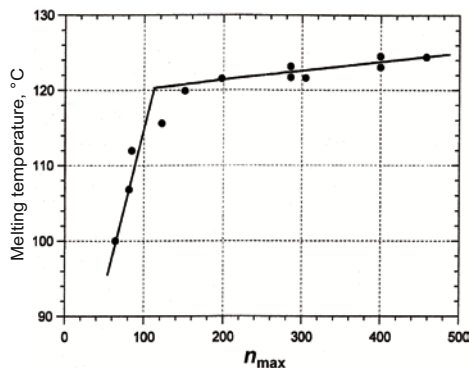
$$n_{\max} = -[\ln(1 - C_M^{\text{copol}}/100)]^{-1} \quad (3.4)$$

Figure 3.4 shows the plot of  $n_{\max}$  as a function of  $C_M^{\text{copol}}$ . As expected, the size of the most abundant ethylene block changes from a very large number,  $\sim 200$  ethylene units, at  $C_M^{\text{copol}} = 0.5$  mol % (an MDPE resin) to a quite small number,  $\sim 10$  ethylene units, at  $C_M^{\text{copol}} = 10$  mol % (a VLDPE resin).



**Figure 3.4** Plot of  $n_{\max}$  value as a function of comonomer content in the copolymer (Equation. 3.4)

Figure 3.5 plots melting temperatures of ethylene/hexene copolymers prepared with a single-site metallocene catalyst (data recorded at a  $10^\circ\text{C}/\text{min}$  heating rate) as a function of the  $n_{\max}$  value. This plot has two distinct ranges. When the copolymers have large  $n_{\max}$  values, from  $\sim 120$  to  $450$  (corresponding to  $C_M^{\text{copol}}$  from  $0.8$  to  $0.3$  mol %), the melting temperature remains approximately constant, in the  $120$  to  $125^\circ\text{C}$  range. When the copolymers have small  $n_{\max}$  values, below  $\sim 120^\circ\text{C}$  (corresponding to  $C_M^{\text{copol}}$  above  $0.8$  mol %), the melting temperature sharply decreases as the  $n_{\max}$  value decreases.



**Figure 3.5** Melting temperatures of ethylene/hexene copolymers prepared with metallocene catalyst as a function of  $n_{\max}$  value

The first part of this correlation (the flat range of the dependence) can be rationalized in view of the chain folding process during crystallization of polyethylene, which is described in the previous section. In the case of ethylene copolymers, the situation is complicated by several circumstances [18–20]:

1. The copolymers have ethylene units arranged in a variety of blocks, from very long to very short (Fig. 1.10).
2. The nature of the loops that connect straight segments of the ethylene blocks in the lamellae (Fig. 1.16) is not uniform; some loops include  $\alpha$ -olefin units (most of them isolated units in E-M-E blocks), other loops are parts of longer folded ethylene blocks.
3. The average thickness of the lamellae depends on the rate of crystallization from the melt, the same phenomenon that occurs for HDPE resins with linear chains.

To avoid the latter problems, the modeling of DSC melting curves of compositionally uniform LLDPE and VLDPE resins described below concentrates on the second part of the plot in Fig. 3.5, the steep dependence between  $T_m$  and  $n_{\max}$ . When the  $n_{\max}$  values are low, the dominant factor determining the melting temperature is the average size  $n$  of crystallizable ethylene blocks M-(E) $_n$ -M, rather than chain folding of long ethylene blocks and lamella thickening during crystallization.

### 3.3.1 Crystallization Process of Compositionally Uniform Ethylene/ $\alpha$ -Olefin Copolymers

The principal assumption of the LLDPE DSC model is that when ethylene blocks M-(E) $_n$ -M in these copolymers crystallize from the melt at a gradually decreasing temperature, the following sequence of events takes place (Table 3.1).

**Table 3.1** Crystallization of Different Blocks M-(E) $_n$ -M in Compositionally Uniform Ethylene/ $\alpha$ -Olefin Copolymers

Length of block, $n$	Limiting length	Type of crystallization and content
Long crystallizable blocks, $n \geq n_{\text{limit}}$	$n_{\text{limit}} \geq n_{\text{max}}$ (Eq. 3.4), content, Eq. 1.18	Primary, at high temperatures; shape is given by Eq. 3.3
Short crystallizable blocks	$n_{\text{limit}} > n > n_{\text{min}}$ , content, Eq. 1.17	Secondary, at low temperatures; shape is given by Eq. 3.5
Short noncrystallizable blocks, $n \leq n_{\text{min}}$	$n_{\text{min}} = 8$ to 9, content, Eq. 1.18	Blocks are too short to crystallize at $\sim 20^\circ\text{C}$

In the beginning of the crystallization process, at relatively high temperatures, all long ethylene blocks with  $n$  higher than a particular limit  $n_{\text{limit}}$  value rapidly crystallize in the chain-folded morphology and provide the framework for the spheru-

lite structure. One can assume that the  $n_{\text{limit}}$  value is slightly higher than the number of ethylene units in the most abundant ethylene sequence,  $n_{\text{max}}$ , which is defined by Eq. 3.4:  $n_{\text{limit}} = k \cdot n_{\text{max}}$  where  $k \sim 1.1$  to  $1.2$ . When the crystallized copolymer is subsequently melted, the  $T_{\text{m}}^{\text{av}}$  value for these lamellae consisting of long blocks is lower than that for linear polyethylene because the  $l_{\text{limit}} = 2.54 \cdot n_{\text{limit}}$  value for them is smaller than for linear polyethylene (see Eq. 3.1 and Fig. 3.5).

Melting curves of these thick lamellae are described by the same model as the one used in Section 3.2 to describe melting of HDPE resins. Similarly to the principal assumption of the model in Section 3.2, the number of ethylene units in these thick lamellae,  $n_{\text{limit}}$ , is not uniform but is also distributed according to the Gauss function in Eq. 3.2. When these thick lamellae melt during a DSC experiment, their melting curve is described by Eq. 3.3 (the Gauss function in the DSC coordinates) but with the maximum at a lower  $T_{\text{m}}^{\text{av}}$ , which is calculated with Eq. 3.1 for the  $n_{\text{max}}$  value. Special attention should be paid when these  $T_{\text{m}}^{\text{av}}$  values for ethylene copolymers are calculated. As Fig. 3.5 shows, the dependence between  $T_{\text{m}}$  and  $n_{\text{max}}$  in the range of the plot at  $n_{\text{max}} < 150$  is very steep, and even a small error in the measurement of the  $C_{\text{M}}^{\text{copol}}$  value (which is carried out either by the infrared or the nuclear magnetic resonance method) can strongly affect the estimation of both the  $n_{\text{max}}$  and the  $T_{\text{m}}$  value.

The second step of the DSC analysis, the stage of crystallization/annealing, is usually carried out at a constant low cooling rate. After the crystallization of long ethylene blocks with  $n \geq n_{\text{limit}}$  is completed, the temperature of the resin sample continues to decrease and the secondary crystallization process, crystallization of the remaining shorter M-(E)<sub>n</sub>-M blocks, begins (Table 3.1). This is a gradual and a much slower process. Such two-stage crystallization processes and their effect on experimental DSC data for melt-crystallized and solution-crystallized polyethylene resins have been thoroughly investigated [22]. Finally, even when the sample is cooled to room temperature, very short ethylene blocks M-(E)<sub>n</sub>-M with  $n$  lower than a particular minimum  $n$  value,  $n_{\text{min}} \sim 8$  to  $9$ , still do not crystallize, although these short blocks can be forced to crystallize at lower temperatures.

### 3.3.2 Model for Secondary Crystallization

This model is suitable only for ethylene copolymers with  $C_{\text{M}}^{\text{copol}}$  values higher than  $\sim 1$  mol %, which is in the range of the plot in Fig. 3.5 where the  $T_{\text{m}}$  value strongly depends on  $n_{\text{max}}$ . The model is based on the following assumptions:

1. Most of these shorter ethylene sequences crystallize in the fully extended form, like short paraffin molecules. Indeed, the  $n$  values in this range vary from  $\sim 50$  to  $120$ , very similar to the minimum equilibrium lamella size for linear polyethylene,  $90$  to  $100$  ethylene units. Surfaces of these thin lamellae do not contain tightly

folded segments of linear chains, as in Fig. 3.1; they consist of branching points in the copolymer chains, which are mostly single  $\alpha$ -olefin units, E-M-E sequences, and the end-groups of the chains.

2. If a resin sample is crystallized slowly, one can assume that each ethylene block with  $n_{\text{limit}} > n > n_{\text{min}}$  cocrystallizes only with ethylene blocks of approximately the same size and that they form lamellae of a relatively uniform small thickness,  $2.54 \cdot n \text{ \AA}$ . The possibility of such an orderly crystallization process depends on the relative values of two rates: the crystallization rate, which is quite high for polyethylene [20], and the cooling rate during the crystallization stage, which is preferably kept low. The fraction of ethylene units in the M-(E) $_n$ -M block, the  $\delta(\text{E})_n$  value in Eq. 1.17, gives the fraction of these units in the lamellae with the thickness of  $2.54 \cdot n \text{ \AA}$ .

The dependence between  $\delta(\text{E})_n$  and  $n$  is represented in a graphic form by the plots similar to those in Fig. 1.10. As discussed above, DSC melting curves are plotted in the coordinates “heat flow  $\Delta H$  as a function of temperature.” If one assumes that the heat of fusion per one ethylene unit does not depend on the lamella thickness, the second of the above assumptions signifies that the heat flow is proportional to the  $\delta(\text{E})_n$  value in Eq. 1.17. To produce a theoretical DSC melting curve for the thin lamellae formed during secondary crystallization, one has to change the coordinates in Fig. 1.10 from “ $\delta(\text{E})_n$  as a function of  $n$ ” to “ $\Delta H$  as a function of  $T_m$ ,” the same transformation as in the model for HDPE resins in Section 3.2. The final expression for the shape of the DSC melting curve of secondary crystals is [16]:

$$\Delta H = (C_M^{\text{copol}}/100)^2 \cdot [T_m^\circ \cdot (\chi/2.54)]^2 \cdot (T_m^\circ - T_m)^{-3} \cdot (1 - C_M^{\text{copol}}/100)^\theta$$

where  $\theta = T_m^\circ \cdot (\chi/2.54)/(T_m^\circ - T_m) - 1$ , as a function of  $T_m(\text{K})$ . (3.5)

### 3.3.3 Combined DSC Model for LLDPE and VLDPE Resins

A combination of Eqs. 3.3 and 3.5 describes the overall shape of DSC melting curves of compositionally uniform ethylene/ $\alpha$ -olefin copolymers. Figure 3.6(a) shows the experimental DSC melting curve of a compositionally uniform ethylene/hexene copolymer containing  $\sim 3.2$  mol % of hexene. The copolymer was prepared with a single-site metallocene catalyst. Figure 3.6(b) shows the calculated DSC curve using a combination of Eqs. 3.3 and 3.5. Curve 1 in Fig. 3.6(b) is calculated with Eq. 3.3; it describes the melting of thick lamellae formed during the primary crystallization process and is similar in shape to the curve in Fig. 3.2(b). Curve 2 in Fig. 3.6(b) is calculated with Eq. 3.5; it describes the melting of thin lamellae formed during the secondary crystallization process. The areas under the two parts of the calculated DSC curve correspond to the fractions of crystallizable material in the two types of lamellae formed during the primary and the secondary crystallization processes; 68 and 32%, respectively.

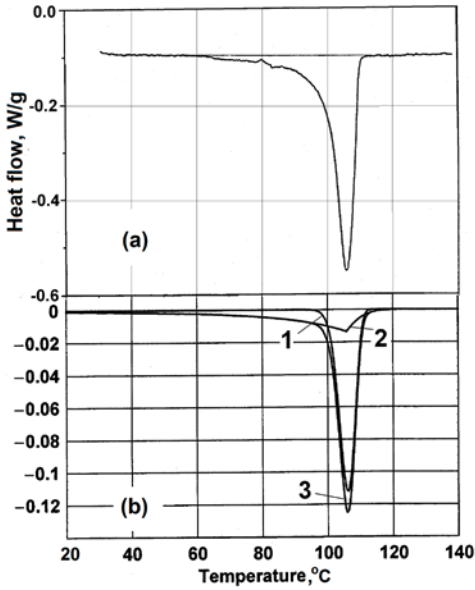


**Figure 3.6** Modeling DSC melting curve of compositionally uniform ethylene/ $\alpha$ -olefin copolymer: (a) Experimental DSC curve of ethylene/hexene copolymer containing 3.2 mol % of hexene prepared with single-site catalyst; (b) Curve 3 is calculated combined DSC curve [16]. Curve 1 is melting of primary lamellae (Eq. 3.3); Curve 2 is melting of secondary lamellae (Eq. 3.5).

Figure 3.7 gives another example of using the combined DSC model for a compositionally uniform ethylene/ $\alpha$ -olefin copolymer, an ethylene/hexene VLDPE resin containing 7 mol % of hexene. This material was also prepared with a single-site metallocene catalyst. A comparison of the two plots in Fig. 3.7 confirms that the combined model gives quite realistic results for ethylene plastomers as well, both

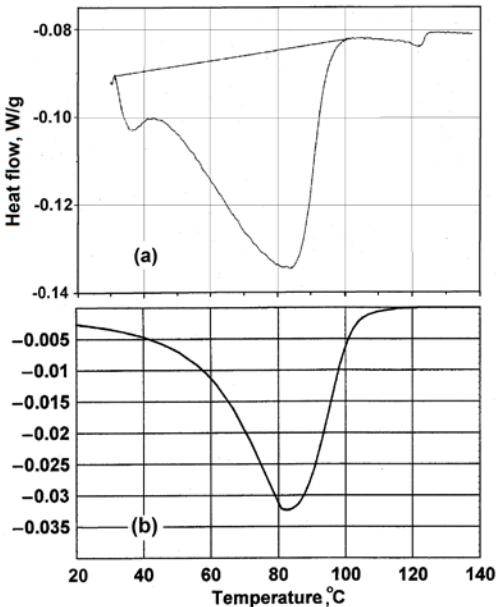


**Figure 3.7** Modeling DSC melting curve of ethylene/ $\alpha$ -olefin plastomer: (a) Experimental DSC curve of ethylene/hexene copolymer containing ~7 mol % of hexene prepared with single-site catalyst; (b) Calculated DSC curve [16], Eqs. 3.3 and 3.5

in terms of the shape of the DSC melting curve and the position of the peak maximum.

The combined model describing the DSC melting curve of a compositionally uniform LLDPE or VLDPE resin is not intended for the precise reproduction of the experimental data. Rather, it provides an interpretation of the experimental data in terms of the two-stage crystallization process described in Table 3.1.

### ■ 3.4 DSC Melting Curves and Melting Points of LLDPE Resins Produced with Multi-Site Ziegler-Natta Catalysts

The discussion in Section 1.8 of Chapter 1 shows that all ethylene/ $\alpha$ -olefin copolymers produced with supported titanium-based Ziegler-Natta catalysts, that is, the overwhelming majority of commodity LLDPE resins, as well as LDLPE resins produced with chromium oxide catalysts, are copolymer mixtures consisting of several components. The components have widely different compositions and molecular weights; see Tables 1.7 and 1.8, Figs. 1.12 and 1.13. Each such copolymer component is produced by a single population of active centers in the catalyst. The minimum number of the polymer components ranges from four to six and the  $\alpha$ -olefin content in them varies from 0.3 to over 15 mol % [7, 8]. Modeling DSC melting curves of such complex copolymer mixtures represents a significant challenge. Obviously, when these mixtures are completely melted and then the temperature is slowly decreased during the crystallization/annealing stage, the longest ethylene blocks in any copolymer component, but mostly the long blocks in the components with the lowest  $C_M^{\text{copol}}$  values, cocrystallize at higher temperatures and produce the thickest lamellae. Similarly, shorter ethylene sequences in all copolymer components cocrystallize at lower temperatures.

The simplest approach to modeling the melting process of such complex mixtures is similar to the model for compositionally uniform copolymers described in Section 3.3. Figure 3.8(a) shows the experimental melting curve of an LLDPE resin produced with a supported Ziegler-Natta catalyst. The average hexene content in the copolymer is 3.6 mol %. Table 3.2 gives the contents and the  $C_M^{\text{copol}}$  values of the copolymer components constituting this resin. Components IV and V have the lowest hexene content and mostly consist of long sequences of ethylene units. Thick lamellae formed from these ethylene sequences melt at a relatively high temperature; they are represented in Fig. 3.8(a) by a narrow peak at  $\sim 128^\circ\text{C}$ . This  $T_m$  value, which is usually cited as “the melting point of an LLDPE resin,” is  $17^\circ\text{C}$  higher than the melting point of a compositionally uniform resin of the same com-

position. (compare to Fig. 3.6). Thinner lamellae formed in this crystal mixture melt at lower temperatures; they produce a characteristic large low-temperature “tail” on the DSC curve in Fig. 3.8 (a).

**Table 3.2** Parameters Used in Modeling DSC Melting Curve of Multi-Component Ethylene/Hexene Copolymer with Average Hexene Content 3.6 mol %

Copolymer component:	I	II	III	IV	V
$C_{M}^{\text{copol}}$ , mol %	15	6.5	4.5	1.3	0.9
Fraction, %	5	20	44	23	8

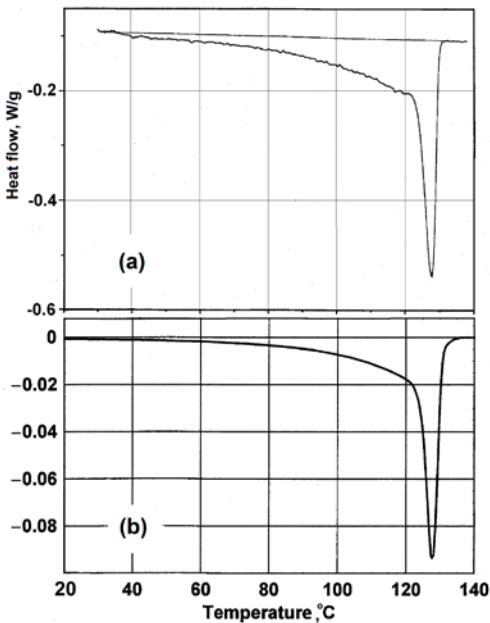


**Figure 3.8** Modeling DSC melting curve of LLDPE resin consisting of several components: (a) Experimental DSC curve of ethylene/hexene copolymer containing 3.6 mol % of hexene prepared with supported Ziegler-Natta catalyst; (b) Calculation for combination of components listed in Table 3.2

To model such melting curves, all crystalline lamellae in these complex mixtures are separated into two populations. The population containing the thickest lamellae is formed at high temperatures from relatively long ethylene blocks during the primary crystallization process. These long ethylene blocks are present mostly in macromolecules belonging to copolymer components IV and V (Table 3.2) but, to some degree, also in component III, although in a much smaller fraction. Component IV is the largest component in the copolymer mixture, and one can assume that the thickness of these lamellae is determined by the number of ethylene units in the most abundant blocks in component IV,  $n_{\text{max}}(\text{IV})$ . This  $n_{\text{max}}(\text{IV})$  value is calculated with Eq. 3.4. According to both DSC models described in Sections 3.2 and 3.3, the thickness of these lamellae is not uniform but is distributed according to the Gauss function distorted in the DSC coordinates (Eq. 3.3).

After these long ethylene blocks form thick lamellae and while the temperature of the resin sample continues to decrease, the secondary crystallization process starts and the population of thinner lamellae begins to form. The secondary crystallization process takes place over a wide temperature range,  $\sim 80^\circ\text{C}$ . Equation 3.5 describes the shape of melting curves of the secondary lamellae in the DSC coordinates. Short blocks  $\text{M}-(\text{E})_n-\text{M}$  in each of the copolymer components V, IV, III, and II contribute to this part of the melting curve proportionally to their content.

Thus, the DSC melting curve of such a multi-component mixture can be also represented by two overlapping distributions: one a Gauss curve in the DSC coordinates (Eq. 3.3) for the thickest lamellae and another one an asymmetric curve for a large number of various thinner lamellae (Eq. 3.5). The final modeling curve calculated for the copolymer mixture in Table 3.2 is shown in Fig. 3.8 (b). The high-temperature DSC peak represents melting of the thick lamellae consisting of long ethylene blocks ( $l \sim 280 \text{ \AA}$ ) that mostly come from copolymer components IV and V. The low-temperature tail in Fig. 3.8 (b) represents melting of the thinner lamellae, which mostly come from copolymer chains in component III ( $\sim 60\%$ ) and II ( $\sim 20\%$ ), as well as the shortest ethylene blocks in components IV and V ( $\sim 20\%$ ). As to component I in this copolymer mixture (Table 3.2), it has very high  $\alpha$ -olefin content and therefore is practically amorphous; it does not contribute anything to the crystallization process.

Although the approach to modeling DSC melting points of two types of resins (compositionally uniform LLDPE resins produced with metallocene catalysts and compositionally nonuniform LLDPE resins produced with Ziegler-Natta catalysts) is the same, it gives drastically different results. In the case of the compositionally uniform resins, the content of  $\alpha$ -olefin is approximately the same for all macromolecules in the resin. As a result, the length of the most abundant ethylene block  $n_{\text{max}}$  steeply decreases as the  $C_{\text{M}}^{\text{copol}}$  value increases (Eq. 3.4), and correspondingly, the melting point of such resins (the maximum point on the DSC curve) rapidly decreases with  $C_{\text{M}}^{\text{copol}}$  value (Fig. 3.3). On the other hand, sharp melting peaks of compositionally nonuniform resins (Fig. 3.8) are produced by the melting of the thickest lamellae from components IV and V (Table 3.2). Active centers in the catalysts that produce these Flory components copolymerize  $\alpha$ -olefins with ethylene very poorly [7, 8]; the comonomer content in these components is always low, and as a result, the respective  $T_{\text{m}}$  values are always high.

To illustrate this difference, Table 3.3 compares estimated melting points for two series of copolymers with  $C_{\text{M}}^{\text{copol}}$  values ranging from 0.5 to 4 mol %. The second row gives the calculated melting points of copolymers that are compositionally uniform. The third and the fourth rows describe compositionally nonuniform copolymers. The fourth row gives estimations of the peak melting points for the compositionally nonuniform copolymers. As described above, these melting points are mostly due to the melting of the longest lamellae formed by the crystallization of components IV and V.

**Table 3.3** Melting Points of Two Sets of Ethylene/ $\alpha$ -Olefin Copolymers

$(C_M^{\text{copol}})_{\text{av}}$ , mol %: Copolymer type	0.5	1.0	2.0	3.0	4.0
Compositionally uniform copolymer; $T_m$ , °C:	130	126	118	113	108
Components IV + V in compositionally nonuniform copolymer; $C_M^{\text{copol}}$ , mol %: <sup>*</sup>	0.2	0.4	0.6	0.8	0.9
Components IV + V in compositionally nonuniform copolymer, $T_m$ , °C:	132	130	128	127	126

<sup>\*</sup> $C_M^{\text{copol}}$  values for combination of components IV and V in copolymer mixtures with the same average  $C_M^{\text{copol}}$  values

Two conclusions follow from this comparison:

1. The average contents of  $\alpha$ -olefins in the sums of components IV and V are always much lower than the average values for the whole copolymers, the  $(C_M^{\text{copol}})_{\text{av}}$  values. As a result, the melting points of compositionally nonuniform LLDPE resins produced with Ziegler-Natta catalysts are always significantly higher than the melting points of compositionally uniform LLDPE resins produced with single-site catalysts.

2. As the  $(C_M^{\text{copol}})_{\text{av}}$  value for a compositionally nonuniform copolymer increases, the  $C_M^{\text{copol}}$  values for the combination of components IV and V also increase, but they always remain relatively low, 0.2 to 0.9 mol % in the examples in Table 3.3. The data in Fig. 3.5 show that this range of copolymer compositions corresponds to the flat part of the curve, where the  $T_m$  value changes relatively little with  $C_M^{\text{copol}}$ . As a result, the melting points of compositionally nonuniform LLDPE resins decrease relatively little as the average content of  $\alpha$ -olefin increases.

## References

1. Bortolussi, F., Broyer, J.-P., Spitz, R., Boisson, C., *Macromol. Chem. Phys.* (2002) 203, p. 2501
2. Piel, C., Karssenberg, F.G., Kaminsky, W., Mathot, V.B.F., *Macromolecules* (2005) 38, p. 6789
3. Koivumaki, J., *Polym. Bull.* (1996) 36, p. 12
4. Bensason, S., Minick, J., Moet, A., Chum, S., Hiltner, A., Baer, E., *J. Polym. Sci., Part B: Polym. Phys.* (1996) 34, p. 1301
5. Aitola, E., Puranen, A., Setälä, H., Lipponen, S., Leskelä, M., Repo, T., *J. Polym. Sci., Part A: Polym. Chem.* (2006) 44, p. 6569
6. Nomura, K., Itagaki, K., Fujiki, M., *Macromolecules* (2005) 38, p. 2053

7. Kissin, Y.V., *Alkene Polymerization Reactions with Transition Metal Catalysts* (2008) Elsevier, Amsterdam, Chapters 2, 3
8. Krentsel, B.A., Kissin, Y.V., Kleiner, V.I., Stotskaya, S.S., *Polymers and Copolymers of Higher  $\alpha$ -Olefins* (1997) Hanser, Munich, Chapter 8
9. Longo, P., Grassi, A., Oliva, L., *Makromol. Chem.* (1990) 191, p. 2387
10. Xu, G.X., Lin, S.A., *Macromolecules* (1997) 30, p. 685
11. Oliva, L., Immirzi, A., Tedesco, C., Venditto, V., Proto, A., *Macromolecules* (1999) 32, p. 2675.
12. Naga, N., Mizunuma, K., Sadatoshi, H., Kakugo, M., *Macromolecules* (1997) 30, p. 2197
13. Palza, H., Lopez-Majada, M., Quijada, R., Benavente, R., Perez, E., Cerrada, M.L., *Macromol. Chem. Phys.* (2005) 206, p. 1221
14. Rulhoff, S., Kaminsky, W., *Macromol. Chem. Phys.* (2006) 207, p. 1450
15. De Rosa, C., Auriemma, F., *Macromolecules* (2006) 39, p. 249
16. Kissin, Y.V., *J. Polym. Sci., Part B: Polym. Phys.* (2011) 49, p. 195
17. Ungar, G., Stejny, J., Keller, A., Bidd, I., *Science* (1985) 229, p. 386
18. Chivers, R.A., Barham, P.J., Martinez-Salazar, D., Keller, A., *J. Polym. Sci., Part B: Polym. Phys.* (1982) 20, p. 1717
19. Barham, P.J., Chivers, R.A., Jarvis, D.A., Martinez-Salazar, J., Keller, A., *J. Polym. Sci., Polym. Lett.* (1981) 19, p. 539
20. Barham, P.J., Jarvis, D.A., Keller, A., *J. Polym. Sci., Part B: Polym. Phys.* (1982) 20, p. 1733
21. Wunderlich, B. *Macromolecular Physics*, vol. 3 (Crystal Melting) (1980) Academic Press, New York
22. Mirabella, F.M., *J. Polym. Sci., Part B: Polym. Phys.* (2001) 39, p. 2800
23. Bassett, D.C., *Principles of Polymer Morphology* (1981) Cambridge University Press, Cambridge, Chapter 7
24. Wunderlich, B., Miello, L., *Makromol. Chem.* (1968) 118, p. 250

## 4

# Crystallinity Degree and Density of Polyethylene Resins

## 4.1 Crystallinity Degree

Most polyethylene resins are semicrystalline plastics. Their crystallinity degree varies from 5 to 10% for VLDPE resins to  $\geq 70\%$  for some HDPE grades.

### 4.1.1 Measurement Methods

The crystallinity degree of polyethylene resins is measured with several physical methods including wide-angle X-ray spectroscopy (WAX), differential scanning calorimetry (DSC), infrared spectroscopy (IR), solid-state  $^{13}\text{C}$ -nuclear magnetic resonance (NMR), ultrasonic method, etc. [1–12].

Figure 4.1 shows the X-ray diffractogram of an ethylene/octene LLDPE resin [3]. The spectrum contains three prominent features: two peaks, one at  $2\theta = 21.20^\circ$  (reflection from the  $\langle 110 \rangle$  plane of the orthorhombic cell) and another at  $23.55^\circ$  (reflection from the  $\langle 200 \rangle$  plane), both due to the crystalline phase of polyethylene; and a broad halo at  $2\theta \sim 19^\circ$  that is due to the amorphous phase. The crystal-

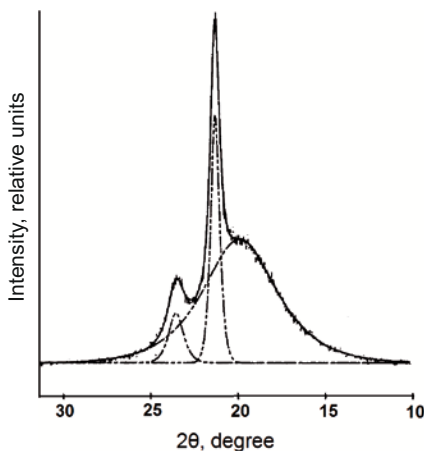


**Figure 4.1** X-ray diffraction pattern of ethylene/octene LLDPE resin [3]

linity degree,  $X$ , is calculated from the areas under the two crystalline-phase peaks,  $S\langle 110 \rangle$  and  $S\langle 200 \rangle$ , and the area under the amorphous halo:

$$X, \% = 100 (S\langle 110 \rangle + K_1 \cdot S\langle 200 \rangle) / (S\langle 110 \rangle + K_2 \cdot S\langle 200 \rangle + K_3 \cdot S\langle \text{halo} \rangle) \quad (4.1)$$

Values of parameters  $K_1$ ,  $K_2$ , and  $K_3$  are listed in Table 4.1.

**Table 4.1** Parameters in Equation 4.1

$K_1$	$K_2$	$K_3$	Ref.
1.43	1.43	0.69	[13, 14]
1.0	1.0	1.235	[2]
1.43	1.43	0.74	[12]
1.46	1.46	0.75	[1]

Figure 4.2 shows the DSC melting curve of an ethylene/hexene LLDPE resin. The heat of fusion,  $\Delta H$ , is calculated as the area under the curve. The crystallinity degree is calculated as  $X, \% = 100 \cdot (\Delta H / \Delta H_0)$  where  $\Delta H_0$  is the heat of fusion for perfectly crystalline polyethylene,  $\Delta H_0 = 283$  to  $302$  J/g ( $67.6$  to  $72.0$  cal/g) [3–6, 12, 15, 16]. The values of the crystallinity degree produced with the wide-angle X-ray and the DSC techniques correlate well in the crystallinity range between  $\sim 10$  and  $\sim 65\%$ , the typical range of MDPE, LLDPE, and VLDPE resins [3].

The  $^{13}\text{C}$ -NMR spin relaxation measurement of a solid polyethylene resin gives magnetization decay curves consisting of three segments: the fast initial decay associated with the amorphous component ( $T_1 \sim 0.3$  s); the intermediate range with

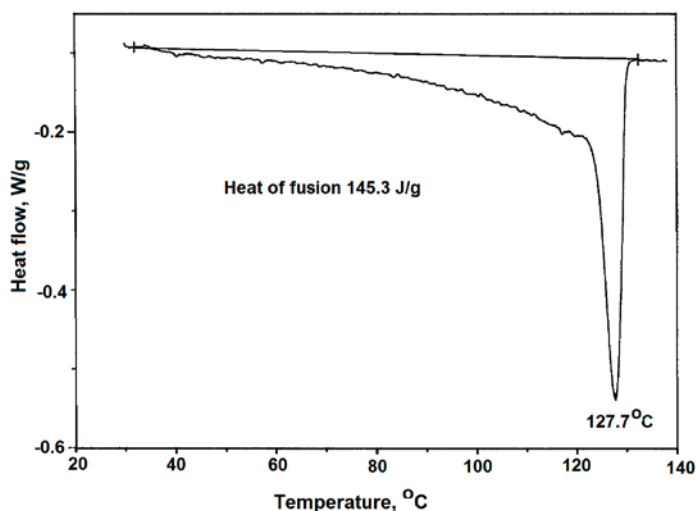


**Figure 4.2** DSC melting curve of ethylene/hexene LLDPE resin,  $C_M^{\text{copol}} = 3.5$  mol %

$T_i \sim 10$  s attributed to the interfacial material; and the range of slow decay due to the crystalline environment ( $T_i \sim 100$  to  $300$  s) [3, 17–19]. Plotting these data in the coordinates “logarithm of the peak height as a function of time” gives the crystallinity degree as the intercept of the slowest decay range [3, 11, 18]. Automated techniques based on this approach are widely used in industry for a rapid measurement of the crystallinity degree and density of polyethylene resins both in the pelletized and the granular form.

IR methods of the crystallinity degree estimation in press-molded polyethylene film (after annealing) are based on the relative absorbance of the  $1894\text{ cm}^{-1}$  band and different measures of the film thickness [2, 6, 12, 20]. If the film thickness is measured directly, the crystallinity degree is calculated as  $X, \% = 100 \cdot K'' \cdot A_{1894}/l$ , where  $A_{1894}$  is the absorbance of the  $1894\text{ cm}^{-1}$  band,  $l$  is the film thickness, in cm, and  $K''$  is an experimentally determined parameter, 16.4 [2] or 18.9 [12]. In other IR methods, the absorbance of the  $1303\text{ cm}^{-1}$  band is used as the internal thickness measure. The crystallinity degree is calculated as  $X, \% = 100 \cdot (A_{1894}/A_{1303}) / (A_{1894}/A_{1303} + K'')$  where  $K'' = 0.36$  [2] or  $0.30$  [12].

#### 4.1.2 Definition of Crystallinity Degree of LLDPE and VLDPE Resins Based on Copolymer Statistics

All commercially produced LLDPE and VLDPE resins are copolymers of ethylene with various  $\alpha$ -olefins, butene, hexene, octane, or methylpentene (see Table 1.1). The molar content of  $\alpha$ -olefin in the copolymers,  $C_M^{\text{copol}}$ , is relatively low, between 2.5 to 3.5 mol % in LLDPE resins and from 5 to 10 mol % in VLDPE resins.

As described in Chapter 1 (Section 1.7), any copolymer macromolecule containing ethylene units, E, and  $\alpha$ -olefin units, M, can be regarded from a statistical viewpoint as a combination of monomer blocks of two types:

1. Ethylene blocks:  $M-(E)_n-M$
2.  $\alpha$ -Olefin blocks:  $E-(M)_m-E$

with each block flanked by two monomer units of the opposite type.

Because the  $C_M^{\text{copol}}$  values for LLDPE and VLDPE resins are relatively low, the average number  $n$  of monomer units in ethylene blocks  $M-(E)_n-M$  is quite high whereas the average number  $m$  of  $\alpha$ -olefin units in blocks  $E-(M)_m-E$  is low; most of the  $\alpha$ -olefin units are isolated in the chains as E-M-E sequences. As a result, the crystallinity and melting point values (Chapter 3) of all LLDPE and VLDPE resins are entirely determined by the presence of long ethylene sequences in the copolymer chains. The statistical parameter which defines the physical meaning of the crystallinity degree is the fraction of ethylene units in the sum of all long ethylene

blocks starting with the block consisting of  $n$  units, that is the fraction of ethylene units in the sum of the blocks  $M-(E)_n-M$ ,  $M-(E)_{n+1}-M$ ,  $M-(E)_{n+2}-M$ , and so on.

$$\Sigma(E)_n = [(C_M^{\text{copol}}/100) \cdot (n - 1) + 1] \cdot \{[1 - (C_M^{\text{copol}}/100)]\}^{n-1} \quad (4.2)$$

A comparison of the experimentally measured crystallinity degree of compositionally uniform ethylene/hexene resins produced with a soluble metallocene catalyst and the computational results using Eq. 4.2 is shown in Fig. 4.3. The crystallinity degree of these polymers was measured by the DSC method at a heating rate of  $10^\circ\text{C}/\text{min}$ . Estimations of the  $n$  value were carried out under the assumption that the crystallization efficiency of polyethylene chains is approximately 0.6, a typical crystallinity level of rapidly crystallized HDPE resins determined from X-ray and DSC data. It follows from the plot that the size of the effective minimum length of the crystallizable ethylene sequences is  $\sim 50$  monomer units.

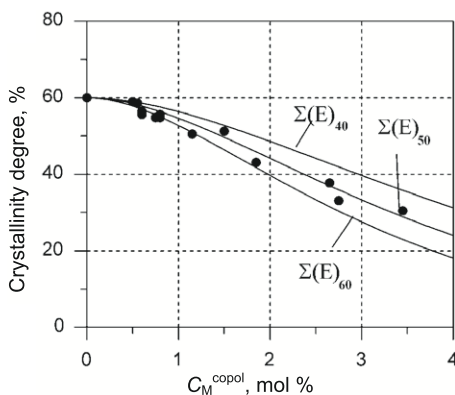


**Figure 4.3** Comparison of experimentally measured crystallinity degree of compositionally uniform ethylene/hexene resins (points) and computational results produced with Eq. 4.2

The packing efficiency of polyethylene chains obviously depends on the crystallization rate of a molten resin. If the polymer samples are crystallized from the melt at a low cooling rate,  $1$  to  $2^\circ\text{C}/\text{min}$ , and then melted at a rate of  $2$  to  $3^\circ\text{C}/\text{min}$  (instead of  $10^\circ\text{C}/\text{min}$  in Fig. 4.3), the packing efficiency increases to  $\sim 0.7$  and, correspondingly, the effective minimum length of the ethylene sequences decreases to  $\sim 40$  ethylene units.

## ■ 4.2 Density

Density is one of the primary characteristics of polyethylene resins. It is the basis of their classification (Chapter 1) and it is universally used as a singular parameter which instantly defines the application range of a given resin.

### 4.2.1 Measurement Methods

The density of polyethylene resins is traditionally measured by the flotation method in density-gradient columns according to ASTM Methods D1505-10 and D2839-10 and by the ultrasound method. Binary liquid systems in density-gradient columns include 2-propanol/water (suitable for the 0.79 to 1.00 g/cm<sup>3</sup> density range) and 2-propanol/ethylene glycol (0.79 to 1.11 g/cm<sup>3</sup> range). The technique is very simple, but has a significant disadvantage because it requires a long sample annealing time for a precise measurement and the measurement itself takes several hours. At the present time, the ultrasonic method (ASTM D4883-08) and the solid-state NMR method (Section 4.1.1) are widely used for a rapid estimation of the polyethylene crystallinity degree and density.

### 4.2.2 Physical Meaning of Polyethylene Density

The physical definition of the density of an ethylene/ $\alpha$ -olefin copolymer is usually based on the simplest model of a semicrystalline material. According to this model, any polyethylene resin consists of only two phases, the crystalline and the amorphous. The model assumes that the values of the specific volumes for the crystalline and the amorphous fractions of the copolymers are additive:

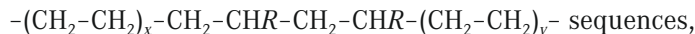
$$1/d = 0.01 \cdot X/d_{\text{cryst}} + (1 - 0.01 \cdot X)/d_{\text{amorph}} \quad (4.3)$$

where  $X$  is the crystallinity degree, %, and  $d$ ,  $d_{\text{cryst}}$ , and  $d_{\text{amorph}}$  are the density of the resin, the density of perfectly crystalline polyethylene, and the density of completely amorphous polyethylene, respectively. The  $d_{\text{cryst}}$  value is usually taken from the density data for linear alkanes (which produce perfect crystals),  $d_{\text{cryst}} = 1.0 \text{ g/cm}^3$ . The  $d_{\text{amorph}}$  value cited in the literature [1, 2, 5, 12, 14–16, 21, 22] varies in a narrow range from  $\sim 0.852 \text{ g/cm}^3$  (the density of highly branched isoalkanes) to  $0.856 \text{ g/cm}^3$ .

One should take into account that articles manufactured from polyethylene nearly always contain two crystalline modifications, the orthorhombic form (the dominant form) and the pseudomonoclinic form (see Section 1.9). Theoretical densities of these modifications are different;  $1.0 \text{ g/cm}^3$  for the orthorhombic form (the same as for crystalline linear paraffins) and  $0.965 \text{ g/cm}^3$  for the pseudomonoclinic form. The pseudomonoclinic modification is stable only at temperatures below  $50 \text{ }^\circ\text{C}$  and converts to the orthorhombic modification at higher temperatures. To achieve reproducibility in the density measurement, the pseudomonoclinic form should be completely converted into the orthorhombic form by annealing at  $80$  to  $100 \text{ }^\circ\text{C}$ .

The model represented by Eq. 4.3 has several shortcomings. First, it does not account for the fact that the presence of short-chain branches in ethylene/ $\alpha$ -olefin

copolymers leads to a small expansion of the **a** and the **b** axes of the orthorhombic cell and, hence, to a decrease of the theoretical  $d_{\text{cryst}}$  value compared to that for linear polyethylene [3, 15, 21, 22]. Second, amorphous regions in the copolymers mostly contain linear sequences of ethylene units,  $-\text{CH}_2-\text{CH}_2-$ , with occasionally inserted single or paired  $\alpha$ -olefin units,  $-\text{CH}_2-\text{CHR}-$ , that is,



and their density can be significantly higher than that of highly branched isoalkanes. To demonstrate this problem, Eq. 4.3, after its transformation,

$$d = d_{\text{cryst}} \cdot d_{\text{amorph}} \cdot [d_{\text{cryst}} - 0.01 \cdot X(d_{\text{cryst}} - d_{\text{amorph}})]^{-1} \quad (4.4)$$

was used to analyze the data for compositionally uniform ethylene/hexene copolymers produced with a single-site metallocene catalyst. Figure 4.4 plots the experimental data in the coordinates of Eq. 4.4 (the crystallinity degree was measured by DSC). Equation 4.4 indeed represents this dependence well. However, the plot shows that the density of the amorphous phase is  $0.877 \text{ g/cm}^3$  rather than  $0.852 \text{ g/cm}^3$  and the density of the crystalline phase is  $0.980 \text{ g/cm}^3$  rather than  $1.00 \text{ g/cm}^3$ . These differences emphasize significant problems associated with the use of the two-phase density model implicit in Eqs. 4.3 and 4.4.

The density of any polyethylene resin (except for that of ethylene homopolymers) is primarily a function of the copolymer composition. Figure 4.5 gives one example of this dependence for the simplest case, compositionally uniform ethylene/hexene copolymers produced with a single-site metallocene catalyst. In theory, this dependence is equivalent to the dependence between the crystallinity degree and the

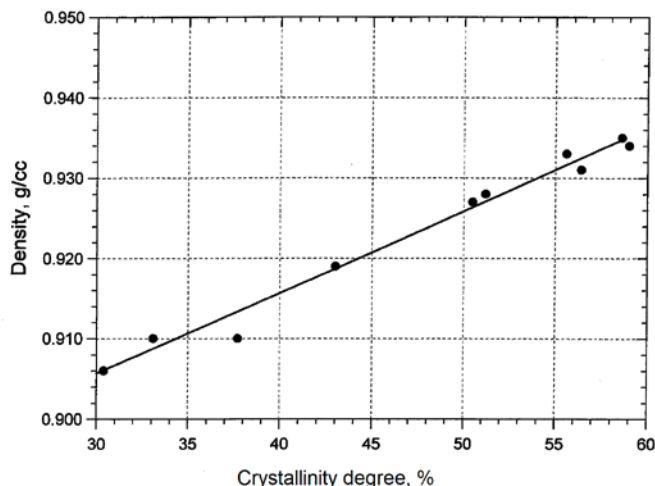


**Figure 4.4** Dependence between density and crystallinity degree for compositionally uniform ethylene/hexene LLDPE and MDPE resins in coordinates of Eq. 4.4

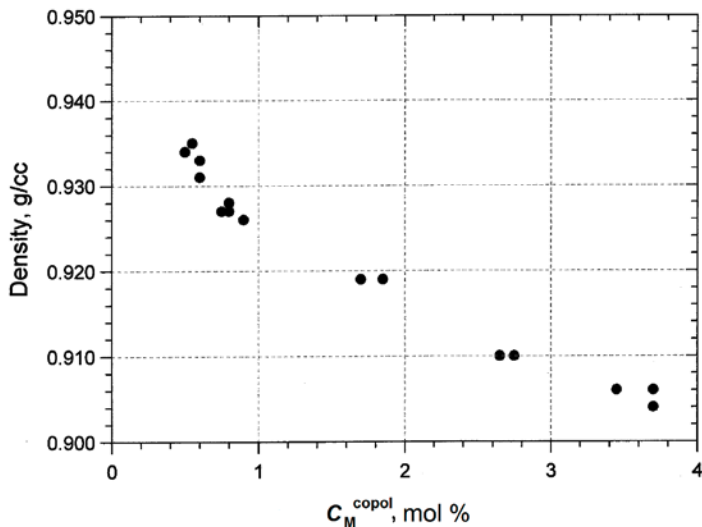


**Figure 4.5** Density of compositionally uniform ethylene/hexene LLDPE and MDPE resins produced with metallocene catalyst as a function of hexene content

copolymer composition shown in Fig. 4.3. The slope of the line in Fig. 4.5 does not depend much on the nature of the  $\alpha$ -olefin (except for propylene), but primarily depends on its content in the copolymer [6, 23].

Three other major factors that affect the resin's density are the thermal history of the sample, the molecular weight of the resin, and the degree of its compositional uniformity.

The role of the first factor is obvious: the faster the polyethylene melt crystallizes, the lower its crystallinity degree and density. When the density is measured, this effect can be avoided by controlled annealing of resin samples before the measurement.

The effect of the resin's molecular weight on its density is quite significant. For example, HDPE resins of a high molecular weight (with a high-load melt index  $I_{21}$  of  $\sim 1$ ) have a maximum crystallinity degree of 70%, and their maximum density is  $\sim 0.95$  g/cm<sup>3</sup>. However, both values increase to  $\sim 80\%$  crystallinity degree and a density of  $\sim 0.96$  g/cm<sup>3</sup> for HDPE resins of a lower molecular weight due to a higher crystallization rate and a better lamella packing. In contrast, HDPE resins of ultra-high molecular weight (over  $\sim 2 \cdot 10^6$ ) have perfectly linear polymer chains but their crystallinity degree is low,  $\sim 30\%$ , and their density is merely  $\sim 0.930$  to  $0.935$  g/cm<sup>3</sup>. In the case of LLDPE resins, the effect of the molecular weight (melt index) is usually accounted for empirically by adjusting the density of a given resin to the "apparent density" the resin would have if its melt index  $I_2$  were 1.0 [24].

The last factor, the uniformity of the compositional distribution in LLDPE resins, is also quite significant and cannot be easily accounted for. To demonstrate its sig-

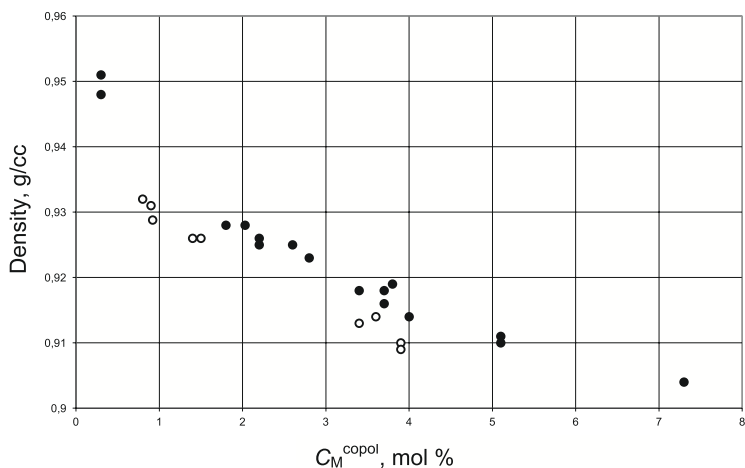


**Figure 4.6** Density of ethylene/hexene LLDPE and MDPE resins produced with Ziegler-Natta catalyst as a function of hexene content; [●] unfractionated resins; [○] narrow fractions

nificance, Fig. 4.6 shows the correlation between the density and the hexene content for ethylene/hexene LLDPE and MDPE resins produced with a Ziegler-Natta catalyst and compares it with the data for fractions of the same copolymers. The fractions were produced in a repeated extraction procedure and they are not perfectly uniform in terms of their compositional distribution. Nevertheless, the densities of the fractions are always noticeably lower than the densities of unfractionated polymers of the same composition. The effect of compositional uniformity on the density is clearly observed when the data in Figs. 4.5 and 4.6 are compared: the density of a compositionally uniform ethylene/ $\alpha$ -olefin copolymer is always lower by  $\sim 0.01$  to  $0.012 \text{ g/cm}^3$  compared to the density of a compositionally non-uniform resin with the same average  $\alpha$ -olefin content.

## References

1. Aggarwal, S.L., Tilley, G.P., *J. Polym. Sci., Part B: Polym. Phys.* (1955) 158, p. 17
2. Hendus, H., Schnell, G., *KGK, Kautsch. Gummi. Kunstst.* (1961) 51, p. 69
3. Clas, S.-D., Heyding, R.D., McFaddin, D.C., Russel, K.E., Scammell-Bullock, V.M., Kelusky, E.C., St-Syr, D., *J. Polym. Sci., Part B: Polym. Phys.* (1988) 26, p. 1271
4. Nowlin, T.E., Kissin, Y.V., Wagner, K.P., *J. Polym. Sci. Part A: Polym. Chem.* (1988) 26, p. 755
5. Ver Strate, G., Wilchinsky, Z.W., *J. Polym. Sci., Part A: Polym. Chem.* (1971) 9, p. 127
6. Beach, D.L., Kissin, Y.V., *J. Polym. Sci., Part A: Polym. Chem.* (1984) 22, p. 3027

7. Peacock, A., *Handbook of Polyethylene: Structures, Properties, and Applications* (2000) Google e-Book
8. Munaro, M., Akcelrud, L., *J. Polym. Res.* (2011) 15, p. 83
9. Lin, W., Cossar, M., Dang, V., *The J. Polym. Test.* (2007) 26, p. 814
10. Standard Test Method for Density of Polyethylene by the Ultrasound Technique (ASTM), D4883-08, <http://www.astm.org/Standards/D4883.htm>
11. Kitamaru, R., Horii, F., Murayama, K., *Macromolecules* (1986) 19, p. 636
12. Tokuzumi, T., *Kobunshi Ronbunshu* (1968) 25, p. 721
13. Nichols, J. B., *J. Appl. Phys.* (1954) 25, p. 340
14. Munos-Escalona, A., Parada, A., *Polymer* (1979) 20, p. 859
15. Bodily, D., Wunderlich, B., *J. Polym. Sci., Part A: Polym. Chem.* (1966) 4, p. 25
16. Runt, J., Harrison, I. R., Dobson, S., *J. Macromol. Sci., Part B. Phys.* (1980) B17, p. 99
17. Axelson, D. E., Mandelkern, L., Popli, R., Mathieu, P., *J. Polym. Sci., Part B: Polym. Phys.* (1983) 21, p. 2319
18. Axelson, D. E., Russell, K. E., *Prog. Polym. Sci.* (1985) 11, p. 221
19. Dujourdy, I., Bazile, J. R., Cohen-Addad, J. P., *Polym. Int.* (1999) 38, p. 558
20. Okada, T., Mandelkern, L., *J. Polym. Sci., Part A: Polym. Chem.* (1967) 5, p. 239
21. Vonk, C. G., In *Integration of Fundamental Polymer Science and Technology*. Lemstra, P. J., Kleintjens, L. A. (Eds.) (1988) Elsevier Applied Science, London
22. Vonk, C. G., Reynaers, H., *Polym. Commun.* (1990) 31, p. 190
23. Dreval, V. Y., Artamonova, S. D., Bobrov, B. N., Kleiner, V. I., Barancheyeva V. V., Litvinov, I. A., Krechekyan, A. S., *Polym. Sci.* (1991) 11, p. 2461
24. Elston, C. T., *U. S. Patent 3 645 882* (1972)

# 5

## End-Use Mechanical Properties of Polyethylene Film

End-use tests of blown and cast film manufactured from low density polyethylene (LDPE), high density polyethylene (HDPE), and linear low density polyethylene (LLDPE) usually include the dart impact test (dart drop test) and the tear test [1–4]. The results of these two tests are used in industry to grade the resins, determine their range of applications and price, and to compare polymerization catalysts and processes. In the case of LLDPE resins, both the dart impact strength and the tear strength of a resin are affected by numerous factors, such as the type of the  $\alpha$ -olefin, copolymer composition, average molecular weight, compositional uniformity, and the type of catalyst [5–7]. Although general information on the mechanical properties of polyethylene resins is readily available in commercial publications, various subtle effects of the resin's structure on the end-use film properties – effects that are often paramount for the successful applications of a given resin – are relatively poorly understood. A better understanding is hindered by the physical complexity of these two seemingly straightforward tests and also by the interaction of various structural factors of the resins that affect the test results.

### ■ 5.1 Mechanical Properties of Polyethylene Resins

Sections 1.9 and 1.10 in Chapter 1 describe principal morphological features and basic mechanical properties of semicrystalline polyethylene resins. Most of these resins are materials with expressed ductile properties. Morphological and mechanical changes in resin samples subjected to stretching are represented by the stress/strain curve shown in Fig. 1.18. The three defining points on the curve are the yield point, the end-of-necking point, and the breaking point. These points are characterized by six parameters:

1. The yield stress,  $\sigma_y$ , and the yield strain,  $\varepsilon_y$ ;
2. The necking stress,  $\sigma_n$ , and the end-of-necking strain,  $\varepsilon_n$ ; and
3. The breaking (tensile) stress,  $\sigma_{br}$ , and the breaking strain,  $\varepsilon_{br}$ .

The  $\varepsilon$  values in Fig. 1.18 are length ratios in the strained and the original sample:  $\varepsilon = \text{elongation} + 1$ ; the minimum  $\varepsilon$  value is 1.

Mechanical changes shown in Fig. 1.18 are accompanied by irreversible structural changes schematically represented in Fig. 1.19. After the yield point is passed, an area consisting of a highly oriented material (the neck) develops in the strained sample. As the stretching proceeds further, two morphological features of a semi-crystalline resin, the spherulites and the microfibrils (see Figs. 1.16 and 1.17), are gradually disassembled until all the material in the tested sample becomes highly oriented. This transformation occurs at a nearly constant stress  $\sigma_n$ . The last stage of the sample stretching is called strain hardening, which involves a simultaneous increase in the strain and the stress. At some point during this stage the oriented material finally breaks.

The length of the strain-hardening range,  $\varepsilon_{br} - \varepsilon_n$ , depends on the grade of the resin. HDPE resins break soon after the onset of strain hardening; their  $\sigma_y$  and  $\sigma_{br}$  values are relatively close. On the other hand, LLDPE resins have a relatively large strain-hardening range and their  $\sigma_{br}$  value is always much higher than the  $\sigma_y$  and  $\sigma_n$  values.

### 5.1.1 Effect of Testing Speed on Mechanical Properties

Both end-use mechanical tests of polyethylene film, the dart impact test and the tear test, are carried out at a high deformation speed (Sections 5.2 and 5.3). Relaxation phenomena in polyethylene are relatively slow, and some mechanical parameters of the resins depend on the deformation speed [8, 9]. These dependencies have been measured experimentally in the range of deformation speeds  $V$  from 0.5 to 150 cm/min (0.2 to  $\sim 60$  in/min) for several ethylene/hexene LLDPE resins, both for compositionally nonuniform resins produced with Ziegler-Natta catalysts and for compositionally uniform resins produced with metallocene catalysts. In most cases, the dependencies between  $V$  and the test parameters,  $\sigma$  or  $\varepsilon$ , can be represented by simple empirical relationships using as a standard a particular value at the deformation speed  $V_{\text{stand}}$  of 50.8 cm/min (20 in/min):

$$\sigma_y(V) = \sigma_y^{\text{stand}} + k(\sigma_y) \cdot \log(V/V_{\text{stand}}), \quad \text{the slope } k(\sigma_y) \approx 0.14 \quad (5.1)$$

$$\sigma_n(V) = \sigma_n^{\text{stand}} + k(\sigma_n) \cdot \log(V/V_{\text{stand}}), \quad \text{the slope } k(\sigma_n) \approx 0.11 \quad (5.2)$$

$$\varepsilon_n(V) - \varepsilon_y(V) = \varepsilon_n^{\text{stand}} - \varepsilon_y^{\text{stand}} + k(\varepsilon_n - \varepsilon_y) \cdot \log(V/V_{\text{stand}}) \quad (5.3)$$

with the slope  $k(\varepsilon_n - \varepsilon_y) \approx 0.5$  to  $0.6$ , depending on the LLDPE grade.

Three other parameters of the stress/strain curve,  $\epsilon_y$ ,  $\epsilon_{br}$ , and  $\sigma_{br}$  values, practically do not depend on the deformation speed.

### 5.1.2 Orientation in Polyethylene Film

Figure 5.1 shows the orientation pattern (orientation of the  $c$  axis, the direction of molecular chains in crystallites) in two types of articles manufactured from polyethylene: a blow-molded item and film.

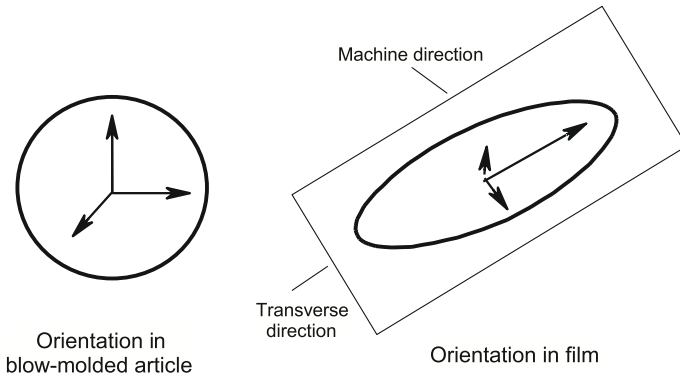


**Figure 5.1** Orientation distribution in blow-molded article and in film

Thick-walled, blow-molded articles are practically isotropic in terms of chain orientation. On the other hand, polymer chains in film are preferably oriented in the machine direction. The level of orientation depends on the resin type; it is highest in HDPE film and significantly lower in film made of LLDPE resins. Several examples of the orientation level in film are given in Table 5.1.

**Table 5.1** Chain Orientation in Crystalline Phase of Polyethylene Film; IR Measurement [14]

Resin type and density, g/cm <sup>3</sup>	Chain orientation in crystallites		
	Machine	Transverse	Thickness
HDPE	0.59 to 0.63	0.39 to 0.35	~0.02
LLDPE, ethylene/butene, 0.923	0.51	0.44	~0.05
LLDPE, ethylene/hexene, 0.918	0.44	0.35	~0.20

The preferred machine-direction orientation in the film explains differences in the film's mechanical properties, which play an especially important role in the measurement of the tear strength (Section 5.3). As an example, Table 5.2 gives experimental data on  $\epsilon_y$ ,  $\epsilon_n$ , and  $\epsilon_{br}$  values of LLDPE film slowly stretched in the machine

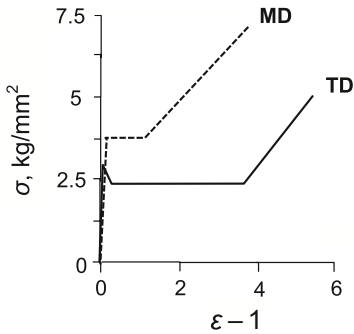


**Figure 5.2** Stress/strain curves of blown ethylene/hexene LLDPE film (density  $0.918 \text{ g/cm}^3$ ) measured in machine direction (MD) and transverse direction (TD); stretching speed  $2.1 \text{ cm/s}$

and transverse directions, and Fig. 5.2 shows experimental stress-strain curves of blown ethylene/hexene LLDPE film ( $0.918 \text{ g/cm}^3$  density) recorded at a stretching speed of  $2.1 \text{ cm/s}$  ( $0.83 \text{ in/s}$ ).

The properties of the film in the two directions are obviously different,  $\sigma_{br}(\text{machine}) > \sigma_{br}(\text{transverse})$  and  $\epsilon_n(\text{machine}) < \epsilon_n(\text{transverse})$ , reflecting differences in the chain orientation. Strain-hardening modules  $M_{\text{str-hard}} = (\sigma_{br} - \sigma_n)/(\epsilon_{br} - \epsilon_n)$  are also noticeably different in the two directions,  $M_{\text{str-hard}}(\text{machine}) \sim 1.3 \text{ kg/mm}^2$  and  $M_{\text{str-hard}}(\text{transverse}) \sim 1.8 \text{ kg/mm}^2$ . Several examples of such measurements for different grades of LLDPE film showed the same trends [1–7]. The highest degree of machine-direction orientation was observed in film manufactured from ultrahigh molecular weight HDPE resins ( $M_w$  over  $1.5 \cdot 10^6$ ). These resins can be processed at high pressure into film that is very strongly stretched and nearly perfectly oriented in the extrusion direction, both in the crystalline and amorphous phases [10, 11]. The data for molecular orientation in HDPE tubing and pipes are not available, but related data for polypropylene pipes also show a certain preferential (although relatively small) degree of molecular orientation in the extrusion direction [12].

**Table 5.2** Elongation Ratio for LLDPE Film (Ethylene/Butene Copolymer, Density  $0.918 \text{ g/cm}^3$ ) at Low Stretching Speed

Stretching direction	$\epsilon_y^a$	$\epsilon_n^a$	$\epsilon_{br}$
Machine	1.2 to 1.3	3.0 to 3.2	4.0 to 4.2
Transverse	1.3 to 1.4	5.5 to 6.0	6.5 to 7.0

a Relaxation to original length takes several seconds

## ■ 5.2 Dart Impact Strength of LLDPE Film

### 5.2.1 Description of Dart Impact Test

The procedure of the dart impact test according to the American Society for Testing and Materials (ASTM) D1709-04 and the International Organization for Standardization (ISO) 7765 is simple [13]. It is shown in Fig. 5.3. A dart with a rounded tip with a curvature radius of  $\sim 16$  mm ( $\sim 0.63$  in) and a thin long stem is loaded with several cylindrical metal weights and dropped from a height of 660 mm (26 in) perpendicularly to the surface of a piece of thin polymer film fastened between two rings 127 mm (5 in) in diameter. The weight of the dart can be varied over a wide range by changing the weights on its stem. The film is usually tested about 20 times at different dart weights until partial or complete rupture occurs. A special protocol for varying the dart weight and calculating the ratio of failure to survival incidents gives the average dart weight needed to break the film (the dart impact strength) [13]. Test results for different grades of polyethylene film vary over a wide range, from  $\sim 50$  to 70 to over 1,000 g. The second ASTM test, ASTM D4272, uses a heavier dart and measures the loss of kinetic energy of the dart by comparing the time of the dart's fall in the test and the time of its free fall in the absence of film.

Mechanical processes occurring during dart impact tests can be clearly seen when the tests are performed on film manufactured from high-quality LLDPE resins. Figure 5.3 shows schematics of various stages of the test. The dart approaches the film at a speed  $V_0$  of  $\sim 3.6$  m/s ( $\sim 142$  in/s). The central part of the film, 22 to 25 mm in diameter, clings to the semispherical surface of the dart head and remains undamaged during the test. At the first stage of the test, the dart bends the film until the stress at the circumference of the central (undamaged) film area exceeds the yield stress of the resin. After that, the area around the undamaged area begins to stretch (Stage 2 in Fig. 5.3). The work of stretching decreases the kinetic energy of the dart, and its speed rapidly decreases (see the quantitative estimation below). If

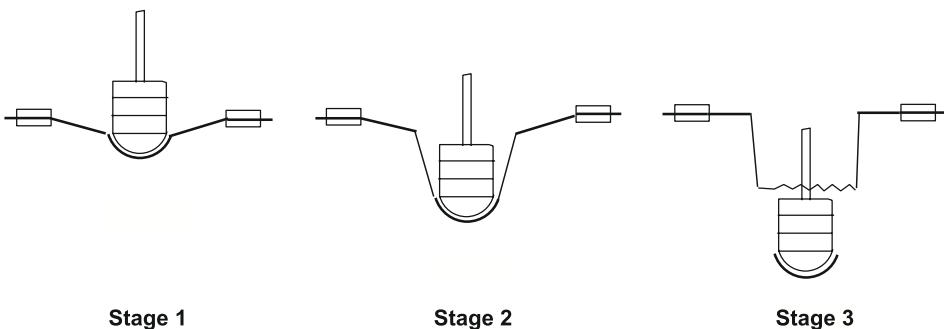


**Figure 5.3** Three stages of dart impact test of semicrystalline film

the kinetic energy of the dart is insufficient to break the film, the dart stops inside the cavity of the stretched film (Stage 2). In the case of film manufactured from a high-quality resin, the depth of the cavity can reach 35 to 40 mm (1.4 to 1.6 in). If the kinetic energy of the dart exceeds the work needed to break the film, the dart makes a round hole in the film and falls through, carrying with it the central undamaged part of the film clinging to its surface (Stage 3). The break line is usually located very close to the circumference of the undamaged film area.

*Deceleration of dart during the test* The falling dart decelerates rapidly during the test; its starting speed,  $V_0$ , is  $\sim 3.6$  m/s ( $\sim 142$  in/s) but is reduced to the final speed  $V_l = 0$  in a fraction of a second. The general expression for the dart speed as a function of the length  $l$  of the film subjected to stretching is [9]:

$$V_l = V_0 \cdot \{1 - 2 \cdot (l/d) \cdot (1 + 2 \cdot l/d) / [(\sigma_{br}/\sigma_n) \cdot (\sigma_{br}/\sigma_n - 1)]\}^{0.5} \quad (5.4)$$

Figure 5.4 gives several examples of the relative dart speed  $V_l/V_0$  as a function of the length  $l$  of the film subjected to irreversible stretching. The calculations were carried out for five  $\sigma_{br}/\sigma_n$  ratios typical for LLDPE resins of various types. The figure shows that the final stages of the dart impact test immediately before the film rupture proceed at a low speed.

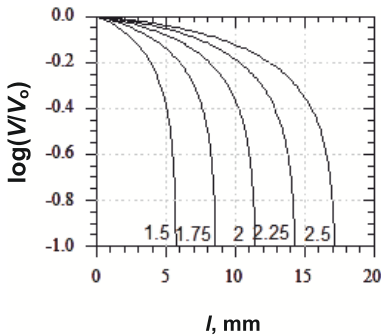


**Figure 5.4** Decrease of dart speed as a function of deformed polymer zone for five different  $\sigma_{br}/\sigma_n$  ratios

The size of the undamaged film area (diameter  $d$ ), which clings to the dart and is torn off when the film fails (Fig. 5.3), was estimated in dart impact experiments with several LLDPE films. The tests were carried out with widely varying dart weights, from very small (barely sufficient to initiate film stretching) to very large, exceeding the dart impact strength of the films. The tests showed that the undamaged area has an elliptical shape with the axis ratio of 1.1 to 1.2. The reason for the elliptical rather than the round shape is the orientation of the material during the film manufacture (Section 5.1.2); the mechanical parameters of the film in the machine direction and the transverse direction are different. The average diameter of the undamaged area is practically independent of the dart weight and of the damage the dart does to the film, see Table 5.3. Similar results were produced with other types of 25- and 38- $\mu$ m-thick films prepared from ethylene/butene, ethylene/

hexene, ethylene/octene, and ethylene/methylpentene resins; the  $d$  values range from 22.5 to 24.1 mm.

**Table 5.3** Effect of Dart Test Parameters on Diameter of Undamaged Zone in LLDPE Film (Density 0.917 g/cm<sup>3</sup>;  $l_2 = 1.0$  g/10 min)

Dart weight, g:	80	120	240	280
Film condition:	not broken	failed	failed	failed
$d^a$ , mm:	23/25	23/25	23/26	22/25

a Minor and major axes of the ellipse

Stretching of the film during a dart impact test is accompanied by strong orientation in the polymer sleeve created by the falling dart (Fig. 5.3, Stages 2 and 3). Analysis of polarized infrared (IR) spectra of the stretched area after the test shows a strong orientation of the polyethylene molecules in the direction of the sleeve. The degree of chain orientation in the test direction is comparable to that achieved by stretching the same film at a high speed to the end-of-necking point [14].

The dart impact test differs from the standard tensile test in two ways:

1. The stretching speed during the dart impact test varies; it is high in the beginning and decreases to zero at the end (if the dart weight is insufficient to break the film). Stretching of the film at the final moment of the test, immediately before the film failure (if the dart mass is slightly higher than the dart impact strength), proceeds at a relatively low speed.
2. Due to the geometrical design of the test, the cross section of the stretched polymer continuously increases as the film stretching progresses.

### 5.2.2 Model of Dart Impact Test

The simplest model of the dart impact test is based on two assumptions:

1. The dart impact strength of the film,  $m_{\text{dart}}$  (g), is defined as the maximum weight of a dart the film can stop without breaking, or the minimum weight of the dart needed to break through the film.
2. Tensile properties of LLDPE can be adequately described by the idealized standard stress/strain curve; see Section 1.10.

The idealized geometry of a film sample is shown in Fig. 5.5(a). Three parameters describe the sample: its thickness  $t$  (mm), the diameter of the test area  $D$  (mm), and the diameter of the central undamaged area of the film clinging to the tip of the dart,  $d$  (mm). In the beginning of the test, the stretching starts at the circumference of the cling area (Stage 1 in Fig. 5.3); the initial cross section of the stretching

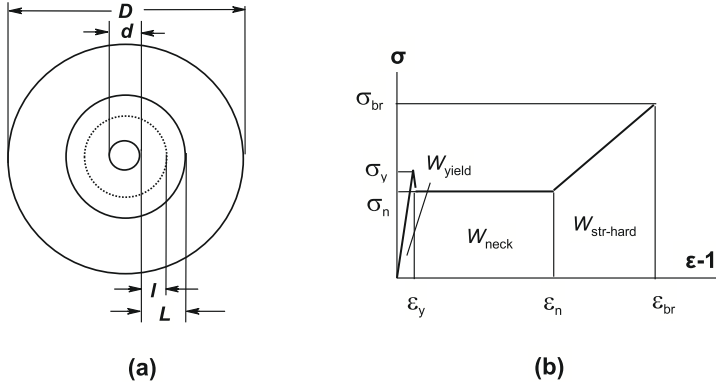


**Figure 5.5** (a) Geometry of dart impact testing; (b) Idealized stress/strain curve of polymer sample

material at this point is  $S_{min} = \pi \cdot d \cdot t$ . As the film stretching progresses, the cross section of the stretched zone increases in a linear manner starting from  $S_{min}$ . When the stretching proceeds to a distance  $l$  (assigned to the original film before the test), the cross section of the film undergoing the yielding is  $S_l = \pi \cdot (d + 2 \cdot l) \cdot t$ . The maximum possible stretching cross section, which is never achieved in real dart impact tests, is  $S_{max} = \pi \cdot D \cdot t$ .

The film breaks when the stress in the smallest cross section,  $S_{min}$ , reaches the breaking stress of the material,  $\sigma_{br}$ . The breaking force  $F_{br}$  at this moment is:

$$F_{br} = \sigma_{br} \cdot S_{min} = \sigma_{br} \cdot \pi \cdot d \cdot t \quad (5.5)$$

The same force  $F_{br}$  is applied to all cross sections of the sample. The maximum distance the necking zone propagates along the film radius ( $L$  in the original film [ $L < D$ ];  $X$  in the stretched film after stress relaxation,  $X/L = \epsilon_n$ ) is defined as:

$$F_{br} = \sigma_y \cdot \pi (d + 2 \cdot L) \cdot t = \sigma_{br} \cdot \pi \cdot d \cdot t \quad (5.6)$$

Equation 5.6 signifies that at the moment when the film fails, the yield stress  $\sigma_y$  is achieved at the distance  $L$  from the undamaged zone, at the point where the cross-section area is  $S_L = \pi (d + 2L) \cdot t$ . Equation 5.6 gives the following expressions for  $L$  and  $X$ :

$$L = (\sigma_{br} - \sigma_y) \cdot d / (2 \cdot \sigma_y) \quad \text{and} \quad X = \epsilon_n (\sigma_{br} - \sigma_y) \cdot d / (2 \cdot \sigma_y) \quad (5.7)$$

According to the definition of the dart impact strength, the weight of the dart sufficient for the film rupture,  $m_{dart}$ , is determined by an expression that equates the kinetic energy of the dart immediately before the impact with the total work of film stretching and breaking,  $W_{total}$ :

$$m_{dart} \cdot V^2 / 2 = W_{total} \quad (5.8)$$

where  $V$  is  $\sim 3.6$  m/s ( $\sim 142$  in/s).

This total work required to strain/stretch the film to the breaking point can be separated into four terms:

$$W_{\text{total}} = W_{\text{yield}} + W_{\text{elast}} + W_{\text{neck}} + W_{\text{str-hard}} \quad (5.9)$$

where  $W_{\text{yield}}$  is the work of elastic stretching to the yield point in all cross sections from  $S_{\text{min}}$  to  $S_{\text{max}}$  (Fig. 5.5(b));  $W_{\text{elast}}$  is the work of elastic stretching in all cross sections from  $S_L$  to  $S_{\text{max}}$ ;  $W_{\text{neck}}$  is the work of necking (i. e., stretching/orientation of the film material from  $l = 0$  to  $L$ ); and  $W_{\text{str-hard}}$  is the work of strain hardening, the additional stretching of the oriented part of the sample to the point when the stress in the smallest cross section reaches  $\sigma_{br}$ .

The second dart impact test, ASTM D4272 [13], measures the loss of kinetic energy,  $\Delta E$ , of the dart breaking the film by comparing the time of the dart fall in the test to the time of its fall in the absence of film. When all the  $\sigma$  values are presented in  $\text{kg}/\text{mm}^2$ , all cross sections in  $\text{mm}^2$ , and all distances in mm, the  $\Delta E$  value for a given film can be estimated as  $\Delta E = 9.81 \cdot 10^{-3} \cdot W_{\text{total}}$  (J).

Figure 5.5 (b) shows three components of the total work required to break the film for a polymer sample with a constant cross section. Analysis of mechanical testing in the case of a film sample with a varying cross section gives the following expressions for each term in Eq. 5.9 [9]:

$$W_{\text{yield}} = 0.125 \cdot \pi \cdot d^2 \cdot t \cdot \sigma_y \cdot (\varepsilon_y - 1) \cdot [(\sigma_{br}/\sigma_y)^2 - 1] \quad (5.10)$$

$$W_{\text{elast}} = 0.25 \cdot \pi \cdot t \cdot \sigma_y \cdot (\varepsilon_y - 1) \cdot (d + 2L)^2 \cdot \ln[D/(d + 2L)] \quad (5.11)$$

$$W_{\text{neck}} = 0.25 \cdot \pi \cdot \sigma_n \cdot (\varepsilon_n - \varepsilon_y) \cdot d^2 \cdot t \cdot [(\sigma_{br}/\sigma_y)^2 - 1] \quad (5.12)$$

$$W_{\text{str-hard}} = (1/6) \cdot \pi \cdot t \cdot (\varepsilon_{br} - \varepsilon_n) \cdot L \cdot [(d \cdot (2 \cdot \sigma_{br} + \sigma_n) + L \cdot (\sigma_{br} + \sigma_n))] \quad (5.13)$$

Obviously, the work of the dart impact is a complex function of all six parameters that characterize the stress/strain curve of a resin: the stresses and the strains at the yield, the end-of-necking, and the breaking points.

The simple model of the dart impact test represented by Eqs. 5.9 to 5.13 has an obvious shortcoming. It does not take into account the large decrease in the stretching speed of the film from the first moment, when  $V \sim 3.6$  m/s ( $\sim 142$  in/s), to the end-point of the test, when  $V \approx 0$ , and this effect on the mechanical properties of the film. The only term in Eq. 5.9 that requires a significant correction to account for the effect of the dart speed is the  $W_{\text{neck}}$  term in Eq. 5.12 [9].

Calculations of the dart impact strength show that different terms in Eq. 5.9 contribute to the impact strength of the film to different degrees. As an example, the following parameters characterize a typical ethylene/hexene LLDPE resin:

$$\sigma_y \sim 1.3 \text{ kg}/\text{mm}^2, \quad \varepsilon_y \sim 1.2, \quad \sigma_n \sim 1.2 \text{ kg}/\text{mm}^2, \quad \varepsilon_n \sim 6.0, \quad \sigma_{br} \sim 2.3 \text{ kg}/\text{mm}^2, \quad \varepsilon_{br} \sim 7.5.$$

The dart impact strength estimation for a 25- $\mu\text{m}$  (1-mil) film prepared from such a resin gives  $m_{\text{dart}} \sim 255$  g. This estimation compares well to the experimental data, which shows a strength from 150 to 200 g. The energy of the falling dart is spent

in the following ways: ~1.5% for stretching the film to the yield point; ~5.5% for elastic deformation of the nonoriented part of the film; ~76% for necking/orientation of the film; and ~17% for overcoming the resin's strain hardening.

Table 5.4 shows the effects of the sample diameter  $D$  and the diameter  $d$  of the undamaged area on the dart impact strength. A change in  $D$  over a wide range has virtually no effect on the calculated test results, provided that  $D \gg d$ . On the other hand, the size of the undamaged area,  $d$ , strongly affects the film strength value. However, the experimental results in Table 5.3 show that this parameter is mostly independent of the resin properties. Also, according to the model, the dart impact strength is proportional to the film thickness (Eqs. 5.10–5.13).

**Table 5.4** Effects of Test Parameters on Dart Impact Strength of 25- $\mu\text{m}$  (1-mil) Film<sup>a</sup>

Test parameters		Dart impact strength
$D$ , mm	$d$ , mm	$m_{\text{dart}}$ , g
100	23	241
125	23	244
150	23	246
127	20	186
127	23	244
127	26	410

<sup>a</sup> Resin parameters:  $\sigma_y = 1.1 \text{ kg/mm}^2$ ,  $\sigma_n = 1.0 \text{ kg/mm}^2$ ,  $\sigma_{br} = 2.0 \text{ kg/mm}^2$ ,  $\epsilon_y = 1.2$ ,  $\epsilon_n = 6$ ,  $\epsilon_{br} = 8$

### 5.2.2.1 Effects of Mechanical Properties of Resins

It follows from Eqs. 5.10 to 5.13 that all the six parameters,  $\sigma_y$ ,  $\epsilon_y$ ,  $\sigma_n$ ,  $\epsilon_n$ ,  $\sigma_{br}$ , and  $\epsilon_{br}$ , affect the dart impact strength in a complex way due to their contributions to the different terms in Eq. 5.9. Computational results for 25- $\mu\text{m}$  (1-mil) film in Table 5.5 demonstrate the effects of LLDPE mechanical properties on the calculated dart impact strength:

1. A pronounced yield threshold,  $\sigma_y/\sigma_n > 1$ , which is typical for many LLDPE resins (assuming the same values of  $\sigma_n$ ,  $\sigma_{br}$ ,  $\epsilon_y$ ,  $\epsilon_n$ , and  $\epsilon_{br}$ ), is detrimental to the dart impact strength, although this effect is not large in the typical range of the  $\sigma_y/\sigma_n$  ratio, 1.05 to 1.10.
2. The Young's modulus of the resin,  $M_Y$ , has virtually no effect on the dart impact strength.
3. An increase of resistance to orientation (a proportional increase of  $\sigma_y$  and  $\sigma_n$ ) produces a strong decrease in the dart impact strength. This trend explains why soft and easily stretchable resins with a uniform compositional distribution exhibit superior dart impact strength.

4. An increase of the orientation potential of a resin (an increase in  $\varepsilon_n$ ) does not affect the dart impact strength.
5. An increase of the tensile strength  $\sigma_{br}$  greatly improves the dart impact strength by allowing the orientation zone in the film to propagate further. An increase in the strain-hardening properties of a resin (a parallel increase of  $\sigma_{br}$  and  $\varepsilon_{br}$ ) produces a similar effect.

**Table 5.5** Effects of LLDPE Mechanical Properties on Dart Impact Strength

<i>Effect of yield threshold <math>\sigma_y/\sigma_n</math> at <math>\sigma_n = 1.0 \text{ kg/mm}^2</math>, <math>\sigma_{br} = 2.5 \text{ kg/mm}^2</math>, <math>\varepsilon_y = 1.2</math>, <math>\varepsilon_n = 5</math>, <math>\varepsilon_{br} = 7</math></i>				
$\sigma_y/\sigma_n$ :	1.02	1.05	1.10	1.15
$m_{\text{dart}}$ , g:	330	318	296	273
<i>Effect of Young modulus, <math>M_y = \sigma_y/(\varepsilon_y - 1)</math></i>				
$\sigma_y/(\varepsilon_y - 1)$ :	7.3	5.5	4.5	3.4
$m_{\text{dart}}$ , g:	293	296	299	304
<i>Effect of resistance to orientation (proportional increase of <math>\sigma_y</math> and <math>\sigma_n</math> at <math>\sigma_y/\sigma_n = 1.1</math>)</i>				
$\sigma_n$ , $\text{kg/mm}^2$ :	0.8	1.0	1.2	1.4
$m_{\text{dart}}$ , g:	500	296	217	152
<i>Effect of increase of orientation potential</i>				
$\varepsilon_n$ :	4.0	6.0	8.0	
$m_{\text{dart}}$ , g:	298	294	289	
<i>Effect of increase of tensile strength</i>				
$\sigma_{br}$ , $\text{kg/mm}^2$ :	2.0	2.5	3.0	
$m_{\text{dart}}$ , g:	203	372	764	

### 5.2.2.2 Comparison of Film Made from Ethylene/Butene and Ethylene/Hexene Copolymers

LLDPE film manufactured from ethylene/butene copolymers is inferior in dart impact strength compared to film manufactured from ethylene/hexene copolymers of the same composition and crystallinity degree (density). The average dart impact strength of 25- $\mu\text{m}$  blown film made from an ethylene/butene copolymer is 80 to 120 g, whereas this parameter for blown film from a common ethylene/hexene copolymer is 150 to 200 g and can reach 400 to 500 g for film from high-strength ethylene/hexene copolymers prepared with special types of Ziegler-Natta catalysts [15]. Table 5.6 lists the mechanical properties of several resins of a different type. The two ethylene/butene resins and the first of the ethylene/hexene resin were produced with the same catalyst; they are similar in density, degree of crystallinity, and molecular weight. The resins have similar yield and necking parameters, but differ noticeably in tensile properties; the ethylene/butene copolymers have a

~30% lower breaking stress. The results in Table 5.6 can be interpreted in the following way. The work required to start a neck,  $W_{\text{yield}}$ , and the work required to stretch elastically the undeformed part of the film,  $W_{\text{elast}}$  are practically the same for both types of film because their yield parameters  $\sigma_y$  and  $\varepsilon_y$  are similar. The film manufactured from an ethylene/butene resin breaks easier in a dart impact test than the film from an ethylene/hexene resin primarily because the breaking stress  $\sigma_{br}$  of the former resin is lower. As a result, the work of necking/orientation,  $W_{\text{neck}}$ , for the film from the ethylene/butene resin is two times lower. The work required to overcome strain hardening,  $W_{\text{str-hard}}$ , is also lower by a factor of 1.5 to 2 for the film from an ethylene/butene copolymer.

**Table 5.6** Mechanical Properties and Estimated Dart Impact Strength 25- $\mu\text{m}$  (1-mil) Film from Compositionally Nonuniform Ethylene/ $\alpha$ -Olefin Resins (Density 0.918 g/cm<sup>3</sup>)

Resin <sup>a</sup>	Mechanical properties <sup>b</sup>						Estimated dart impact parameters <sup>b</sup>					
	$\sigma_y$	$\varepsilon_y$	$\sigma_n$	$\varepsilon_n$	$\sigma_{br}$	$\varepsilon_{br}$	$m_{\text{exp}}$	$m_{\text{calc}}$	$W_{\text{yield}}$	$W_{\text{elast}}$	$W_{\text{neck}}$	$W_{\text{str-hard}}$
E/B	1.01	1.27	0.94	6.4	1.53	9.9	~100	160	2	8	67	29
E/B	1.03	1.36	0.98	5.1	1.56	8.9	~120	105	2	14	39	14
E/H	1.20	1.45	1.04	5.7	2.39	8.7	~200	320	7	23	136	43
E/H	1.24	1.40	1.05	5.3	2.94	8.7	~580	640	12	25	229	157

a E/B – ethylene/butene resins, E/H – ethylene/hexene resins

b All  $\sigma$  values are in kg/mm<sup>2</sup>, all  $W$  values are in kg · mm, both  $m_{\text{dart}}$  values are in g

The last two rows in Table 5.6 compare the results for film made from two different ethylene/hexene copolymers; the first one a resin produced with a standard Ziegler-Natta catalyst and another one a “super-strength” resin produced with a modified catalyst [15]. The two resins are identical in most of their tensile parameters. The superior dart impact strength of film made from for the “super-strength” resin is determined by a ~20% higher  $\sigma_{br}$  value and, respectively, by a higher contribution of  $W_{\text{neck}}$  and  $W_{\text{str-hard}}$  terms to the  $W_{\text{total}}$  value (Eq. 5.9).

### 5.2.2.3 Effect of Copolymer Composition

The dart impact strength of film from all ethylene/ $\alpha$ -olefin resins of a similar average molecular weight significantly increases as the  $\alpha$ -olefin content in them increases; that is, when their density and the crystallinity degree decrease [1, 2, 5, 6]. The data in Table 5.7 provide an explanation of this dependence. As the butene content in an ethylene/butene copolymer increases from ~3.5 to 4.4 mol %, all the  $\sigma$  values of the material decrease while all the  $\varepsilon$  values remain essentially the same. Paradoxically, the mechanically weaker film has a higher dart impact strength (its  $W_{\text{neck}}$  and  $W_{\text{str-hard}}$  values are higher) because the lower  $\sigma_y$  value of the material allows the film to stretch farther under the falling dart (and to absorb

more of the dart's energy) before the stress in the smallest cross section of the film reaches  $\sigma_{br}$ . A still further increase in the butene content to  $\sim 5.5$  mol % decreases all the  $\sigma$  values even more, but the dart impact strength value remains approximately the same.

**Table 5.7** Effect of Resin Density and Copolymer Composition on Mechanical Properties and Dart Impact Strength of 25- $\mu\text{m}$  (1-mil) Film from Compositionally Nonuniform Ethylene/Butene Copolymers

Property <sup>a</sup>	Mechanical properties <sup>b</sup>							Estimated dart impact strength <sup>b</sup>				
	$\sigma_y$	$\varepsilon_y$	$\sigma_n$	$\varepsilon_n$	$\sigma_{br}$	$\varepsilon_{br}$	$m_{exp}$	$m_{calc}$	$W_{yield}$	$W_{elast}$	$W_{neck}$	$W_{str-hard}$
0.921/3.5	1.32	1.14	1.07	5.7	1.91	8.9	$\sim 120$	145	1	5	62	27
0.917/4.4	0.96	1.33	0.89	5.4	1.75	8.9	$\sim 280$	240	4	12	87	56
0.910/5.5	0.64	1.53	0.60	5.8	1.35	8.9	$\sim 230$	235	6	15	82	53

a Density,  $\text{g}/\text{cm}^3/C_M^{copol}$ , mol %

b All  $\sigma$  values are in  $\text{kg}/\text{mm}^2$ , all  $W$  values are in  $\text{kg} \cdot \text{mm}$ , both  $m_{dart}$  values are in g

The same effect is characteristic for film made from ethylene/hexene LLDPE resins. An increase of the hexene content from 2.3 to 3.2 mol % and the respective decrease in density from 0.923 to 0.917  $\text{g}/\text{cm}^3$  results in a significant decrease of all three  $\sigma$  values. This change leads to an increase of the calculated dart impact strength from  $\sim 230$  to  $\sim 290$  g.

#### 5.2.2.4 Compositionally Uniform and Compositionally Nonuniform Resins

LLDPE resins of high compositional uniformity are produced with single-site metallocene catalysts. Table 5.8 lists the mechanical properties of several resins of this type and compares their estimated and experimentally measured dart impact strength. A comparison with the data in Table 5.6 and in Fig. 5.6 shows that, overall, compositionally uniform resins are softer and are more easily stretched (their  $\sigma_y$  and  $\sigma_n$  values are lower). However, their necking range is typically shorter

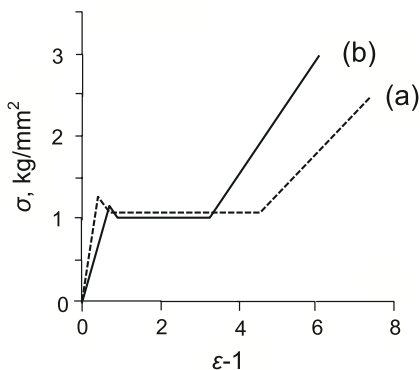


**Figure 5.6** Stress/strain curves for ethylene/hexene copolymers of the same crystallinity degree (density): (a) Compositionally nonuniform resin; (b) Compositionally uniform resin

( $\varepsilon_n \sim 4.5$  rather than 5.5), and the strain-hardening range,  $\varepsilon_{br} - \varepsilon_n$ , is longer, indicating that resins of this type exhibit more expressed rubber-like properties in the oriented state.

The high dart impact strength (both experimentally determined and predicted by the model) for film made from such materials is mostly attributed to their strain-hardening properties; the  $W_{\text{str-hard}}$  term in the  $W_{\text{total}}$  value (Eq. 5.9) for them is significantly higher than for film from compositionally nonuniform LLDPE resins.

**Table 5.8** Mechanical Properties and Dart Impact Strength of 25- $\mu\text{m}$  (1-mil) Film from Compositionally Uniform Ethylene/ $\alpha$ -Olefin Resins

Resin <sup>a</sup>	Mechanical properties <sup>b</sup>							Estimated dart impact strength <sup>b</sup>				
	$\sigma_y$	$\varepsilon_y$	$\sigma_n$	$\varepsilon_n$	$\sigma_{br}$	$\varepsilon_{br}$	$m_{\text{exp}}$	$m_{\text{calc}}$	$W_{\text{yield}}$	$W_{\text{elast}}$	$W_{\text{neck}}$	$W_{\text{str-hard}}$
E/H, 0.917	1.14	1.93	1.02	4.6	3.04	7.8	>800	830	33	57	263	197
E/H, 0.916	1.03	1.80	1.00	4.4	2.76	8.1	>800	720	26	44	200	204
E/MP, 0.914	0.96	1.46	0.89	4.3	2.33	7.6	>800	460	11	11	136	131

a E/H - ethylene/hexene copolymers, MP - ethylene/methylpentene copolymer; density in  $\text{g}/\text{cm}^3$

b All  $\sigma$  values are in  $\text{kg}/\text{mm}^2$ , all  $W$  values are in  $\text{kg} \cdot \text{mm}$ ,  $m_{\text{dart}}$  values are in  $\text{g}$

The model of the dart impact test has several deficiencies. It describes a perfect film break taking place along the circumference of the cling zone (Fig. 5.3). In reality, such a break is observed only for compositionally uniform resins, which produce weakly oriented film. Most other types of blown LLDPE film become partially oriented in the manufacturing process. When a dart impacts such a film, it often produces one or two cracks stretched in the machine direction of the film tangentially to the cling zone. The formation of the cracks qualifies such tests as a failure, although no complete breaking of the films really occurs. The degree of orientation in the film (and the probability of film cracking) increases with decreasing  $\alpha$ -olefin content in the copolymers, increasing the resin crystallinity degree (density), and increasing the tendency to orientation during the film manufacture. This phenomenon explains discrepancies between high dart impact strength predictions for MDPE film and its relatively low experimentally measured “dart impact strength,” which in reality should be called “dart-cracking strength.”

## ■ 5.3 Tear Strength of LLDPE and LDPE Film

The tear strength is the second important end-use mechanical parameter of blown and cast film manufactured from HDPE, LLDPE, and LDPE resins [1–4]. Commercial publications providing general data on properties of polyethylene resins usually contain the results of tear strength; for example, see refs. [5–7]. However, all this information is strictly empirical and provides practically no insight with regard to possible correlations between the resin structure and its basic mechanical properties on one side and its end-use film properties on the other.

### 5.3.1 Description of Tear Test

The Elmendorf tear test is carried out according to ASTM D1922 and ISO 6383-2 on a special apparatus following a standard procedure [16]. Several rectangular samples 76 mm (3") in width and 63 mm (2.5") in length are cut from a roll of film in two directions: the machine direction of the roll and the transverse direction. The principal part of the Elmendorf apparatus is a pendulum with an arm length of 40.6 cm (16 in). The weight of the pendulum can be varied from 200 to 1,600 g depending on the tear strength of the film. The pendulum is fixed in the horizontal position, and the long edge of the film is fastened by two clamps (see Fig. 5.7 (a)), one attached to the pendulum and another to the body of the apparatus. A cut is made with a razor in the middle of the wide side of the film. The cut leaves the undamaged length of the film equal to 43 mm (~1.7 in). The end of the cut, the point where the tear starts, extends ~5 mm beyond outer edges of the clamps.

When the pendulum is released, its swing motion rapidly tears the uncut length of the film, as shown in Figs. 5.7 (b) and 5.7 (c). Due to the geometry of the Elmendorf apparatus, the film is completely torn when the pendulum reaches the lowest point of its swing. Without the film, the linear speed at this point would be the highest, ~1.2 m/s (~in/s), but the film-tearing process slows down the pendulum. The duration of the single test is less than 0.5 s. The energy loss of the pendulum is measured and used to calculate the tear strength of the film. Test results for several samples of the same film are averaged and presented as the weight of the pendulum, in g, which is sufficient to bring the pendulum to a halt at the moment when the film is completely torn.

### 5.3.2 Physical Details of Tear Test

The principal goal in the analysis of the tear process is to visualize all the steps occurring during film tearing in the terms conventionally used to describe stand-

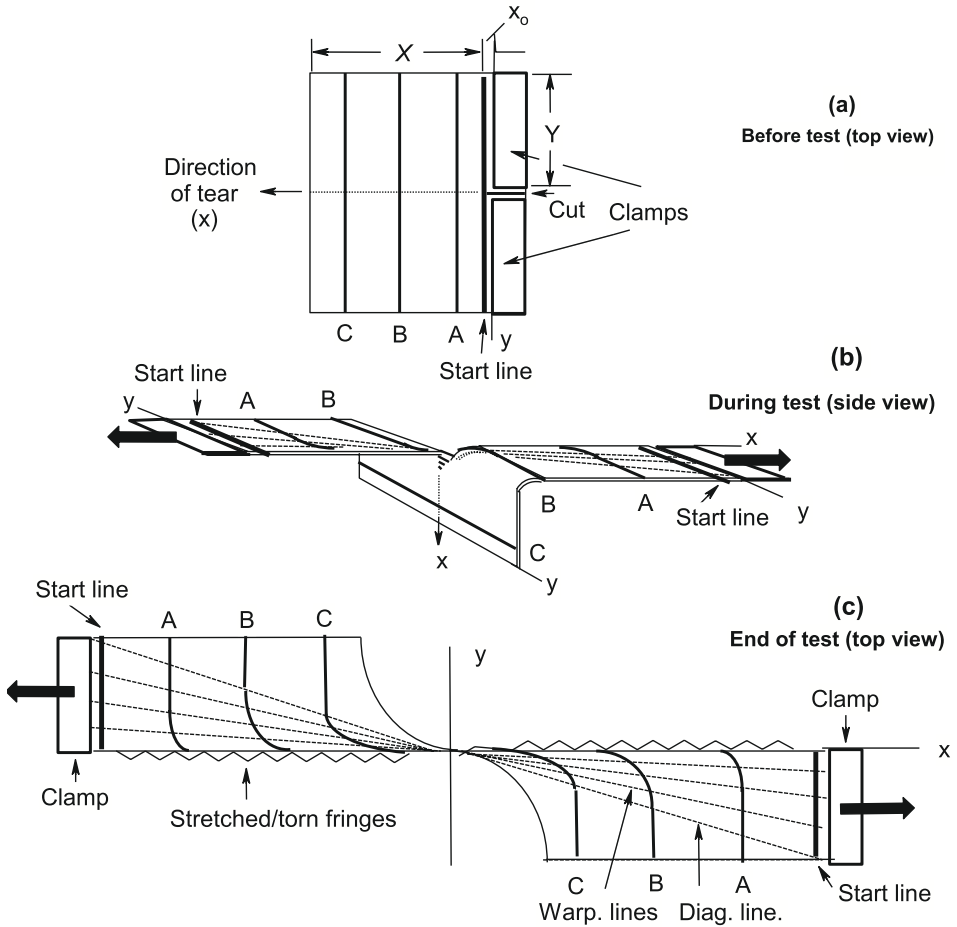


**Figure 5.7** Schematics of Elmendorf tear test

ardized mechanical testing of semicrystalline plastics (Section 1.10). Mechanical processes that occur during the tear test can be seen best when high quality LLDPE film is used [17]. As Fig. 5.7 (b) shows, the tearing process is accompanied by temporary twisting of the still undamaged part of the film, which is now positioned perpendicularly to the plane of the pendulum movement. The twisting results in an apparent turning of the  $x$  coordinate by  $\sim 90^\circ$  whereas the direction of the  $y$  coordinate, which is perpendicular to the tear direction, remains unchanged. The original direction of the  $x$  coordinate is restored at the moment the film is completely torn, as shown in Fig. 5.7 (c).

Tearing of a film sample during the test occurs very rapidly, and its direct observation is difficult. Only a few features are easily noticeable. The first one is the formation of border fringes: narrow, strongly stretched borders along the tear line, which are very schematically presented in Fig. 5.7 (c). Figure 5.8 shows the microphoto-

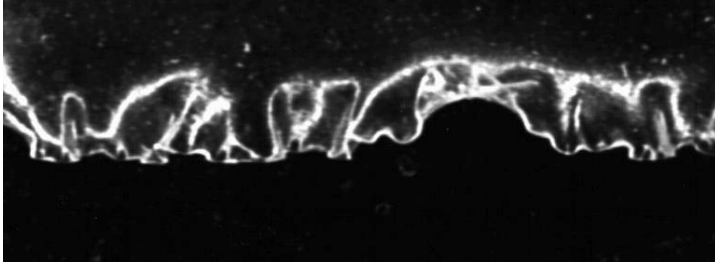


**Figure 5.8** Microphotograph of oriented fringes in transverse-torn LLDPE film; magnification  $\times 100$ , length of fringes  $\sim 0.7$  mm

graph of a typical fringe. The fringes are usually small; their lengths vary from  $\sim 0.3$  to  $\sim 1$  mm, depending on the type of film and the tear direction.

The second directly observable feature is straining of the area in the film between the  $x$  coordinate and the diagonal lines shown in Fig. 5.7 (b). For convenience of observation, three lines (A, B, and C) were drawn on the film perpendicular to the tear direction before the test (Fig. 5.7 (a)). The straining results in bending of these lines. The bending increases with the length of the tear (Fig. 5.7 (c)). The shape of the bent lines can be measured in torn film samples after the test.

When the tear test is performed on any film sample produced by the film-blowing method, a well-known aberration in the test might occur. Although the tear is supposed to propagate along the  $x$  coordinate, it often changes its path and ends up propagating in the  $y$  direction. The reason for the change is the large difference in the orientation pattern in the film. Some types of blown film are quite strongly machine- or transverse-oriented. As a result, their tear strength in the two directions is significantly different, and the tear direction may shift by following the path of the least resistance.

Additional features of the tear test become noticeable if the tear is carried out at a low speed [17]. The first such feature is very strong warping of film regions along the tear line. The directions of the warping lines are shown in Figs. 5.7 (b) and 5.7 (c). The second feature is high stress in some parts of the film during the test. The stress is present in the area between the tear line and the last warping line (the diagonal line in Fig. 5.7 (c)) while all other parts of the film are not stressed at all.

Figure 5.9 gives details of an interrupted tear test. Only the film segments strained during the test are shown. The tearing involves three parts of the film, Region I and two adjacent Regions II (Fig. 5.9 (a)). The central part, Region I, is affected most strongly. This region has the form of an isosceles triangle; its base is positioned along the  $x$  axis at  $y = 0$ , and the region is twisted with respect to the  $x$  coordinate. Region I is always small; its altitude is usually less than  $\sim 3$  to 4 mm. A small section of Region I in the middle of the triangle base, the area about to be torn apart, is strongly and irreversibly stretched and under the breaking stress,  $\sigma_{br}$ .

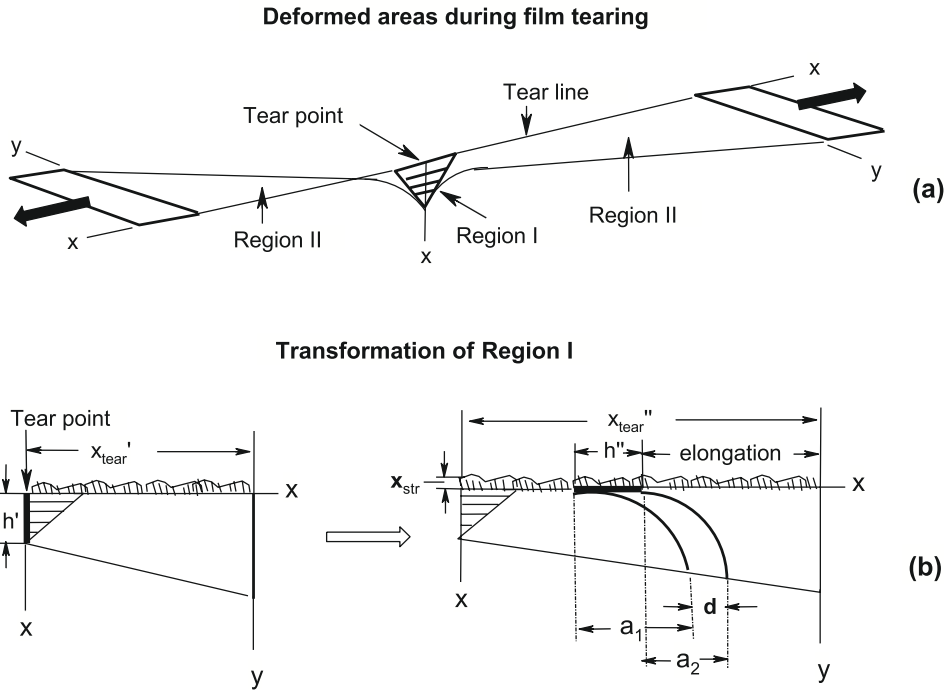


**Figure 5.9** (a) Stressed/stretched film regions during tear test; (b) Transformation of Region I during passing of tear point along its altitude

Figure 5.9 (b) shows schematically what happens with one-half of Region I when the tear point continues to travel along the altitude of the triangle (along the  $x$  coordinate). At the moment when the tear point reaches the position shown at left in Fig. 5.9 (b), the height of Region I (its altitude) is  $h'$ , which can be approximately estimated experimentally as shown below. As the tear point travels along the altitude toward the vertex of Region I, the altitude  $h'$  becomes slightly elongated and gradually splits into two halves,  $h''$ , positioned along the  $x$  coordinate. This change is shown in the right part of Fig. 5.9 (b), at a moment when the tear point has moved far ahead ( $x_{\text{tear}}'' \gg x_{\text{tear}}'$ ).

Several important visual observations become possible if such slow tearing is stopped midway and the sample is held under stress only slightly below  $\sigma_{br}$  [17]:

1. The size of Region I in the strained sample, both its base and altitude, change relatively little when the total length of the tear increases.
2. In several tests, a short distance along the  $x$  axis was marked (like  $h'$  in Fig. 5.9 (b)), and the tear was allowed to propagate along the marked distance. The measurement of its both halves ( $h''$ ) showed that after the torn film was subsequently relaxed,  $h''$  were only slightly higher than  $h'$ .

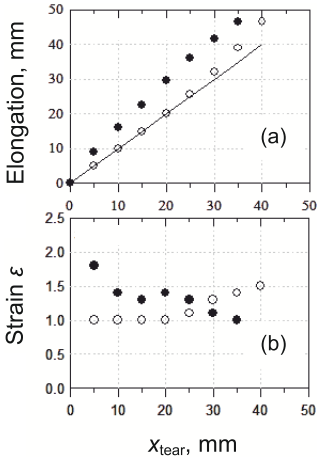


**Figure 5.10** (a) Irreversible elongation along tear line (distances between  $x_{\text{tear}} = 0$  and ends of curved lines) in relaxed LLDPE film torn in transverse (●) and machine (○) direction; (b) Irreversible strain  $(a_1 - a_2)/\mathbf{d}$  (see Fig. 5.9(b)) in LLDPE film torn in transverse (●) and machine (○) direction

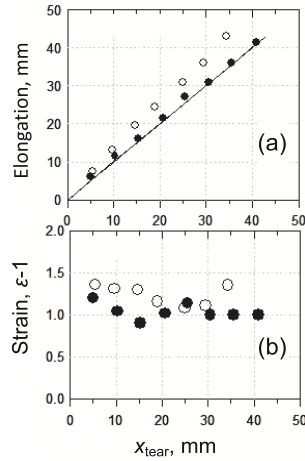


**Figure 5.11** (a) Irreversible elongation along tear line (distances between  $x_{\text{tear}} = 0$  and ends of curved lines) in relaxed LDPE film torn in transverse (●) and machine (○) direction; (b) Irreversible strains  $(a_1 - a_2)/\mathbf{d}$  (see Fig. 5.9(b)) in LDPE film torn in transverse (●) and machine (○) direction

These observations were confirmed in a more quantitative manner. Prior to testing, a large number of lines were drawn on the film perpendicular to the  $x$  coordinate, similar to lines A, B, and C in Fig. 5.7(a), with short distances  $\mathbf{d}$  between the lines. The tearing process transformed the end of each line into a curve (Fig. 5.9(b)). After the tests, the lines remained curved and each ended with a short, strongly oriented fringe shown in Fig. 5.8.

Measurements carried out with completely torn and relaxed film samples show that the  $a_1 - a_2$  distances are approximately proportional to  $h''$  and the  $(a_1 - a_2)/\mathbf{d}$  ratios give the level of irreversible strain in the film along the tear line,  $\epsilon_{\text{film}}$ . Figures 5.10 and 5.11 show dependences for the total elongations along the tear line and the  $\epsilon_{\text{film}}$  values for samples of blown film manufactured from LLDPE and LDPE and torn in the machine and the transverse direction. Figure 5.12 gives  $x_{\text{fringe}}$  values for the two types of film.

Figure 5.11 shows that the strain in the LLDPE film ( $\epsilon_{\text{film}}$ ) along the tear line depends on the tear direction. Tearing in the machine direction proceeds easily and without any noticeable strain except for the last stage before the complete breaking of the film. In contrast, tearing in the transverse direction results in the development of a significant permanent strain ( $\epsilon_{\text{film}} > \epsilon_y$ ) in the beginning of the tearing process (at low  $x_{\text{tear}}$ ); whereas the final stages of the tearing proceed without any noticeable additional straining. Because the film used in the transverse and the machine-direction tests is made from the same LLDPE resin, these results can only

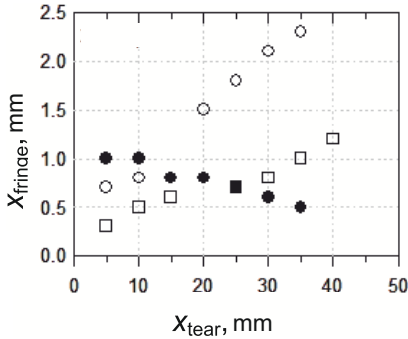


**Figure 5.12** Length of stretched/oriented fringes  $x_{\text{str}}$  in LLDPE film torn in machine direction ( $\square$ ) and in LDPE film torn in transverse ( $\bullet$ ) and in machine ( $\circ$ ) direction

be reconciled if one takes into consideration that the polymer chains in blown HDPE and LLDPE film are always preferably oriented in the machine direction. (see Section 5.1.2) [14, 18, 19]. The data in Fig. 5.10 show that even a small difference in the degree of chain orientation in LLDPE film significantly affects the tear behavior. The strain always significantly exceeds  $\varepsilon_y$ , which is most probably caused by rapid machine  $\rightarrow$  transverse reorientation of polymer chains in the course of tearing.

LDPE film exhibits a very complex pattern of chain/crystal orientation [18, 19]. Figure 5.10 shows that the tear pattern in this film is reversed; the initial straining is slightly higher in the film torn in the machine direction, but overall, the straining during the tearing in both directions is relatively small and the  $\varepsilon_{\text{film}}$  value is close to the respective  $\sigma_y$  values. In general, the  $\varepsilon_{\text{film}}$  values for both types of film are within 1.0 and 1.3. This means that every time the tear point advances by a distance  $h'$  along the  $x$  coordinate, the length of the partially torn sample,  $2x_{\text{tear}}$ , increases by  $2h'' \approx 2 \cdot \varepsilon_{\text{film}} \cdot h'$  (Fig. 5.9 (a)).

Figure 5.9 (a) shows that two other areas of the film are also strained during the tear test, Regions II. These are two orthogonal trapezoids with their large bases equal to the width of the clamp,  $Y$ , and their small bases corresponding to  $h'$  of Region I. The stresses and the strains at any point of Regions II along the  $x$  coordinate are very uneven and depend on the position along the  $y$  coordinate. The highest strains are along the tear line at  $y = 0$ , but judging by the data in Figs. 5.10 and 5.11, all these strains are lower than  $\varepsilon_y$ . The yet undamaged part of the film in advance of the apex of Region I (Fig. 5.9) does not experience any strain.

### 5.3.3 Model of Tear Test

Significant complications arise when an analytical solution is attempted to describe stretching of a combination of Region I and the two adjacent Regions II (Fig. 5.9). One reason for the difficulty is strong twisting and warping of all the stress-affected parts of the film, a fact obvious from Figs. 5.7 (b) and 5.9 (a). The second

reason is a very uneven distribution of stresses and strains in Region I. Obviously, the center of the base in Region I is under the breaking stress. However, the overall strain in the base of the triangle is smaller than either  $\sigma_{br}$  or  $\sigma_n$  due to cohesion of the material in the base and the underlying sections of Region I. The cohesion level is different when the test is carried out in different directions of the film (Figs. 5.10 and 5.11).

The model of the tear test [17] divides a combination of Region I and the two adjacent Region IIs into a large number of primitive elements. Figures 5.13 (a) and 5.13 (d) show the top primitive element from Fig. 5.9 (a) and its internal coordinates. The element consists of two narrow equilateral trapezoids fused at their small bases,  $dx_{tear}$ , which is the distance that corresponds to the elemental step along the tear line. The coordinate origin in the primitive element is positioned in its middle (the narrowest point); any distance from the origin is designated as  $\xi$  (Fig. 5.13 (d)). The minimum length of the first element at the beginning of the tearing process is  $2x_0$  (10 mm or  $\sim 0.4$  in), its length at any given  $x_{tear}$  is  $2 \cdot (x_{tear} + x_0)$ , and its maximum length is  $2 \cdot (X + x_0)$  ( $\sim 96$  mm or  $\sim 3.8$  in). Each primitive element is twisted  $180^\circ$  with respect to the  $x$  coordinate (Fig. 5.10 (a)); this twisting does not affect the mechanics of its straining.

During the test, the primitive element is gradually stretched until the stress at  $\xi = 0$  (in the narrowest cross section,  $S_{min}$ ) reaches the breaking stress,  $\sigma_{br}$ . At this moment, all the elements positioned below the top element in Fig. 5.9 (a) are under lower stresses, and the narrowest cross section of the last element, at the apex of Region I, reaches the yield point ( $\sigma_y$  and  $\epsilon_y$ ). After the two parts of the top primitive element are torn apart under the breaking stress (Fig. 5.13 (c)), Region I is reconstituted. The next primitive element becomes the most-stressed element; all underlying elements are additionally strained, and the bottom point of Region I propagates down the  $x$  coordinate by the distance  $dx_{tear}$ . In other words, *the tear test consists of a cascade of straining and breaking of the primitive elements* until  $x_{tear}$  reaches  $X$  and  $\xi$  reaches  $X + x_0$ .

Figure 5.13 signifies that all the stages of stretching/straining of the primitive element are in effect the stages of a standard tensile test of an object with a linearly variable cross section, the smallest in the middle ( $S_{min} = t \cdot dx_{tear}$ ) and the largest at both ends,  $S_{max} = t \cdot dY$  where  $t$  is the film thickness.

At the moment when the primitive element is about to break into two halves (Fig. 5.13 (b)), its total length substantially increases. First of all, the two irreversibly deformed parts,  $2x_{str}$ , lengthen to  $2x_{fringe}$ . The deformation in both strained  $x'_{str}$  parts varies from the breaking strain  $\epsilon_{br}$  in the smallest cross section  $S_{min}$  to  $\epsilon_y$  at their opposite ends,  $S_{str}$ . The remaining parts of the element, each with the length  $x_{tear} + x_0 - x_{str}$ , are elastically strained, and their strain gradually decreases starting from  $\epsilon_y$ . When the primitive element is torn and relaxed (Fig. 5.13 (c)), both its irreversibly stretched parts at  $x_{fringe} = \epsilon_n \cdot x_{str}$  appear as fringes on the torn

**Model: deformation of element EL**

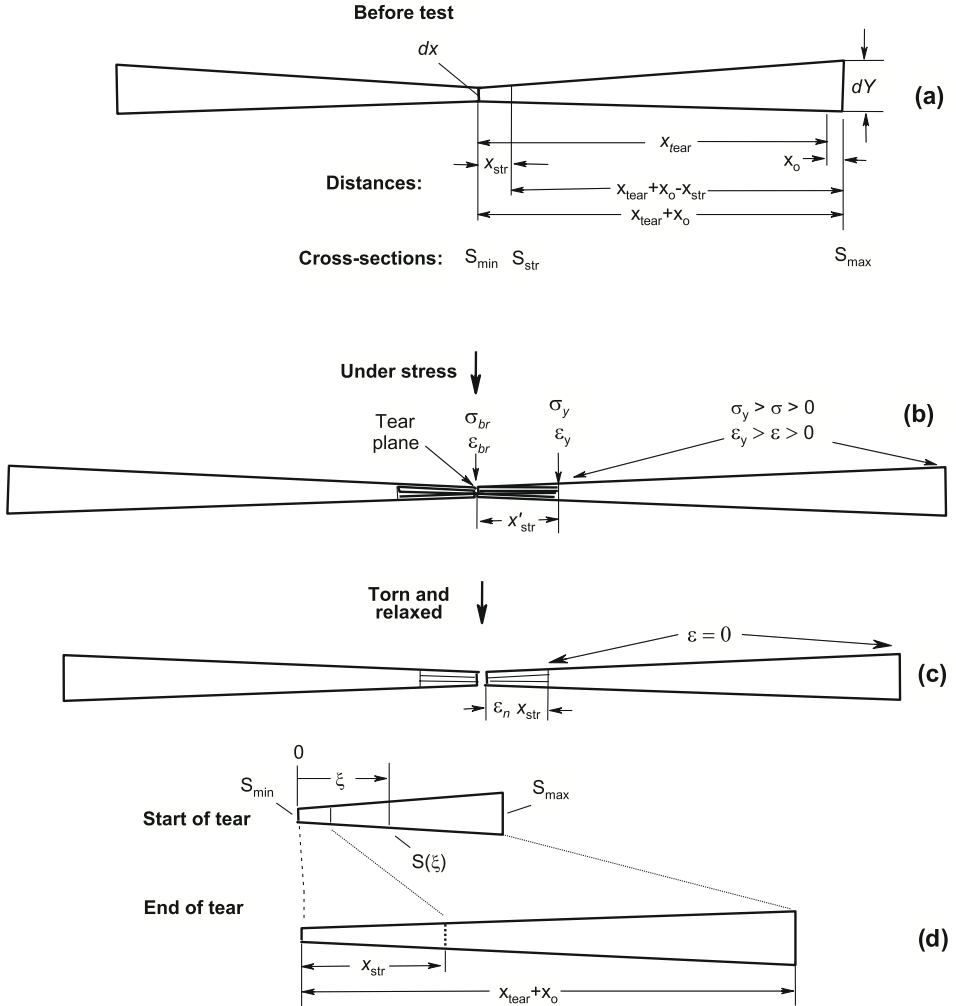


**Figure 5.13** Deformation of primitive element: (a) Before test; (b) During test, under stress; (c) After test, torn and relaxed; (d) Internal coordinate and relationships between original and stretched parts in one half of primitive element

halves of the film (Figs. 5.9 (b), and 5.12). In principle, the previously elastically strained parts of the element should contract to their unstrained combined length,  $2 \cdot (x_{\text{tear}} + x_0 - x_{\text{str}})$ . However, polyethylene resins do not have sharp clear-cut yield points and these distances in the relaxed film can be noticeably higher.

The goal of the model is to describe the shape of the primitive element in Fig. 5.13 at different points of the tear propagation along the  $x$  coordinate and to calculate the total work of tearing each such element. After the tear test is completed, the energy loss of the pendulum is equal to the work of the gradual (one primitive ele-

ment after another) tearing of a piece of film,  $W_{\text{total}}$ . By definition of the test, the tear strength (tear resistance) of the film is equal to the potential energy of the pendulum with the weight  $m_{\text{tear}}$  (g) released at a  $90^\circ$  angle and stopped at the lowest point of its swing due to the film's resistance to tear:

$$W_{\text{total}} = 2 \cdot m_{\text{tear}} \cdot g \cdot l \cdot \sin^2(90^\circ/2) = m_{\text{tear}} \cdot g \cdot l (g \cdot \text{m}^2/\text{s}^2) \quad (5.14)$$

Here  $l$  is the pendulum length, 40.6 cm (16 in), and  $g = 9.81 \text{ m/s}^2$ .

As with the model of the dart impact test in Section 5.2, the total work required to strain/stretch and break all the primitive elements one after another,  $W_{\text{total}}$  in Eq. 5.14, is separated into four parts:

$$W_{\text{total}} = W_{\text{yield}} + W_{\text{neck}} + W_{\text{str-hard}} + W_{\text{elast}} \quad (5.15)$$

The first three terms in Eq. 5.15 describe the work spent on deformation of the parts of all the primitive elements from  $\xi = 0$  to  $\xi = x_{\text{str}}$  (Fig. 5.13). They are:

1.  $W_{\text{yield}}$ , the work of elastic stretching in cross sections of all the elements from  $\xi = 0$  to  $\xi = x_{\text{str}}$  to the yield point;
2.  $W_{\text{neck}}$ , the work of necking, that is, stretching/orientation of the film material from  $\xi = 0$  to  $\xi = x_{\text{str}}$ ; and
3.  $W_{\text{str-hard}}$ , the work of strain hardening, additional straining of oriented parts in all the elements to the point at which the stress in the smallest cross sections reaches  $\sigma_{br}$ .

The last term in Eq. 5.15,  $W_{\text{elast}}$ , is the work of sub-yield elastic stretching in cross sections of all the primitive elements beyond  $\xi = x_{\text{str}}$  up to  $\xi = x_{\text{tear}} + x_0 - x_{\text{str}}$ .

Straining of a primitive element proceeds along the  $\xi$  coordinate, with the origin positioned in the middle of the element. Cross-section areas  $S(\xi)$  of the element at a distance  $\xi$  from the origin are given by Eq. 5.16 [17]:

$$S(\xi) = [t \cdot dx_{\text{tear}}] \cdot [1 + \xi \cdot (dY/dx - 1)/(x_{\text{tear}} + x_0)] \quad (5.16)$$

For every such cross-section area, the work of deformation  $W_{i,\xi}$  is the product of the force  $F_{i,\xi} = \sigma_i \cdot S(\xi)$  and the distance of the force application,  $d\xi$ , from  $\xi$  to  $\xi + d\xi$ .

Although analytical forms for all the terms of  $W_{\text{total}}$  in Eq. 5.15, ( $W_{\text{yield}}$  [total],  $W_{\text{neck}}$  [total],  $W_{\text{str-hard}}$  [total] and  $W_{\text{elast}}$  [total]) are desirable, some final expressions, after two integration steps, are very cumbersome due to the complex shape of the primitive element. These calculations can be carried out only by numerical integration of respective differential equations.

*Calculation of  $W_{\text{yield}}$ :*

$$W_{\text{yield}}(\text{element}) = \sigma_y \cdot (\epsilon_y - 1) \cdot [t \cdot dx_{\text{tear}}] \cdot [x_{\text{str}} + [r_{\text{tear}}/(\sigma_{br}/\sigma_y - 1) - 1] \cdot 0.5 \cdot x_{\text{str}}^2/(x_{\text{tear}} + x_0)] \quad (5.17)$$

$$W_{\text{yield}}(\text{total}) = \int_{x_{\text{tear}}=0}^X W_{\text{yield}}(\text{element}) \cdot dx_{\text{tear}} \quad (5.18)$$

Calculation of  $W_{\text{neck}}$ :

$$W_{\text{neck}}(\text{element}) = 2 \cdot \sigma_{br} \cdot (\varepsilon_n - \varepsilon_y) \cdot t \cdot r_{\text{tear}} \cdot (x_{\text{tear}} + x_0) \cdot dx_{\text{tear}} \quad (5.19)$$

$$W_{\text{neck}}(\text{total}) = \int_{x_{\text{tear}}=0}^X W_{\text{neck}}(\text{element}) \cdot dx_{\text{tear}} = 2 \cdot \sigma_{br} \cdot (\varepsilon_n - \varepsilon_y) \cdot t \cdot r_{\text{tear}} \cdot X \cdot (0.5 \cdot X + x_0) \quad (5.20)$$

Calculation of  $W_{\text{str-hard}}$ :

$$W_{\text{str-hard}}(\text{element}) = 2 \cdot \sigma_{br} \cdot [t \cdot dx_{\text{tear}}]^2 \cdot (\varepsilon_{br} - \varepsilon_n) \cdot [S(\xi)^{-1} \cdot d\xi] \quad (5.21)$$

$$W_{\text{str-hard}}(\text{total}) = \int_{x_{\text{tear}}=0}^X W_{\text{str-hard}}(\text{element}) \cdot dx_{\text{tear}} \quad (5.22)$$

Calculation of  $W_{\text{elast}}$ :

$$W_{\text{elast}}(\text{element}) = \int_{\xi=x_{\text{str}}}^{x_{\text{tear}}+x_0-x_{\text{str}}} (\sigma_{br}^2 / \sigma_y) \cdot (\varepsilon_y - 1) \cdot [S_{\text{min}}^2 / S(\xi)] \cdot d\xi \quad (5.23)$$

$$W_{\text{elast}}(\text{total}) = \int_{x_{\text{tear}}=0}^X W_{\text{elast}}(\text{element}) \cdot dx_{\text{tear}} \quad (5.24)$$

The model defined by Eqs. 5.17 to 5.24 has only one adjustable parameter, the ratio  $r_{\text{tear}} = x_{\text{str}} / (x_{\text{tear}} + x_0)$ . Estimations of  $r_{\text{tear}}$  in Fig. 5.12 give its range from 0.06 to 0.08. This model of the tear test and the numerical calculations with Eqs. 5.15 to 5.24 reveal several important features of the test and afford an estimation of the effects of the resins' mechanical properties on the tear strength of film. As a test of the model reliability, the following experimentally determined parameters typical for a commercial LLDPE resin were used to estimate the average tear strength of film:

$$\sigma_y = 1.3 \text{ kg/mm}^2, \quad \varepsilon_y = 1.2, \quad \sigma_n = 1.2 \text{ kg/mm}^2, \quad \varepsilon_n = 6.0, \quad \sigma_{br} = 2.5 \text{ kg/mm}^2, \quad \varepsilon_{br} = 7.5.$$

Calculations for 25- $\mu\text{m}$  (1-mil) film prepared from such a resin without account for the orientation effect give the tear strength in the range of 170 to 220 g, a correct order of magnitude of the tear strength when compared to the experimental data (see below). The energy of the pendulum is spent in the following way:

1. Stretching the narrow part of each primitive element to the yield point,  $W_{\text{yield}} = 1.1\%$ ;
2. Necking/orientation of this part of the element,  $W_{\text{neck}} = 73.4\%$ ;

3. Overcoming strain hardening in the element,  $W_{\text{str-hard}} = 20.0\%$ ; and
4. Elastic deformation of the nonoriented part of the element,  $W_{\text{elast}} = 5.5\%$ .

It is very informative to compare two calculated values:

(a) The work of tearing a piece of film in the tear test, which is essentially the strain/stress test in the course of which narrow strands of film break one after another, and

(b) The work of stretching and breaking of a rectangular piece of film with the cross section  $S_{\text{max}} = t \cdot X$ , the length  $2Y$ , and with the same mechanical parameters.

The calculations show that the work of breaking the film in the tear test,  $W_{\text{total}} = 90 \text{ kg} \cdot \text{mm}$ , constitutes merely 11 % of the work required to break the same piece of film when it is tested in the standard mechanical test.

### 5.3.3.1 Effect of Pendulum Speed

Some mechanical parameters of polyethylene resins depend on the deformation rate, mostly due to the relatively slow relaxation phenomena described in Section 5.1.2. The necking stage is the crucial part of the film tearing, and only the effect of the tearing speed  $V$  on  $\sigma_n$  and  $\varepsilon_n$  values was considered in the tear test model. The same resin, when stretched at a high speed typical for the tear test, is slightly stiffer during the necking stage, and its final necking strain is noticeably higher. These two effects increase the calculated tear resistance. For example, the tear strength estimation for the film produced from the LLDPE resin with the above set of  $\sigma$  and  $\varepsilon$  values increases from  $\sim 220$  to  $\sim 260 \text{ g}$ .

### 5.3.3.2 Effects of Mechanical Properties of Resins

All six parameters that determine the shape of the stress/strain curve,  $\sigma_y$ ,  $\varepsilon_y$ ,  $\sigma_n$ ,  $\varepsilon_n$ ,  $\sigma_{br}$ , and  $\varepsilon_{br}$ , affect the tear strength of film in a complex way due to their contribution to different terms in  $W_{\text{total}}$  (Eq. 5.15). The computational results for 25- $\mu\text{m}$  (1-mil) film are presented in Table 5.9. They show the predicted effects of mechanical properties of LLDPE resins on the calculated tear strength of film. A pronounced yield threshold,  $\sigma_{br}/\sigma_y > 1$ , which is typical for some LLDPE resins of higher density (crystallinity degree), does not affect the tear strength of the film. Calculations show also that the value of the Young's modulus, the  $M_Y = \sigma_y/(\varepsilon_y - 1)$  ratio, has virtually no effect on the tear resistance. An increase of resistance to orientation (a proportional increase of  $\sigma_y$  and  $\sigma_n$ ) also produces only a modest increase of the tear strength, whereas an increase of the orientation (necking) potential (an increase in  $\varepsilon_n$  at constant  $\varepsilon_{br} - \varepsilon_n$ ) significantly increases the tear strength. An increase in the strain-hardening (tensile) modulus  $M_{\text{str-hard}} = (\sigma_{br} - \sigma_n)/(\varepsilon_{br} - \varepsilon_n)$  (an increase of  $\sigma_{br}$  at a constant  $\sigma_n$ ) also strongly increases the tear strength by allowing the orientation zone in each primitive element to propagate farther. Finally, an improvement in strain-hardening properties of a resin (a parallel increase of  $\sigma_{br}$  and  $\varepsilon_{br}$  at a constant  $M_{\text{str-hard}}$ ) also greatly increases the tear strength of the film.

**Table 5.9** Effects of LLDPE Mechanical Properties on Film Tear Strength

<i>Yield threshold, <math>\sigma_y/\sigma_n = 1.2 \text{ kg/mm}^2</math>, <math>\sigma_{br} = 3.0 \text{ kg/mm}^2</math>, <math>\epsilon_y = 1.2</math>, <math>\epsilon_n = 6</math>, <math>\epsilon_{br} = 8</math></i>					
$\sigma_y/\sigma_n$	1.02	1.05	1.10	1.15	
Tear strength $m_{tear}$ , g	267	258	270	271	
<i>Resistance to orientation; proportional increase of yield stress and necking stress at <math>\sigma_y/\sigma_n = 1.1</math></i>					
$\sigma_n$ , kg/mm <sup>2</sup>	0.8	1.0	1.2	1.4	1.6
Tear strength $m_{tear}$ , g	259	264	270	276	281
<i>Increase of orientation potential (<math>\epsilon_{br} = \epsilon_n + 2.0</math>)</i>					
$\epsilon_n$	4.0	6.0	8.0		
Tear strength $m_{tear}$ , g:	200	270	340		
<i>Increase of strain hardening modulus <math>M_{str-hard} = (\sigma_{br} - \sigma_n)/(\epsilon_{br} - \epsilon_n)</math>; <math>\sigma_n = 1.2 \text{ kg/mm}^2</math></i>					
$M_{str-hard}$ , kg/mm <sup>2</sup>	1.0	1.5	2.0		
Tear strength $m_{tear}$ , g	285	360	440		
<i>Increase of strain hardening region (<math>\sigma_n = 1.2 \text{ kg/mm}^2</math>, <math>M_{str-hard} = 1.0</math>)</i>					
$\epsilon_{br} - \epsilon_n$ :	2.0	3.0	4.0		
Tear strength $m_{tear}$ , g	285	390	500		

### 5.3.3.3 Effect of Film Orientation

Large differences between the tear strength in the machine and the transverse direction in blown LLDPE film is one of the most well-known characteristics revealed in tear tests. Two examples of the difference are presented in Table 5.10. This difference is the consequence of chain orientation in LLDPE film.

**Table 5.10** Effect of Orientation on Mechanical Properties and Tear Strength of Blown Film from Ethylene/Hexene LLDPE Resins

Density, g/cm <sup>3</sup>	Direction of test	Mechanical properties						Tear strength $m_{tear}$ , g	
		$\sigma_y$ , kg/mm <sup>2</sup>	$\epsilon_y$	$\sigma_n$ , kg/mm <sup>2</sup>	$\epsilon_n$	$\sigma_{br}$ , kg/mm <sup>2</sup>	$\epsilon_{br}$	calculated	experiment <sup>a</sup>
0.918	Machine	1.6	1.1	1.6	3.3	6.1	6.8	~370	300
	Transverse	1.5	1.1	1.4	7.1	4.8	9.0	~470	670
0.917	Machine	0.9	1.1	0.9	3.1	5.8	6.8	~320	440
	Transverse	1.0	1.1	0.9	7.2	4.8	9.4	~470	740
0.917	Machine	0.9	1.1	0.9	3.9	5.3	7.3	~340	460
	Transverse	0.9	1.1	0.9	6.9	5.1	9.2	~480	600

a Experimental data adjusted to film thickness 25- $\mu\text{m}$  (1-mil)

Two features of the orientation pattern in the film are important for its tear strength. First, the  $c$  axis in the crystalline phase (the axis that corresponds to the direction of extended polymer segments in lamellae) in blown HDPE and LLDPE film is always preferably oriented in the machine direction. Table 5.1 gives several examples of the orientation pattern in typical LLDPE film. Second, the fraction of polymer chains in the crystalline phase oriented in the thickness direction of the film is always low, < 20% rather than 33% in the absence of orientation. Consequently, the averaged mechanical strength of film is higher than the strength of an isotropic sample of the same resin.

This difference in orientation results in noticeable differences in the stretching process and in mechanical properties between the machine and the transverse direction of the film. For example, estimations of the tear resistance corresponding to mechanical properties of the film shown in Fig. 5.2 give the following results:

Tear strength (machine direction) ~ 290 g;

$W_{\text{yield}} \sim 1\%$ ,  $W_{\text{neck}} \sim 48\%$ ,  $W_{\text{str-hard}} \sim 45\%$ ,  $W_{\text{elast}} \sim 6\%$ .

Tear strength (transverse direction) ~ 380 g;

$W_{\text{yield}} \sim 1\%$ ,  $W_{\text{neck}} \sim 77\%$ ,  $W_{\text{str-hard}} \sim 19\%$ ,  $W_{\text{elast}} \sim 3\%$ .

The model of the tear test correctly predicts a higher tear resistance in the transverse direction for the film and explains the difference as mostly due to a significantly higher  $\epsilon_n$  value in this direction.

Table 5.11 contains several examples in which the mechanical properties and tear resistance of blown ethylene/hexene LLDPE film were experimentally measured in the machine and the transverse direction. A comparison between the experimentally measured tear strength and the estimations shows that the model correctly predicts the range of tear resistance and the differences between the tear properties in the two directions of film.

**Table 5.11** Comparison of Mechanical Properties and Tear Strength of Blown Film Made from Two LLDPE Resins (Density 0.918 g/cm<sup>3</sup>,  $l_2 = 1.0$ )

Copolymer	Direction of test	Mechanical properties						Tear strength $m_{\text{tear}}$ for 50- $\mu\text{m}$ (2-mil) film, g	
		$\sigma_y$ , kg/mm <sup>2</sup>	$\epsilon_y$	$\sigma_n$ , kg/mm <sup>2</sup>	$\epsilon_n$	$\sigma_{br}$ , kg/mm <sup>2</sup>	$\epsilon_{br}$	calculated	experiment
Ethylene/butene	machine	1.1	1.1	1.1	3.4	3.5	6.8	~460	350
	transverse	1.1	1.1	1.0	6.4	2.8	8.3	~520	590
Ethylene/hexene	machine	1.2	1.1	1.2	4.7	4.1	8.0	~690	820
	transverse	1.1	1.1	1.0	7.5	4.7	9.5	~950	1200

### 5.3.3.4 Comparison of Tear Strength of Ethylene/Butene and Ethylene/Hexene Copolymers

Film manufactured from ethylene/butene LLDPE resins is inferior in tear resistance to film manufactured from ethylene/hexene LLDPE resins of the same composition and density (crystallinity level), as the examples in Table 5.12 show [2, 4–7, 15]. The principal difference between these two types of resins is a lower  $M_{\text{str-hard}}$  value for ethylene/butene copolymers [9]. Table 5.12 compares the mechanical properties and tear strength of the two types of blown film. Both resins were prepared using the same polymerization catalyst; they have the same crystallinity degree (density 0.918 g/cm<sup>3</sup>) and molecular weight ( $I_2 = 1.0$ ) [6]. The calculations show that the inferior tear strength of the film made from the ethylene/butene resin is indeed mostly the consequence of its lower  $\sigma_{br}$  value.

**Table 5.12** Mechanical Properties of Two Types of LLDPE Film [5]

Property	Ethylene/butene		Ethylene/hexene	
	MD <sup>a</sup>	TD <sup>a</sup>	MD <sup>a</sup>	TD <sup>a</sup>
Yield strength $\sigma_y$ , kg/mm <sup>2</sup>	0.96	0.97	0.86	0.79
Breaking strength $\sigma_{br}$ , kg/mm <sup>2</sup>	5.42	3.60	6.74	3.90
Elongation ratio at break $\varepsilon_{br}$	5.80	~8.5	3.43	~8.0
Dart drop strength $m_{\text{dart}}$ , g	100		81	
Elmendorf tear strength $m_{\text{tear}}$ , g	80	400	300	750

a MD - machine direction, TD - transverse direction

### 5.3.3.5 Low Density Polyethylene

LDPE resins contain both short-chain branches of different sizes and long-chain branches. These homopolymers have a reduced crystallinity level compared to HDPE resins prepared in catalytic homopolymerization reactions of ethylene, and they have lower melting points, 110 to 120 °C compared to ~135 °C for HDPE resins. Table 5.13 lists the mechanical properties of two commercial LDPE resins.

**Table 5.13** Mechanical Properties and Estimated Tear Strength of LDPE Resins

Resin, density	Direction of test	Mechanical properties						Tear strength $m_{\text{tear}}$ for 50- $\mu\text{m}$ (2-mil) film, g	
		$\sigma_y$ , kg/mm <sup>2</sup>	$\varepsilon_y$	$\sigma_n$ , kg/mm <sup>2</sup>	$\varepsilon_n$	$\sigma_{br}$ , kg/mm <sup>2</sup>	$\varepsilon_{br}$	calculated	experiment
LD100 [6]	Machine	1.1	1.3	1.0	3.0	2.5	4.3	~260	150
0.923	Transverse	1.1	1.3	1.0	4.5	2.2	6.5	~340	120
LDPE 132I [7]	Machine	1.2	1.3	1.1	4.0	3.2	5.7	~410	300
0.921	Transverse	1.2	1.3	1.1	5.3	2.9	7.6	~500	180

A comparison with Tables 5.11 and 5.12 shows that most mechanical properties of LDPE resins are similar to those of catalytically produced LLDPE resins except for a noticeably lower  $\sigma_{br}$  value. Machine and transverse orientation levels in LDPE film are relatively close [18, 19]. As a result, the experimentally measured tear strength in both directions of the film is also usually similar.

Calculations for 25- $\mu\text{m}$  (1-mil) film support these results and demonstrate that the main reason for a relatively low tear strength of LDPE film compared to LLDPE film is lower  $\sigma_{br}$  and  $\sigma_n$  values and the resulting lower  $W_{\text{neck}}$  and  $W_{\text{str-hard}}$  values:

LDPE (machine direction):  $W_{\text{total}} \sim 85 \text{ kg} \cdot \text{mm}$

( $W_{\text{yield}} < 1$ ,  $W_{\text{neck}} \sim 58$ ,  $W_{\text{str-hard}} \sim 17$ ,  $W_{\text{elast}} \sim 8 \text{ kg} \cdot \text{mm}$ )

LLDPE (machine direction):  $W_{\text{total}} \sim 140 \text{ kg} \cdot \text{mm}$

( $W_{\text{yield}} < 1$ ,  $W_{\text{neck}} \sim 110$ ,  $W_{\text{str-hard}} \sim 25$ ,  $W_{\text{elast}} \sim 3 \text{ kg} \cdot \text{mm}$ )

## ■ 5.4 Comparison of Factors Determining Results of Tear Test and Dart Impact Test of LLDPE Film

The dart impact test and the tear test are the two most important end-use tests of film manufactured from LLDPE and LDPE resins. The models of the dart impact test (Section 5.2) and the tear test (Section 5.3) provide the basis for a comparison of both tests in terms of the mechanical parameters of semicrystalline resins; that is, the stresses and strains at the yield, the end-of-necking, and the breaking points.

These two models show that, formally speaking, the standard mechanical test of a film sample (such as ASTM D882, ISO 257-3), the dart impact test (ASTM D1709, ISO 7765), and the Elmendorf tear test (ASTM D1922, ISO 6383-2) are variations of the same mechanical test but that they greatly differ in testing conditions:

1. The standard mechanical test is carried out with a strip of film of a constant cross section and at a relatively low stretching speed.
2. The dart impact test is carried out at a high stretching speed; its conditions correspond to stretching of a sample of a resin with a linearly varying cross section, see Fig. 5.5.
3. The tear test corresponds to cascading high-speed tests of very narrow strips of film with variable cross sections and different lengths, see Fig. 5.13.

Table 5.14 compares the work of film breaking in these three types of mechanical tests. The results were calculated for 25- $\mu\text{m}$  (1-mil) film made from a hypothetical high-quality LLDPE resin with the following mechanical properties:

$$\sigma_y = 1.3 \text{ kg/mm}^2, \varepsilon_y = 1.2, \sigma_n = 1.2 \text{ kg/mm}^2, \varepsilon_n = 6.0, \sigma_{br} = 3.0 \text{ kg/mm}^2, \varepsilon_{br} = 8.0$$

The comparison shows that, in principle, the dart impact test and the tear test measure the same properties of the film but on a different scale because of major differences in the implementation of the respective tests. The only noticeable difference between both of these end-use tests and the standard mechanical test (apart from elastic straining of the nonoriented part of the film, which is absent in the standard test) is a higher contribution of the work of strain hardening in the standard test. This difference is easily explained: the strain-hardening stage in the standard test involves the whole length of the sample (Fig. 1.18), whereas this stage is restricted only to the narrowest parts of the film adjacent to the tearing line in the tear test (Figs. 5.7 and 5.8) and to a narrow cross section of the film (the circumference of the dart) in the dart impact test (Fig. 5.3).

**Table 5.14** Comparison of Results of Different Tests for LLDPE Film with Parameters  $\sigma_y = 1.3$ ,  $\sigma_n = 1.2$ ,  $\sigma_{br} = 3.0$  (all in  $\text{kg/mm}^2$ );  $\varepsilon_y = 1.2$ ,  $\varepsilon_n = 6.0$ ,  $\varepsilon_{br} = 8.0$

Test	$W_{\text{total}}$ kg · mm	$W_{\text{yield}}$ %	$W_{\text{neck}}$ %	$W_{\text{str-hard}}$ %	$W_{\text{elast}}$ %
Standard mechanical test (cross section 1.0 mm <sup>2</sup> )	1,088	1.2	65.2	33.7	-
Tear test (total cross section 1.09 mm <sup>2</sup> )	109	0.9	75.9	18.1	5.0
Dart drop test (minimum [9] cross section 0.58 mm <sup>2</sup> )	350	1.7	69.3	25.5	3.5

## References

1. James, D.E., In *Encyclopedia of Polymer Science and Engineering*, vol. 6, 2<sup>nd</sup> ed. Kroschwitz, J.I. (Ed.) (1988) John Wiley & Sons, New York, p. 429
2. Krentsel, B.A., Kissin, Y.V., Kleiner, V.I., Stotskaya, S.S., *Polymers and Copolymers of Higher  $\alpha$ -Olefins* (1997) Hanser, Munich, Chapter 8
3. *Ethylene Polymers, HDPE; Ethylene Polymers, LLDPE; Ethylene Polymers, LDPE*, In *Encyclopedia of Polymer Science and Technology*, vol. 2, 3<sup>rd</sup> ed. Mark, H.F., Kroschwitz, J.I., (Eds.) (2003) Wiley-Interscience, New York
4. Kissin, Y.V., In *Kirk-Othmer Encyclopedia of Chemical Technology*, vol. 17 (1996) John Wiley & Sons, New York, p. 756

5. ExxonMobil Chemical Company: <http://www.exxonmobilchemical.com/Chem-English/brands/polyethylene-ldpe-exxonmobil-grades-and-datasheets.aspx?In = products-services>
6. Dow Chemical Company: <http://www.dow.com/polyethylene/na/en/prod/index.htm>
7. Lyondell Company: [www.lyondell.com/Lyondell/Products/polymers/LinearLowDensity-Polythylene](http://www.lyondell.com/Lyondell/Products/polymers/LinearLowDensity-Polythylene)
8. Strella, S., In *Engineering Design for Plastics* Baer, E. (Ed.) (1964) Reinhold, New York, Chapter 12
9. Kissin, Y.V., *Macromol. Mater. Eng.* (2008) 293, p. 66
10. Ward, I.M., *Polym. Eng. Sci.* (1984) 24, p. 724
11. Zachariades, A.E., Porter, R.S., *J. Macromol. Sci., Part B: Phys.* (1981) 19, p. 377
12. Tonkopicj, E.A., Friedman, M.L., Kissin, Y.V., Malkin, A.Y., Zharova, I.L., Gul, V.E., *Plast. Massy* (1975) 10, p. 56
13. Standard Test Methods for Impact Resistance of Plastic Film by the Free-Falling Dart Method, ASTM D1709-04 09A(ISO 7765-1); <http://www.astm.org/Standards/D1709.htm>, and D4272-09 (ISO 7765-2), Standard Test Method for Total Energy Impact of Plastic Films by Dart Drop, <http://www.astm.org/Standards/D4272.htm>
14. Kissin, Y.V., *J. Polym. Sci, Part B: Polym. Phys.* (1992) 30, p. 1165
15. Crotty, V.J., Firdaus, V., Hagerty, R.O., *SPE Polyolefins VIII International Conference.* (1993) Houston, TX, p. 192
16. Elmendorf tear test. Propagation Tear Resistance of Plastic Film and Thin Sheeting by Pendulum Method, ASTM D1922 (ISO 6383-2); [www.ptli.com/testlopedia/tests/ElmendorfD1922.asp](http://www.ptli.com/testlopedia/tests/ElmendorfD1922.asp)
17. Kissin, Y.V., *Macromol. Mater. Eng.* (2011) 296, p. 729
18. Krishnaswamy, R.K., *J. Polym. Sci, Part B: Polym. Phys.* (2000) 38, p. 182
19. Pazur, R.J., Prud'homme, R.E., *Macromolecules* (1996) 29, p. 119

# 6

## End-Use Testing of High Molecular Weight HDPE and MDPE Resins

### ■ 6.1 Top Load Test of HDPE Containers

Top load testing (or crush testing) is the measurement of resistance of a household container (usually a bottle) or an industrial container to a compressive load and the measurement of the load under which the container is irreversibly deformed or collapses. The compressive strength of bottles and cans made of polyethylene resins must be high enough to withstand the capping process, stacking, storage, and shipment. The majority of household and industrial containers are single-use articles, and special government regulations for environmental protection have been developed to limit the amount of resin spent for their manufacture.

Several standard procedures for the top load/crush tests are practiced [1–4]. The two main procedures are the dynamic and the static top load tests. In the dynamic test, a container is placed between two platens and the top movable platen compresses the container at a constant speed. The container is crushed until it collapses. Several parameters are recorded during the test: the breaking force (load) and the downward deflection of the top platen at this point, the yield force, and the crushing force at a given distance of the platen travel, usually between 12 and 25 mm (0.5 to 1 in). Such tests provide information for optimization of the force leading to deformation and failure of a container and for identification of excessively thinned areas in the wall of the container resulting from a poor wall-thickness distribution.

Containers with packaged liquid products (beverages, milk, liquid detergents, etc.) are often stacked for a significant period of time. The bottom container in the stack is continually stressed under a constant load. Static test methods subject such containers, empty or filled, to a predetermined static load. The test measures the crushing yield load (the load under which an increase in a downward deflection occurs even without any further increase of the load) and the crushing deflection, a decrease in the height of the container at the crushing load.

### 6.1.1 Mechanics of Top Load Test

Figure 6.1(a) shows the schematics of a typical top load test. The tested container is usually a thin-walled bottle of the simplest configuration with a cylindrical body, a short, relatively thick neck (the thread on the neck is not shown), and a conical transitional section between the neck and the cylindrical body. The essential dimensions of the container are diameters  $D_1$  and  $D_2$ ; wall thicknesses  $t_1$ ,  $t_2$ ,  $t_3$ , and  $t_4$ ; the height of the conical section  $h_1$ ; and the height of the cylindrical part of the bottle  $H$ . The height of the neck ( $h_2$ ) is irrelevant for the test results.

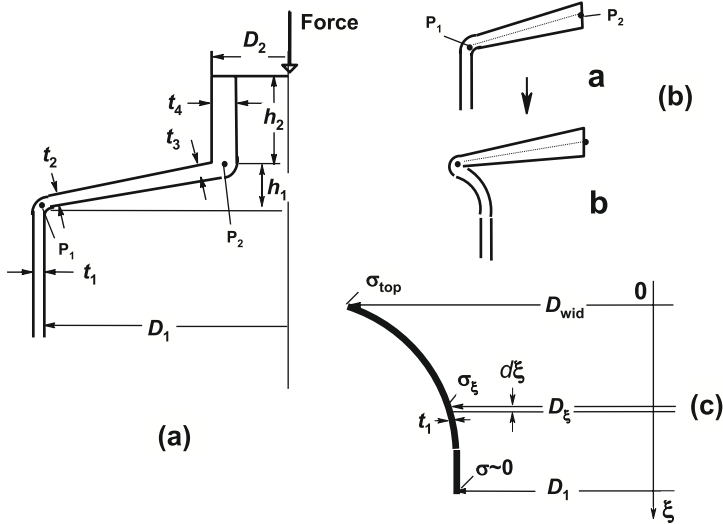


**Figure 6.1** (a) Schematics of top load test; (b) Moment of initial failure; (c) Stresses in model, Equation 6.3

A crushing force is uniformly applied to the top of the neck and the bottle is compressed until it collapses. Visual observations show that if  $t_1 < t_2 < t_3$  (a typical case) one can neglect the downward bending of the transitional section of the bottle and assume that when the top load increases this section moves as a rigid pivot, which rotates at points  $P_1$  and  $P_2$ . Figure 6.1 (b) shows the initial part of the test in an exaggerated form as an **a**  $\rightarrow$  **b** transition. The downward movement of the top platen, which corresponds to the downward deflection of the neck, *def*, produces an increase in the diameter of the upper part of the cylindrical section. The diameter of the widened rim of the cylindrical body,  $D_{wid}$ , is:

$$D_{wid} = 2[h_1^2 + 0.25 \cdot (D_1 - D_2)^2 - (h_1 - def)^2]^{0.5} + D_2 \quad (6.1)$$

This widening leads to stretching of the circumference at the top of the cylindrical body from  $\pi \cdot D_1$  to  $\pi \cdot D_{wid}$ . When the  $(\pi \cdot D_{wid})/(\pi \cdot D_1)$  ratio approaches the value of the yield strain  $\epsilon_y$ , the upper part of the cylindrical body enters the zone of in-

elastic deformation on the stress/strain curve (see Fig. 1.18). To evaluate the maximum *reversible* downward deflection of the bottle's neck,  $def_{\max}$ , it is necessary to introduce a tolerance factor, a coefficient  $\gamma = (\varepsilon_{\max} - 1)/(\varepsilon_y - 1)$ , which determines the permissible *elastic* expansion of the upper rim of the cylindrical section from  $\pi \cdot D_1$  to  $\pi \cdot \varepsilon_{\max} \cdot D_1$ . The  $\gamma$  value is chosen between 0.8 and 0.9. The  $def_{\max}$  value is determined by equating the maximum diameter of the expanded upper part of the cylindrical section,  $\varepsilon_{\max} \cdot D_1 = [\gamma \cdot (\varepsilon_y - 1) + 1] \cdot D_1$ , and the geometrical changes that take place after the **a**  $\rightarrow$  **b** transition and are expressed by Eq. 6.1, that is,  $[\gamma \cdot (\varepsilon_y - 1) + 1] \cdot D_1 = D_{\text{wid}}$ . A solution of this equation for  $def_{\max}$  gives the maximum elastic downward deflection of the bottle's neck:

$$def_{\max} = h_1 - (h_1^2 + 0.25 \cdot (D_1 - D_2)^2 - 0.25 \cdot \{[\gamma \cdot (\varepsilon_y - 1) + 1] \cdot D_1 - D_2\}^2)^{0.5} \quad (6.2)$$

This model has an obvious limit for the  $def_{\max}$  value; it cannot exceed the height of the transitional section  $h_1$ . The condition  $def_{\max} = h_1$  corresponds to the point at which the transitional section flattens (see Fig. 6.1(a)). Respectively, the  $D_{\text{wid}}$  value in Eq. 6.1 cannot exceed  $2[h_1^2 + 0.25(D_1 - D_2)^2]^{0.5} + D_2$ .

The deformation in the cylindrical part of the bottle during the **a**  $\rightarrow$  **b** transition is a complex process described in the science of structural mechanics as the collapse of a thin rigid shell under a distributed load. The model presented below gives the simplest semi-empirical variant of this deformation stage. Figure 6.1(c) shows the schematics of the model. The rim of the deformed cylindrical wall is stretched from  $\pi \cdot D_1$  to the circumference slightly below the point of irreversible deformation,  $\pi \cdot [\gamma \cdot (\varepsilon_y - 1) + 1] \cdot D_1$ . Taking into account the definition of the elastic (Young's) modulus  $M_Y = \sigma_y/(\varepsilon_y - 1)$ , this upper layer is under the stress  $\sigma_{\text{top}} = M_Y \cdot (\varepsilon_{\max} - 1) = M_Y \cdot \gamma \cdot (\varepsilon_y - 1)$ . The principal assumption of the simple top-load model is that the stress in an arbitrary elementary section of the cylindrical wall below its upper rim decreases according to the exponential law:

$$\sigma_\xi = \sigma_{\text{top}} \cdot \text{Exp}(-k \cdot \xi) = M_Y \cdot \gamma \cdot (\varepsilon_y - 1) \cdot \text{Exp}(-k \cdot \xi) \quad (6.3)$$

Here  $\xi$  is the distance of the section from the top of the cylinder, and  $k$  is an empirical parameter. The diameter of this section is  $D_\xi = \varepsilon_\xi \cdot D_1 = (\sigma_\xi/M_Y + 1) \cdot D_1$ . The elemental work of stretching a ring section with the cross-section  $t_1 \cdot d\xi$  and the length  $\pi \cdot D_1$  to the length  $\pi \cdot D_\xi = \pi \cdot \varepsilon_\xi \cdot D_1$  is

$$dW_\xi = \sigma_\xi \cdot [\text{Cross section}] \cdot [\text{Distance}] = \sigma_\xi \cdot [t_1 \cdot d\xi] \cdot [\pi \cdot (\varepsilon_\xi - 1) \cdot D_1] = \pi \cdot \sigma_\xi^2 \cdot (t_1 \cdot D_1/M_Y) \cdot d\xi \quad (6.4)$$

The introduction of the expression for  $\sigma_\xi$  from Eq. 6.3 into Eq. 6.4 and integration from  $\xi = 0$  to  $h_1$  gives the final expression for the work of deforming the cylindrical section of the bottle to the point when its elastic recovery after lifting the top load is still possible:

$$W_{\text{top-load}}^{\text{elast}} \approx (\pi \cdot D_1 \cdot t_1/2k) \cdot M_Y \cdot \gamma^2 \cdot (\varepsilon_y - 1)^2 \cdot [1 - \text{Exp}(-2k \cdot H)] \quad (6.5)$$

Because the  $\varepsilon_y$  value does not depend much on the type of high density polyethylene (HDPE) resin, Eq. 6.5 provides the general assessment of the top-load test. The work of compressing the cylindrical part of a bottle to a point just before the beginning of its inelastic deformation (signifying the failure of the bottle in the test) is proportional to two parameters of the bottle: the wall thickness of the cylindrical body,  $t_1$ , and its diameter,  $D_1$ . The  $W_{\text{top-load}}^{\text{elast}}$  value is also proportional to a single mechanical parameter of the resin, its stiffness (the value of Young's modulus  $M_Y$ ). The maximum top load a container can carry before the start of irreversible deformation is:

$$\text{Top load}_{\text{elast}} = W_{\text{top-load}}^{\text{elast}} / \text{def}_{\text{max}} \quad (6.6)$$

The maximum top load is proportional to the  $W_{\text{top-load}}^{\text{elast}}$  value but also strongly depends on the configuration of the transitional section between the threaded neck and the cylindrical body, as illustrated in Eq. 6.2. The latter dependence explains the large variability in the design of this transitional section, which is aimed at achieving an even distribution of the top load across the container's body and at avoiding excessive local strain areas, such as those at points  $P_1$  and  $P_2$  in Fig. 6.1.

This simple model of the top load test provides a realistic estimation of the maximum top load. As an example, the values of  $W_{\text{top-load}}^{\text{elast}}$  (Eq. 6.5),  $\text{def}_{\text{max}}$  (Eq. 6.2), and  $\text{Top load}_{\text{elast}}$  (Eq. 6.6) were evaluated for a small, thin-walled bottle with the geometry shown in Fig. 6.1 and with the following dimensions:  $D_1 = 61$  mm (2.4 in);  $D_2 = 21$  mm (0.83 in); the wall thickness  $t_1 = 0.35$  mm (0.014 in); the height of the transitional section  $h_1 = 5$  mm (0.2 in); and the height of the cylindrical body  $H = 140$  mm (5.5 in). When such a bottle is manufactured from a stiff HDPE resin characterized by a high secant 1% modulus of 150 kg/mm<sup>2</sup> (1,500 MPa) (which is close to  $M_Y$ ) and a low yield strain  $\varepsilon_y$  of 1.02 to 1.03, the maximum reversible deformation is  $\sim 2$  mm; the work of deformation (depending on the values of  $\gamma$  and  $k$  parameters) ranges from 4 to 4.5 kg · mm, and the estimation of the top load weight varies from 2 to 2.5 kg.

## ■ 6.2 Dynamic Burst Test of HDPE Tubing and Pipes

Bimodal HDPE and medium density polyethylene (MDPE) resins are widely used for the manufacture of pipes (diameter  $> 1$  cm or  $\sim 0.4$  in) and tubing (diameter  $< 1$  cm). These materials revolutionized water and gas distribution systems; they are light, corrosion-resistant, and represent the safest choice in case of earthquakes [5]. A special type of polyethylene resin was developed for pipe manufac-

ture and biomedical applications: radiation or chemically cross-linked polyethylene resins (PEX), which contain chemical links between macromolecules. The cross-linking makes polyethylene more resistant to creep and chemical corrosion, more durable at high temperatures, and allows the material to remain flexible under subfreezing temperatures [6–8].

Two types of tests were developed for polyethylene pipes and tubes: burst tests and static tests [9–11]. The burst tests are carried out at temperatures from  $\sim 20$  to  $90^\circ\text{C}$  at an internal pressure (air or water) ramping to  $\sim 20$  MPa (200 atm, 3,000 psi). The static tests (sustained pressure tests) are carried out at a constant pressure below the burst pressure to determine the time-to-failure.

The mechanical interpretation of the dynamic test is straightforward; it is equivalent to the stress/strain test described in Section 1.10 of Chapter 1. As the internal pressure (the stress) increases, the pipe initially bulges when the stress in a small area of the wall (usually a defect or a bubble) exceeds the yield stress  $\sigma_y$ , and soon after that the bulged wall bursts under the breaking stress  $\sigma_{br}$ . (The  $\sigma_y$  and the  $\sigma_{br}$  values for HDPE resins are relatively close.) Although the dynamic tests are performed by ramping the internal pressure until the pipe bursts, the meaningful goal of the testing is to determine the maximum internal pressure a pipe can withstand without the wall bulging. In general, the strain at this point is  $\gamma \cdot (\epsilon_y - 1) + 1$  where  $\gamma$  is the tolerance coefficient, 0.8 to 0.9, the same as in Eqs. 6.2 to 6.5, and respectively, the stress is  $\gamma \cdot \sigma_y$ . Because the yield strain of HDPE resins (the elongation at the moment when the bulge appears) is a nearly constant value, the crucial parameter determining the outcome of the dynamic burst test is the resin stiffness (Young's modulus),  $M_Y = \sigma_y / (\epsilon_y - 1)$  [12, 13].

## ■ 6.3 Static Burst Test and Long-Term Fatigue in Polyethylene

Static burst tests of pipes and tubes are carried out in the first range of the stress/strain curve in Fig. 1.18, before the stress reaches the yield point. The behavior of many polymers, including HDPE and MDPE resins, under a low stress is very different from their behavior in relatively rapid dynamic burst tests. It is governed by a phenomenon called long-term fatigue. This phenomenon in polymers (it is also called creep-to-rupture or stress cracking) is well researched.

### 6.3.1 Principal Equation for Low-Stress Failure

Plastic materials strained for a long time fail at a lower stress than the same materials strained for a shorter time. Even a relatively small stress, if applied for a sufficiently long time, will invariably result in mechanical failure. In engineering practice, the dependence between the stress  $\sigma$  applied to a polymer sample and the time  $\tau$  it takes to break the sample is usually presented in the coordinates “ $\log(\tau)$  as a function of  $\sigma$ ,” as shown in Fig. 6.2. For many polymers, including HDPE resins, such plots are linear:

$$\log(\tau) = A - K \cdot \sigma \quad (6.7)$$

where  $A$  and  $K$  are parameters which depend on the mechanical properties of a resin. Equation 6.7 does not hold at  $\sigma \rightarrow 0$ .

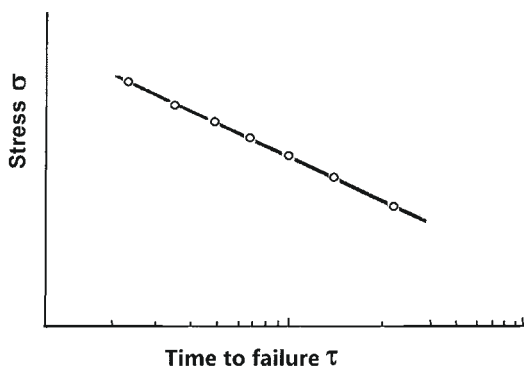


**Figure 6.2** Standard presentation of long-term fatigue data for polymers

A general physical theory has been developed to describe linear dependencies represented by Eq. 6.7 as a manifestation of the universal mechanism of polymer failure [14–16]. The theory is based on numerous experimental results on the long-term fatigue of polymers at different temperatures. The most convincing results were obtained for strongly oriented polymer filaments, which usually break under stress without any noticeable elongation. These results, when presented in the coordinates of Eq. 6.7, produce plots schematically shown in Fig. 6.3. Such plots reflect a well-known fact that an increase in temperature accelerates the polymer failure under stress, provided that the temperature is not so high as to facilitate a substantial creep.

The data in Fig. 6.3 were described by the universal equation:

$$\tau = \tau_0 \cdot \text{Exp}[(U_0 - \gamma \cdot \sigma)/(k_B \cdot T)] \quad (6.8)$$

where  $k_B$  is Boltzmann constant and temperature  $T$  is in kelvin. The  $\tau_0$  value in Eq. 6.8 corresponds to the shortest time-to-failure for any polymer; it is  $\sim 10^{-12}$  to  $10^{-13}$  s, the value that is close to the vibrational frequency of the C–C bond in a

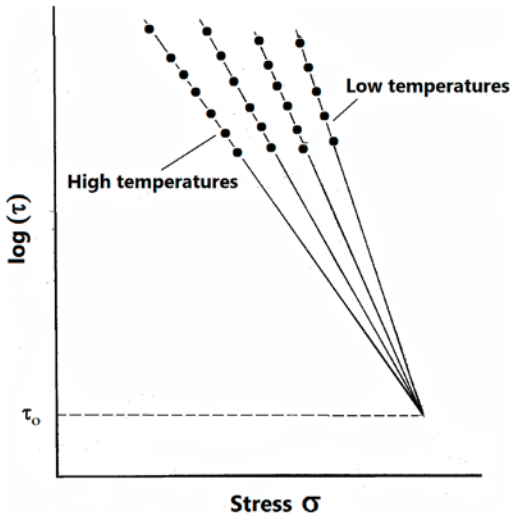


**Figure 6.3** Long-term fatigue data for polymers in coordinates of Equation 6.8

polymer chain. The  $U_0$  term in Eq. 6.8 is the initial potential energy barrier for a polymer failure. Its value, which was experimentally estimated for oriented polypropylene film, is  $\sim 56$  kcal/mol; it is close to the energy of the C-C bond. The  $\gamma$  parameter in Eq. 6.8 is a structure-dependent parameter that reflects the uniformity of stress distribution across the cross section of a polymer sample. Equation 6.8 signifies that the external stress decreases the potential energy barrier for the C-C bond rupture at a particular temperature and thus increases the frequency of a spontaneous C-C bond rupture caused by vibrational fluctuations. Thus, Eq. 6.8 provides the physical meaning to parameters  $A$  and  $K$  in Eq. 6.7. Detailed mechanistic studies of failure in LDPE resins at various temperatures give significant support to this theory in general and have supplied many quantitative details [17].

The theory represented by Eq. 6.8 provides a convenient simplified physical model for the description of many phenomena related to time-dependent properties of polymers, including environmental stress cracking (see Section 6.4). Experimental data for HDPE and MDPE resins with density from 0.94 to 0.95 g/cm<sup>3</sup> and with a high-load melt index  $I_{21} \sim 1$  (such resins are used for the fabrication of pipes) also support this theory. When pipes made from these resins are tested under below-burst pressure, the dependence between the time-to-failure and the stress is well described by Eqs. 6.7 and 6.8, although a deviation from these dependencies is observed for other types of resins at low stresses [18, 19].

### 6.3.2 Physical Mechanism of Polymer Failure under Low Stress

The phenomenological mechanism of gradual polymer failure under low stress includes several distinct stages:

craze nucleation → craze growth → craze failure (crack initiation)  
→ crack propagation.

Numerous studies describing details of this cascade of events in polyethylene resins have been published [8, 20–25]. Studies of the static fatigue fracture in HDPE resins identified the following features of the polymer failure under low stress [8, 23, 26]:

1. The crack initiation stage (“induction time”) occupies the largest fraction of the total time between the stress application and the sample failure. In contrast, the crack propagation stage is, in relative terms, very rapid. Figure 6.4 gives an example of a relationship between the crack initiation and the propagation rate in the bending test of a notched polyethylene sample [26].

2. The rate of the slow craze-growing stage is controlled by the stress intensity [24, 25, 27, 28]. The resistance of polyethylene to the initiation of fracture under a static load is related to a large extent to its resistance to voiding [21, 26, 29]. This latter process depends on a combination of numerous structural factors, such as the lamellae thickness, the size of amorphous regions, the degree of crystal perfection, the number of tie molecules and entanglements, and so on. All these factors

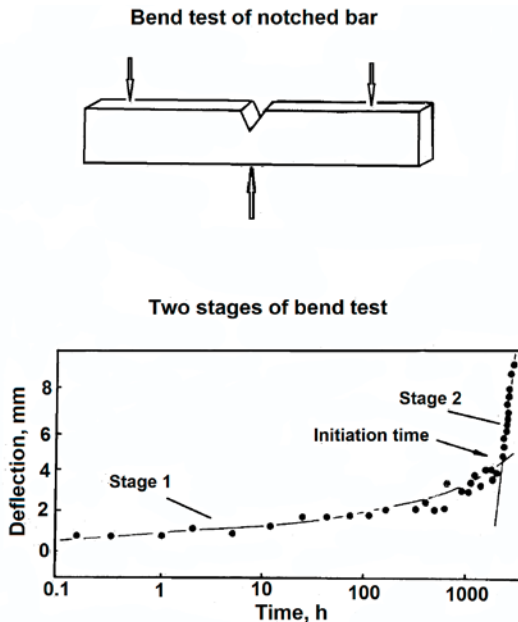
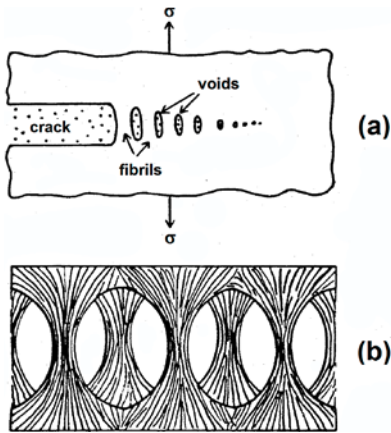


**Figure 6.4** Two stages of crack failure in bend test of notched bar; data from [26]



**(b) Figure 6.5** (a) Deformation of crack tip and crack propagation; (b) Schematic structure of fibrils

make the prediction of resistance of polyethylene resins to crack initiation quite unreliable.

3. Figure 6.5 schematically depicts the process of crack propagation through a polymer [30] based on nuclear magnetic resonance (NMR) imaging data for amorphous polymers [29] and polyethylene [21, 22]. After the first cracks are initiated at the points of the maximum stress intensity (at the surface of the sample), the crack propagation stage (the fast stage of the fatigue failure) begins. This stage is mostly controlled by the effective viscosity of the polymer medium. Once the crazes on the path of the growing crack have nucleated, the local stress level at the tip of the crack exceeds the yield stress of the polymer. As a result, a small area between the tip of the crack and the closest craze starts to stretch and is gradually transformed into bundles of oriented macromolecules called craze fibrils. The craze fibrils steadily increase in length and eventually fail. The quantitative theory of the crack growth predicts that the crack growth rate is proportional to the yield stress of the resin and reciprocal to the square of the Young's modulus and the intrinsic viscosity of fibrils in the craze [22] (see Fig. 6.5 (b)).

4. Low-density and high-density cross-linking in polyethylene, either by radiation or chemical, increases the fatigue resistance on both the crack initiation and propagation stages [8, 23].

Generally speaking, the growth of oriented craze fibrils during the low-stress tests (Fig. 6.5) is identical to the yielding and the neck formation in polymer samples during a tensile test (Section 1.10). The craze fibrils are highly oriented [17, 22, 30, 31]. Such fibrils can bear a significantly greater stress than the bulk of the resin sample [26]. As obvious from Fig. 6.5, the cracks propagate because the craze fibrils gradually rupture [26]. Figure 6.6 shows the end result of the slow cracking, a surface of a fractured MDPE sample [19] covered with broken craze fibrils consisting of bundles of oriented polymer molecules.

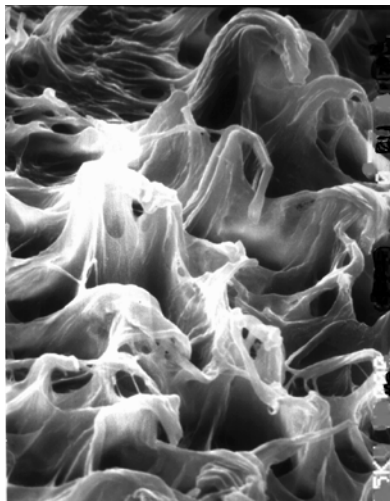


**Figure 6.6** Scanning electron micrograph of fracture surface of MDPE sample; magnification x1000

The overall mechanical behavior of HDPE and MDPE resins under low-stress conditions is predominantly affected by the molecular entanglement network that is present in the resin melt prior to crystallization. This entanglement network is mostly provided by high molecular weight macromolecules in the resins. A similar explanation based on the entanglement mechanism is used to calculate ultimate draw ratios in polyethylene [32, 33]. The same entanglement mechanism explains why adding high molecular weight material to a polyethylene resin enhances its resistance to fracture. It also explains why an increase of the average molecular weight of a polyethylene resin is always accompanied by a decrease in the crack propagation rate [34]. The same theory was also used to explain deformation and failure processes in amorphous polymers [35–37].

Polyethylene resins with a broad molecular weight distribution fail relatively easily under low stress. This deficiency is the consequence of peculiarities of polymer crystallization from the melt [38]. The crystallization process is usually accompanied by fractionation of polymer constituents. High molecular weight components in such polymers crystallize at the highest temperatures whereas low molecular weight and branched macromolecules crystallize the last, at relatively low temperatures. This fractionation can be clearly observed in differential scanning calorimetry (DSC) studies of polyethylene resins described in Chapter 3. As a consequence of spontaneous fractionation, the low molecular weight and branched macromolecules concentrate in interlamellar regions (Figs. 1.16 and 1.17) and in the areas between spherulites. These macromolecules do not form good links between structural elements within the spherulites (between the lamellae) and between the spherulites themselves. These inter-spherulite regions, as well as the centers of spherulites, are the starting points of the initial crazes, which develop under stress.

The degree of interconnectedness between spherulites can be somewhat controlled by crystallization conditions. For example, rapidly quenched pipe-grade MDPE resins have relatively homogeneous morphology; their spherulites consist of lamellae that are merely  $\sim 160 \text{ \AA}$  thick. However, annealing these samples increases segregation of their material into separate crystallite populations and produces poorly connected large spherulites with thicker lamellae,  $\sim 270 \text{ \AA}$ . As a result, the annealing significantly degrades the crack propagation resistance of the materials due to a lower concentration of tie molecules [39]. In addition, a significant local stress can develop even in unstrained articles (containers, pipes) during the later stages of crystallization. The existence of this stress also affects the crack growth rate [40].

## ■ 6.4 Environmental Stress-Cracking Resistance

Resistance to environmental stress cracking (ESCR) is one of the two most important end-use properties of HDPE and MDPE resins formulated for applications in household and industrial containers (the second such property being stiffness). Resistance to environmental stress cracking is also an important property of LDPE and LLDPE resins used as cable and wire insulation materials.

### 6.4.1 Description of ESCR Test

The simplest ESCR test for polyethylene resins is called the bent strip test. It provides a good graphic description of macroscopic changes accompanying the environmental stress cracking. Figure 6.7 shows several stages of the test. A compression-molded strip of a resin is bent close to  $180^\circ$  and positioned in a metal

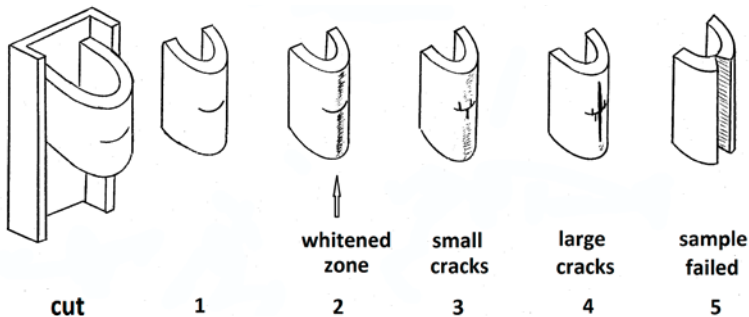
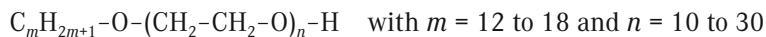


**Figure 6.7** Stages of bent strip environmental stress cracking test

holder. The bent strip is notched with a razor parallel to the long edge of the strip (to concentrate the stress in this area) and placed in a bath with detergent solution in water.

The most common detergents are non-ionic liquid detergents; they are usually used as 10% solutions in water. The detergents have the following structures:



The detergent most often used in the bent strip test is called Igepal® CO-630, it has the second structure with  $n = 9$ .

In the beginning of the test, the sample shows no visible traces of stress for a significant period of time and the curvature of the bend remains unchanged; Stage 1 in Fig. 6.7. The first manifestation of the polymer yielding to stress is an increase in the bend curvature and the development of a whitened area around the cut, indicating the formation of numerous crazes and voids in the material (Stage 2). After a certain time, one or several small cracks develop along the bend line (Stage 3). The cracks usually initiate somewhere at the original notch, which serves as a stress concentrator. Some of the cracks (those in the zone with the minimum radius of curvature and, therefore, the highest stress concentration) propagate faster than other cracks (Stage 4). In some samples, polyethylene fibrils (craze fibrils) can be seen bridging the sides of the cracks. The moment when the sample fails is defined as the moment when the cracks propagate to the sides of the strip. The time-to-failure is usually determined visually by a technician who periodically examines several strips made from the same resin submerged in the detergent solution.

#### 6.4.2 Physics of Environmental Stress Cracking

The original phenomenological definition of environmental stress cracking states that it is a failure in the surface-initiated brittle fracture of a polyethylene specimen under stress in contact with a sensitizing medium in the absence of which the fracture would not occur under the same stress [4, 38, 41, 42]. Although many other polymers suffer from the environmental stress cracking phenomenon [38, 41, 43, 44], this phenomenon is particularly troublesome for polyethylene products made of HDPE and MDPE resins due to their wide use for the manufacture of containers for transportation and storage of household soaps and industrial detergents.

Environmental stress cracking is closely related to the fracture of plastics under a sub-yield stress discussed in Section 6.3 [42]. Detailed studies of the rupture surface of HDPE and LDPE samples by the scanning electron microscopy method [18,

19, 45–49] showed that the fracture surfaces are always ductile. However, the size of the deformation zones, especially for HDPE resins, can be so small that the newly formed surface appears to an unaided eye as an outcome of a brittle rupture. Microscopic observations reveal however that highly oriented craze fibrils (similar to those in Fig. 6.6) are indeed present on the fracture surfaces, but their size (which strongly depends on the speed of crack propagation) is usually very small.

Detergents are by no means the only sensitizing agents that can cause environmental stress cracking. Various alcohols, silicon oils (such as mold-release agents used during fabrication), ketones, phenols, esters, halogenated hydrocarbons, mineral and vegetable oil, and even some low-molecular-weight polymers can produce similar effects [31, 38, 47]. Environmental stress cracking is essentially a physical phenomenon involving neither a chemical reaction between polyethylene and a detergent nor large-scale swelling typical for solvent-initiated cracking [38]. This does not mean, however, that the surfactants do not interact with polyethylene at all. Infrared spectroscopic observations indicate that polyethylene absorbs about 1% of a detergent and water, both of which concentrate in the regions between spherulites [50]. This localized plasticization of polyethylene is the essential feature of the phenomenon. When microcracks appear in polyethylene, they propagate along the weakest boundaries in the material, which are the borders between neighboring spherulites and the borders between microfibrils and lamellae within the spherulites; that is, they propagate through the areas where the detergent/water micelles concentrate [18, 45, 51].

### 6.4.3 Structural Parameters of HDPE Resins Affecting ESCR

All three principal structural properties of polyethylene resins, the crystallinity degree (density), the molecular weight, and the molecular weight distribution, affect their ESCR [38].

*Molecular weight* An increase in the molecular weight (a decrease in the melt index) is nearly always accompanied by an increase in ESCR. The dependence between the time-to-failure under ESCR conditions at a particular stress level and the melt index of HDPE resins is very strong. For example, a decrease of the  $I_2$  value of an HDPE resin from 2.0 to 0.3 results in an increase of the time-to-failure from two to over 600 h. Similarly, a decrease of the  $I_2$  value of an LDPE resin from 20 to 0.3 is accompanied by an increase of the time-to-failure from 20 minutes to ~7000 h [38]. Obviously, HDPE resins with the highest possible molecular weight (from the fabrication point of view) should be used in detergent-sensitive applications. However, the dependence between the time-to-failure and the molecular weight is not linear; after a certain high melt index is reached, the ESCR decreases precipitously. The value of the melt index corresponding to a nearly complete loss of the ESCR is

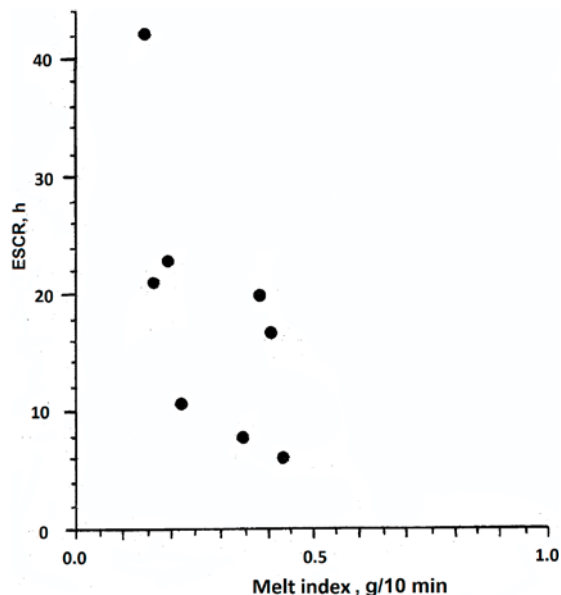


**Figure 6.8** Effect of melt index on ESCR of HDPE resins; data from [46]

different for different resin types and should be experimentally determined in each particular case. Unfortunately, the dependence between the ESCR and the melt index is usually affected by variations in other properties of the resin; these are secondary effects that are difficult to eliminate completely. Figure 6.8 shows that these effects make the correlation between ESCR and the melt index for HDPE resins in the density range of 0.950 to 0.955 g/cm<sup>3</sup> less clear-cut [46].

*Molecular weight distribution* The width of the molecular weight distribution significantly affects the ESCR [38]. Polymer components with low molecular weight, which are always present in resins with a broad molecular weight distribution, are especially detrimental for ESCR [38]. Extraction of these components produces a very large increase in ESCR, and concurrently, the addition of low molecular weight waxes to polyethylene resins decreases their ESCR [38]. The ESCR is the highest for HDPE resins with a large fraction of high molecular weight macromolecules [18, 52]. The longest polymer chains in these resins are the source of interlamellar tie molecules, which play the crucial role in ESCR [53].

A direct quantitative assessment of the concentration of tie molecules has proved to be difficult, but several indirect experimental techniques have been developed. They include polarization IR spectroscopy [54], crystallization fractionation [55], and step-wise isothermal crystallization [13]. One such technique involves deformation of MDPE or LLDPE film followed by a chlorination reaction and by analysis of polarized infrared spectra. This technique provides the means of ranking resins of comparable density but with different molecular weight and molecular weight distribution in terms of their resistance to crack propagation [54]. The tie mole-

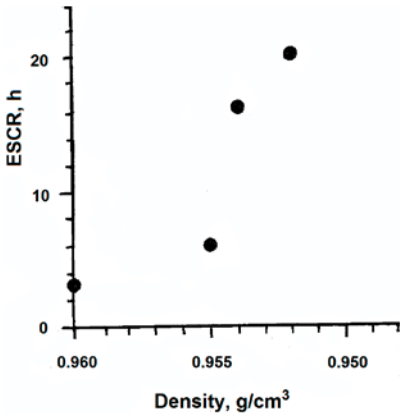


**Figure 6.9** Effect of density on ESCR of HDPE resins; data from [46]

cules can be also partially separated from the bulk of HDPE resins through the use of the preparative crystallization fractionation (CRYSTAF) technique with 1,2,4-trichlorobenzene as a solvent; the polymer fraction rich in tie molecules crystallizes between 75 and 85 °C [55]. ESCR of the resins increases when the molecular weight and the content of this fraction increase.

*Crystallinity level* The effect of the crystallinity degree (density) on the ESCR is also very difficult to present in a concise form. Depending on testing conditions, an increase in the crystallinity degree and density can produce either an increase or a decrease in ESCR [38]. The bent strip ESCR test shown in Fig. 6.7 is essentially a constant strain test. Therefore, polymer components with a low crystallinity degree in the tested strips are subjected to a lower stress level at the same strain compared to the highly crystalline components, since the tensile modulus of the polyethylene resins of low crystallinity (MDPE, LLDPE, LDPE) is lower (Section 1.10). Consequently, a reduction in the crystallinity degree and density generally leads to a higher ESCR [38, 46]. However, experimental data relating ESCR and polyethylene density are usually very scattered and are affected by other factors. The most important of them are the variations in the molecular weight and the molecular weight distribution (Fig. 6.9), as well as the length of side-groups in ethylene/ $\alpha$ -olefin copolymers [56]; the longer the side chain (for example, in ethylene/octene copolymers) the higher is the ESCR.

In addition to the structural parameters of polyethylene resins, their ESCR is also affected by numerous processing parameters [18, 38, 57]: the temperature, the speed of extrusion, the speed of cooling, melt orientation during fabrication, and other factors. These parameters affect the morphological features of the articles, such as the size and the quality of spherulites and crystallites, chain orientation, the degree of chain entanglement, and so on. None of these effects have yet been studied in sufficient detail to yield a simple and coherent set of rules. However, the existence of these effects imposes significant restrictions on the interpretation of ESCR test results.

#### 6.4.4 Relationship between ESCR and Long-Term Fatigue in Polyethylene

On the quantitative level, general features of environmental stress cracking can be better understood if this type of polymer failure is analyzed within the framework of long-term stress fatigue (Sections 6.3.1 and 6.3.2). The theory that describes the linear dependencies shown in Eq. 6.7 proposes the general polymer failure mechanism [14, 15] represented by the universal expression shown in Eq. 6.8. This theory also points to a convenient starting point for the description of many phenomena related to environmental stress cracking. These two types of cracking of high molecular weight HDPE and MDPE resins used for fabrication of pipes ( $I_{21} \sim 1$ , density from 0.94 to 0.95 g/cm<sup>3</sup>) were studied by subjecting the pipes to internal pressure [18, 19]. In the absence of a surfactant, the dependence between the time-to-failure and the stress for many HDPE samples is well described by Eq. 6.7. However, when the testing is carried out in the presence of a detergent (1% of Igepal® CO-630 solution in water), a clear deviation from the linear logarithmic dependence is observed in the high  $\tau$ /low  $\sigma$  range. Figures 6.10 and 6.11 emphasize the surfactant effect by plotting the experimental data from [18] in the coordinates “ $\sigma_d/\sigma_a$  as a function of  $\log(\tau)$ ,” where  $\sigma_d$  and  $\sigma_a$  are the stresses in the presence of the detergent solution and in air, respectively. Thus, the  $\sigma_d/\sigma_a$  ratio is the measure of the environment-related weakening of polyethylene.

Plotting experimental data in these coordinates allows separation of two effects: the universal time-dependent polymer properties discussed in Section 6.3 and the environmental stress cracking effect as such. Plotting in these coordinates also provides the answer to an important question about environmental stress cracking: what reduction in stress is required to enable an HDPE or a MDPE sample to survive under some particular conditions for a particular period of time?

The plots in Figs. 6.10 and 6.11 identify two types of environmental stress cracking behavior. Some HDPE samples in Fig. 6.10 show a relatively mild effect (that is, good ESCR); their rupture stress is reduced by only ~20% after 1,000 h of testing

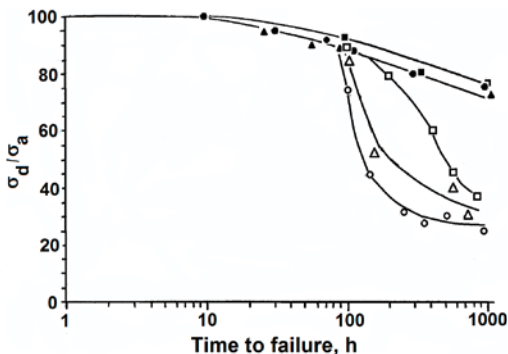


**Figure 6.10** Effect of detergent solution on long-term fatigue of HDPE resins: ▲, ■, ● are HDPE resins with high ESCR; △, □, ○ are HDPE resins with low ESCR. Experimental data from [18]

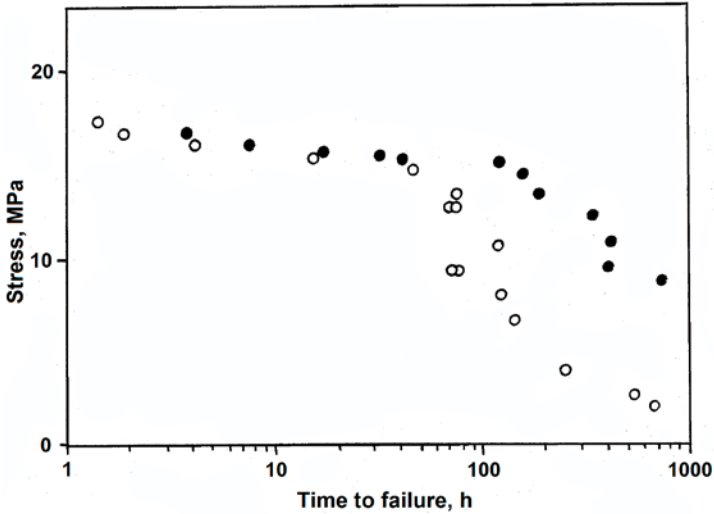


**Figure 6.11** Correlation between stress and time-to-failure for MDPE (ethylene/butene copolymer with density 0.940 g/cm<sup>3</sup>); data from [19]

in the presence of the detergent (top curves). Other HDPE samples have very poor ESCR; to survive for 1,000 h, their rupture stress should not be higher than 25 to 30% of the stress they can bear in air (bottom curves). The comparison of different curves in Fig. 6.10 shows also that the HDPE samples that have longer lifetimes at low stresses also have better resistance to environmental stress cracking: the cracking-resistant samples survive for much longer times (both in air and in the presence of a detergent) than the cracking-prone samples.

Several features related to the loss of strength under the environmental stress cracking conditions for HDPE resins follow from the analysis of the data in Figs. 6.10 and 6.11:

1. The resistance of polyethylene to environmental stress cracking at a relatively high stress (close to the yield stress) does not decrease appreciably in the presence of a detergent, most probably, because the survival time under these conditions, a few hours, is not long enough for the environment-related cracks to develop. In other words, the environmental stress cracking can be clearly observed only at a low stress level when the time-to-failure exceeds 50 h.
2. The resistance to environmental stress cracking is related to long-term fatigue (creep) properties, which suggests a similarity in the rupture mechanism [16]. The changes in the polyethylene structure or processing parameters that improve its long-term stability also improve its ESCR.
3. The fact that a significant period of time is required for environmental stress cracking to manifest itself suggests that it is a diffusion-related process. Either a significant time is required for detergent solution to diffuse into a resin or the de-

tergent-induced structural changes involve diffusion-controlled rearrangements of polymer chains.

These features of environmental stress cracking suggest a modified definition of the phenomenon [18, 58]: environmental stress cracking is an acceleration of the long-term stress-fatigue process in polyethylene caused by several types of surface-active agents that facilitate crack propagation.

#### 6.4.5 Mechanism of Environmental Stress Cracking

The mechanism of the polyethylene failure under environmental stress cracking conditions represents a special case of the general mechanism describing the mechanical failure of polymers under low stress, which is discussed in Section 6.3.2. As with the process of failure under low stress, the mechanism includes four distinct stages [59, 60]:

craze nucleation (the longest stage) → craze growth →  
craze failure (crack initiation) → crack propagation.

The overall mechanical behavior under the conditions of environmental stress cracking is similar to that of the failure under low stress; it is dominated by the molecular entanglement network, which is formed in the polymer melt prior to crystallization [38] (Section 6.3.2). Crystallization of most polyethylene resins from the melt leads to a spontaneous fractionation of their components. The low molecular weight and branched macromolecules crystallize at the latest stage and concentrate in interlamellar and inter-spherulite regions. These short polymer chains cannot serve as good links between the lamellae and between the spherulites. The principal feature responsible for the ESCR is the presence of tie molecules of a high molecular weight, which reinforce mechanically weak areas between and within spherulites and mitigate the effects of polymer fractionation [18, 38, 45–49]. The content of tie molecules in an HDPE resin can be artificially increased, for example, by co-blending a small amount of a semicrystalline ethylene block copolymer with the resin [61] or by co-blending an HDPE resin with a high molecular weight LLDPE resin, especially if such an LLDPE resin contains a small amount of long-chain branches [62].

Two subjects are important for the discussion of the mechanism of environmental stress cracking: the role of the detergent and the role of the solvent for the detergent. A detailed analysis of the liquid environment and its effect on the ESCR of LDPE and HDPE resins shows several important effects [17, 27, 30, 41, 52, 60].

Figure 6.12 compares crack propagation phenomena in an HDPE resin in three different environments: air, water, and 10% solution of Igepal CO-630 in water [27]. The dependence obtained in the air test shows the complex fatigue behavior typi-

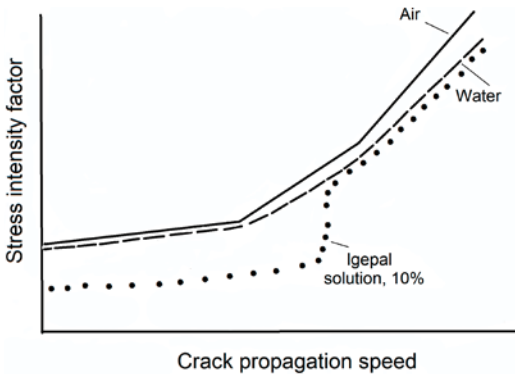


**Figure 6.12** Crack propagation speed in HDPE in three environments; data from [30]

cal for HDPE resins in general (Section 6.3.2). Cracks start to grow at a certain finite stress level, and the crack propagation rate at low stresses increases rapidly with an increase in the stress, but the acceleration of the crack propagation at high stresses is less pronounced. The behavior of the same HDPE resin in the water environment is mostly the same as in air, which means that water is not an effective sensitizing agent. Introduction of the detergent changes several features of the dependence between the stress and the crack growth rate:

1. The minimum stress required for the crack to grow decreases about twofold.
2. A new stage in the crack propagation phenomenon appears: the speed of the crack growth at a particular stress does not depend on the stress level.
3. The environmental stress cracking phenomenon manifests itself at relatively low stresses. For this reason, the high-stress range of the curve in Fig. 6.12 (the range in which the specific effect of the detergent disappears) is of little concern under the real-life conditions. However, an enormous difference exists in the speed of crack propagation between solutions of Igepal CO-630 in different solvents (Fig. 6.13).

The ESCR of polyethylene resins strongly depends on the concentration of the detergent (Igepal CO-630 in this case) in water [63, 64]. The largest reduction in the time-to-failure occurs at the concentration of  $\leq 0.1\%$ . An additional increase to  $\sim 20$

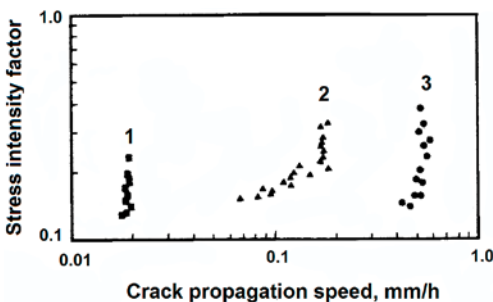


**Figure 6.13** Environment effect on crack propagation speed in HDPE resin; data from [30]. Solvents for Igepal CO-630: (1) ethanol, (2) ethylene glycol, and (3) water

to 25% leads to an additional reduction of the time-to-failure, but the change is minimal when the detergent concentration reaches ~50%, and a further concentration increase from 50 to 100% does not produce any effect at all. Low molecular weight organic liquids, when used by themselves, exhibit some effect. The effect is independent of such properties of the liquids as viscosity and surface tension.

The environmental effect strongly depends on the interaction between the components in the liquid. The cracks propagate slowly when exposed to 10% solution of Igepal CO-630 in ethanol, whereas colloidal solutions of the same detergent in ethylene glycol or water are 20 to 30 times more aggressive. The effect of Igepal CO-630 solution in ethylene glycol increases with the detergent concentration and becomes more pronounced after the critical micelle concentration is reached. Increasing the detergent concentration from 0.001 to 2% produces a 25-fold increase in the crack growth rate [17].

The environmental stress cracking effect of detergent solutions strongly depends on temperature [17, 51, 57]; this dependence can be described by the Arrhenius equation. The activation energy of the process does not depend on the detergent concentration but it strongly depends on the hydrophilic-lipophilic balance of the detergent. Detergents usually used for ESCR testing exhibit a combination of both lipophilic properties due to their oxyethylene chains and hydrophilic properties due to alcohol groups at the end of the chains. An increase in the lipophilic activity (an increase in the length of the oxyethylene chain) produces an increase in the activation enthalpy of crack propagation.

The application of hydrostatic pressure to the detergent solution reduces the crack propagation speed [17]. This change is probably related to the fact that the crazing process is accompanied by an increase in volume and therefore would be hindered as the hydrostatic pressure increases. When silicon oils are used in environmental stress cracking tests, an increase in oil viscosity is accompanied by a noticeable decrease in the crack propagation speed [27].

Based on these observations, a plasticization model of the environmental stress cracking phenomenon has been proposed [30, 31, 60]. The model is related to the general crack propagation model shown schematically in Fig. 6.5. Thermodynamic calculations indicate that a significant stress at the tip of the crack and in the craze that precedes the crack tip greatly increases the permeability of the polymer. This change produces local swelling, significant plasticization of the amorphous phase, and the reorganization of the chain entanglement. All these effects lead to a decrease in the load-bearing capability of the amorphous phase. Indeed, electron microscopic studies confirmed the effect of aggressive agents on the polymer morphology at the deformation stage [46, 47, 51, 60]. The chemicals that cause environmental stress cracking decrease cohesion between lamellae and microfibrils in spherulites and thus facilitate the crack propagation. Although environmental stress cracking is inherently a slow-developing phenomenon, it is nevertheless

affected by low viscosity of some agents. It is possible that the enhanced aggressive properties of detergent solutions in water can be partially attributed to their lower effective viscosity. Although this mechanism of environmental stress cracking is well supported by the experimental evidence, it is the least persuasive in explaining the very high effectiveness of colloidal detergent solutions as agents of environmental stress cracking compared to other organic liquids, which also swell polyethylene.

## ■ References

1. Standard Test Method for Column Crush Properties of Blown Thermoplastic Containers, (ASTM) D2659-11; <http://www.astm.org/Standards/D2659.htm>
2. Standard Test Method for Compression Resistance of a Container under Constant Load, ASTM D4577-05 (2010); <http://www.astm.org/Standards/D4577.htm>
3. Column Crush Properties of Blown Thermoplastic Containers, ASTM D2659-95; <http://www.astm.org/DATABASE.CART/HISTORICAL/D2659-95.htm>
4. Deutsches Institut Fur Normung E. V. (DIN) 55440-1:99; Packaging Compression Test
5. Gahleitner, M., *eXPRESS Polym. Lett.* (2011) 5, p. 936, doi:10.3144/expresspolymlett.2011.91
6. Standard Specification for Crosslinked Polyethylene (PEX) Tubing, ASTM F876-10e1; <http://www.astm.org/Standards/F876.htm>
7. Standard Specification for Crosslinked Polyethylene (PEX) Hot- and Cold-Water Distribution Systems, ASTM F877-11a; <http://www.astm.org/Standards/F877.htm>
8. Baker, D. A., Bellare, A., Pruitt, L., *J. Biomed. Mater., Res., Part A* (2003) 66, p. 146
9. Test Method for Time-to-Failure of Plastic Pipe Under Constant Internal Pressure, ASTM D1598-02 (2009); <http://www.astm.org/Standards/D1598.htm>
10. Test Method for Resistance to Short-Time Hydraulic Pressure of Plastic Pipe, Tubing, and Fittings, ASTM D1599-99 (2011); <http://www.astm.org/Standards/D1599.htm>
11. Standard Test Method for Obtaining Hydrostatic Design Basis for Thermoplastic Pipe Materials or Pressure Design Basis for Thermoplastic Pipe Products, ASTM D2837-11; <http://www.astm.org/Standards/D2837.htm>
12. Bohm, L. L., Enderle, H. F., Fleißner, M., *Adv. Mater. Sci.* (1992) 4, p. 234
13. Cazenave, J., Seguela, R., Sixou, B., Germain, Y., *Polymer* (2006) 47, p. 3904
14. Zhurkov, S. N., *J. Polym. Sci., Part A: Polym. Chem.* (1972) 10, p. 1509
15. Kausch, H. H., Williams, J. G., In *Encyclopedia of Polymer Science and Engineering*, Mark, H. F., Kroschwitz, J. I. (Eds), vol. 7 (1986) John Wiley & Sons, New York, p. 360
16. Rose, L. J., Channell, A. D., Frye, C. J., Capaccio, G., *J. Appl. Polym. Sci.* (1994) 54, p. 2119
17. Ohde, Y., Okamoto, H., *J. Mater. Sci.* (1980) 15, p. 1539

18. Lustiger, A., Markham, R.L., *Polymer* (1983) 24, p. 1647
19. Lustiger, A., Corneliussen, R.D., *J. Mater. Sci.* (1987) 22, p. 2470
20. Friedrich, K., *Adv. Polym. Sci.* (1983) 52–53, p. 225
21. Kasakevich, M.L., Moet, A., Chudnovsky, A., *J. Appl. Polym. Sci.* (1990) 39, p. 395
22. Brown, N., Lu, X., *Polymer* (1985) 36, p. 543
23. Pruitt, L.A., *Biomaterials* (2005) 26, p. 902
24. Parsons, M., Stepanov, E.V., Hiltner, A., Baer, E., *J. Mater. Sci.* (2000) 35, p. 2659
25. Favier, V., Giroud, T., Strijko, E., Hiver, J.M., G'Sell, C., Hellinckx, S., Goldberg, A., *Polymer* (2002) 43, p. 1375
26. Barry, D., Delatycki, O., *J. Polym. Sci., Polym. Phys. Ed.* (1987) 25, p. 883
27. Tonyali, K., Rogers, C.E., Brown, H.R., *Polym. Eng. Sci.* (1987) 27, p. 82
28. Tonyali, K., Rogers, C.E., Brown, H.R., *J. Macromol. Sci., Part B: Phys* (1989) 28, p. 235
29. Adriaensens, P., Storme, L., Carleer, R., Vanderzande, D., Gelan, J., Litvinov, V.M., Marissen, R., *Macromolecules* (2000) 33, p. 4836
30. Tonyali, K., Rogers, C.E., Brown, H.R., *Polymer* (1987) 28, p. 1472
31. Brown, H.R., *Polymer* (1986) 19, p. 1186
32. Smith, P., Lemstra, P.J., Booiij, H.C., *J. Polym. Sci., Part B: Polym. Phys.* (1981) 19, p. 877
33. Irvine, P.A., Smith, P., *Macromolecules* (1986) 19, p. 240
34. Marshall, G.P., Culver, L.E., Williams, J.G., In *Plastics and Polymers* (1970) 38, p. 95
35. Donald, A.M., Kramer, E.J., *Polymer* (1983) 24, p. 1063
36. Donald, A.M., Kramer, E.J., *Polymer* (1982) 23, p. 461
37. Kramer, E.J., In *Developments in Polymer Fracture-1*, Andrews, E.H. (Ed.) (1979) Applied Science Publishers, London, Chapter 3
38. Howard, J.B., In *Engineering Design for Plastics*, Baer, E. (Ed.) (1964) Reinhold Publishing Corp., New York, p. 742
39. Strebel, J.J., Moet, A., *J. Polym. Sci., Part B: Polym. Phys.* (1995) 33, p. 1969
40. Lu, X., Brown, N., *Polymer* (1987) 28, p. 1505
41. Wright, D.C., *Environmental Stress Cracking of Plastics* (1996) Rapra Technology, Shawbury, Great Britain, Chapter 1
42. Ayyer, R., Hiltner, A., Baer E., *J. Mater. Sci.* (2007) 42, p. 7004
43. Williams, J.G., Marshall, G.P., *Proc. Roy. Soc., A* (1975) 342, p. 55
44. Howard, J.B., In *Crystalline Olefin Polymers, Part II*, Raff, R.A.V., Doak, K.W. (Eds.) (1964) Interscience, New York
45. Hase, T.W., McRae, P.H., *SPE J.* (1968) 24, p. 27
46. Hannon, M.J., *J. Appl. Polym. Sci.* (1974) 18, p. 3761
47. Singleton, C.J., Roche, E., Geil, P.H., *J. Appl. Polym. Sci.* (1977) 21, p. 2319
48. Bandyopadhyay, S., Brown, H.R., *Polymer* (1978) 19, p. 589
49. Bandyopadhyay, S., Brown, H.R., *J. Mater. Sci.* (1977) 12, p. 2131

50. Frayer, P.D., Tong, P.P., Dreher, W.W., *Polym. Eng. Sci.* (1977) 17, p. 27
51. Ghanbari-Siahkali, A., Kingshott, P., Breiby, D.W., Arleth, L., Koch, C., Almdal, K.K., *Polym. Degrad. Stab.* (2005) 89, p. 442
52. Aiba, M., Osawa, Z., *Polym. Degr. Stab.* (1998) 61, p. 1
53. Lustiger, A., Corneliussen, R.D., *J. Polym. Sci, Part B: Polym. Phys.* (1986) 25, p. 1625
54. Lustiger, A., Ishikawa, N., *J. Polym. Sci, Part B: Polym. Phys.* (1991) 29, p. 1047
55. Soares, J.B.P., Abbott, R.F., Kim, J.D., *J. Polym. Sci, Part B: Polym. Phys.* (2000) 38, p. 1267
56. Bubeck, R.A., Baker, H.M., *Polymer* (1982) 23, p. 1680
57. Soni, P.L., Geil, P.H., *J. Appl. Polym. Sci.* (1979) 23, p. 1167
58. Lustiger, A., In *Failure of Plastics* (1986) Hanser, Munich, p. 305
59. Bubeck, R.A., *Polymer* (1981) 22, p. 682
60. Lagaron, J.M., Pastor, J.M., Kip, B.J., *Polymer* (1999) 40, p. 1629
61. Lustiger, A., Avinash, G., *U.S. Patent* 6 153 703 (2000)
62. Schellenberg, J., Fienhold, G., *Polym. Eng. Sci.* (1998) 38, p. 1413
63. Qian, R., Lu, X., Brown, N., *Polymer* (1993) 34, p. 4727
64. Tonyali, K., Brown, H.R., *J. Mater. Sci.* (1987) 22, p. 3287

# INDEX

---

## Index Terms

## Links

### A

Active center	8
Additivity rules, for viscosity	43

### B

Bimetallic catalysts	6	18	51	
Bimodal resins	7	9	18	19
	51			
Blocks, in copolymers	20	21	62	63
	75	76		
Branches				
– short-chain	1			
– long-chain	1	10	11	37
	53	54		
Branching degree	2			
Breaking point, stress and strain	28	83	84	
Burst test, dynamic, for pipes and tubing	118	119		
Burst test, static, for pipes and tubing	119			

### C

Capillary, melt flow throughm	37			
Catalysts, effects on resin properties				
– bimetallic	6	18	25	26

## Index Terms

## Links

Catalysts, effects on resin properties (*Cont.*)

	51	52		
– chromium oxide	5	6	7	17
	18	24		
– metallocene	5	7	15	25
	26			
– Ziegler-Natta	4	5	6	16
	17	23	48	
Chain orientation	85	86	108	109
Chain propagation reactions	8	9		
Chain transfer (termination) <i>reactions</i>	9			
Chromium-containing catalysts	5			
Classification, of polyethylene resins	2	3		
Compositional uniformity	22	23		
Copolymer chain statistics	20	21		
Copolymerization reactions	9			
Cross-linking, polyethylene	119			
Crystaf	22			
Crystal forms of polyethylene	28	77		
Crystallinity degree				
– definition	75			
– effect of copolymer composition	75	76		
– measurement methods	73			

## **D**

Dart impact strength of LLDPE film

– definition	87			
– of ethylene copolymers	92			
– measurement	87			

## Index Terms

## Links

Dart impact strength of LLDPE film ( <i>Cont.</i> )		
– model	89	
Density of polyethylene resins		
– definition	75	
– effect of copolymer composition	77	
– measurement methods	77	
– use in classification	2	3
Density-gradient columns	77	
Differential scanning calorimetry (DSC)	57	74
Distribution of monomer units in copolymers	20	21
 <b>E</b>		
Effective viscosity, additivity rules	45	46
Elmendorf tear strength – see Tear strength		
Environmental stress cracking resistance (ESCR)		
– definition	126	132
– effect of density	129	
– effect of molecular weight	127	128
– measurement methods	125	126
– mechanism	130	
 <b>F</b>		
Failure, low-stress	119	
Flory-Schulz molecular weight distribution	13	14
Fractionation methods	22	

## Index Terms

## Links

### **G**

Gas-phase polymerization technology	6			
Gel permeation chromatography (GPC)	12	14		

### **H**

Heat of fusion of polyethylene	74			
Hydrogen, chain transfer agent	9			

### **I**

Infrared spectroscopy	26	75	85	86
	89			

### **L**

Lamella	26			
Long-chain branching	1	10	11	37
	53	54		
Low density polyethylene (LDPE)	2	7	8	110
Low-stress failure	119			

### **M**

Melt flow rate	35	36		
Melt flow ratio, definition	37			
Melt index	2	35	36	
– definition	35	36		
– of Newtonian liquid	40			

## Index Terms

## Links

Melt index (*Cont.*)

– of non-Newtonian liquid

45      46      48

– of polyethylene resins

36      37      46

Melting curve, model

– HDPE

58

– LLDPE

61

Melting points

– of linear polyethylene (HDPE)

58

– of ethylene copolymers

66

Metallocene catalysts

5      15      18      23

Methylalumoxane (MAO)

5

Modeling:

– dart impact test

89

– Elmendorf tear test

102

– melting point, HDPE

58

– melting point, ethylene copolymers

66

– top load test

116

Molecular weight distributions

– theory

10

– GPC analysis

13      14

Molecular weights of polyethylene resins

10      11

– control with hydrogen

9      10

– measurement methods

12

Monodisperse polyethylene

41      42

Morphology, of polyethylene resins

26

## **N**

Necking stage, stress and strain

28      83      84

Newtonian liquid

37      40

**Index Terms****Links**

Nomenclature, of polyethylene resins	2	3		
Non-Newtonian liquid	37	45	48	
Nuclear magnetic resonance (NMR)	75	76		

**O**

Orientation, of chains	85	86	108	109
Orthorhombic cell	28	77		

**P**

PEX	119			
Pipes, testing	118	119		
Plastomers	2	3	67	68
Polyethylene resins				
– applications	4			
– bimodal	7	18	19	53
	54			
– branching degree	1			
– classification	2	3		
– compositionally nonuniform	22	23	94	95
– compositionally uniform	22	23	25	95
	96			
– definition	1			
– morphology	26			
– multi-Flory	15	16	17	18
	19	51		
– nomenclature	2	3		
– single-Flory	15	45		
Polymerization degree	12			

## Index Terms

## Links

Polymerization rate	10	
Polymerization reactors		
– gas-phase	6	7
– solution	7	8
– slurry (particle-type)	6	
Polymorphism of polyethylene	28	77
Pseudo-monoclinic cell	28	77

## **R**

Radical reactions		
– cross-linking	119	
– polymerization	7	8

## **S**

Secant modulus	29	30	118
Shear rate, definition	39		
Shear strain, definition	39		
Slurry polymerization technology	6		
Solution polymerization technology	7	8	
Spherulite	27	28	30
Statistics of copolymer chains	20	21	
Stress-strain curve	29		

## **T**

Tear strength of LLDPE film		
– definition	97	
– of ethylene copolymers	97	107

## Index Terms

## Links

Tear strength of LLDPE film (*Cont.*)

– measurement	97		
– model	102		
Top load test, for containers			
– definition	115		
– measurement	115	116	
– model	116		
Tref	22		
Tubing, testing	118	119	

## U

Uniformity, compositional	22		
---------------------------	----	--	--

## V

Viscosity

– definition	39		
– effective	44		
– zero-shear	38		

## X

X-ray spectroscopy	26	73	74
--------------------	----	----	----

## Y

Yield stress and strain	28	83	84	
Young modulus	29	92	93	107
	117	118		

## **Index Terms**

## **Links**

### **Z**

Zero-shear viscosity

– additivity rules

43

44

– definition

38

39